

THE FLORIDA STATE UNIVERSITY  
COLLEGE OF ARTS AND SCIENCES

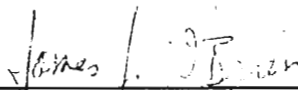
WIND-DRIVEN VARIABILITY OF THE TROPICAL  
PACIFIC AND ATLANTIC OCEANS

by

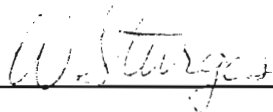
ANTONIO J. BUSALACCHI JR.

A Dissertation submitted to the  
Department of Oceanography  
in partial fulfillment of the  
requirements for the degree of  
Doctor of Philosophy

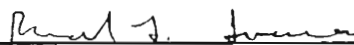
Approved:

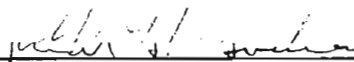
  
\_\_\_\_\_

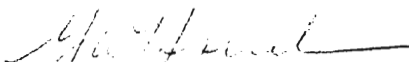
Professor Directing Dissertation

  
\_\_\_\_\_

  
\_\_\_\_\_

  
\_\_\_\_\_

  
\_\_\_\_\_

  
\_\_\_\_\_

Chairman, Department of Oceanography

December, 1982

## ABSTRACT

Models incorporating a single baroclinic mode and realistic coastline geometry are used to analyze the linear, dynamic response to estimates of the interannual wind field over the tropical Pacific and the seasonally varying winds of the tropical Atlantic. The interannual variability of the tropical Pacific is studied for the period January, 1961 to December, 1978. Model pycnocline variations at several locations are similar to the observed sea level fluctuations. El Niño events are depicted as periods when the pycnocline is persistently deep along the eastern boundary. Remotely forced equatorial Kelvin waves are responsible for this response. The character of each simulated El Niño is strongly dependent on the relation between zonal wind stress changes in the western and central equatorial Pacific. A rapid shoaling of the pycnocline in the western tropical Pacific during each El Niño is caused by westward-propagating Rossby waves. Interannual pycnocline displacements in the central equatorial Pacific are determined by the superposition of Kelvin waves excited to the west and first-mode Rossby waves generated to the east.

The forced periodic response to the seasonal wind field of the tropical Atlantic is a spatially dependent combination of a locally forced response, Kelvin waves, Rossby waves, and multiple wave reflections. The seasonal displacements of the model pycnocline are compared with observed dynamic height. Annual and semiannual fluctuations dominate the seasonal signal throughout the basin. In general, the distribution of amplitude and phase are similar for fluctuations dominate the seasonal signal throughout the basin. In general, the distribution of amplitude and phase are similar for annual changes in dynamic height and pycnocline depth. Major features

of the seasonal response are reproduced, e.g. an east-west tilting of the equatorial pycnocline about a pivot point, the seasonal pycnocline movement along the northern and southern coast of the Guinea Gulf, and a significant change of phase in the ocean variability north and south of the ITCZ. The relative importance between local and remote forcing is determined for several parts of the basin. The wind-driven annual signal in the Gulf of Guinea is due to zonal wind stress fluctuations west of the gulf. The seasonal response in the western equatorial and northernmost parts of the basin are primarily local.

#### ACKNOWLEDGMENTS

This work was supported by the National Science Foundation under grants ATM7920485 and OCE8119052. Partial support for the tropical Atlantic study was provided by a NOAA cooperative agreement NA80RAH00002 during a visit to the Joint Institute for Marine and Atmospheric Research (JIMAR) at the University of Hawaii during the summer of 1981. Computations were performed at the National Center for Atmospheric Research, the Florida State University Computing Center, and the Hawaii Institute of Geophysics.

It is with the deepest respect and appreciation that I thank Dr. James J. O'Brien for his ideas, support, and guidance as my major professor. I thank him for the motivation he provided through his encouragement and infectious enthusiasm. In addition, I wish to express my gratitude for the countless opportunities allowing me to interact with some of the top people in our field. I am also grateful for the time taken by Drs. Steve Blumsack, Ya Hsueh, Richard Iverson, and Wilton Sturges while serving on my doctoral committee. The benefits reaped from discussions with Drs. Mark Cane, Allan Clarke, John Kindle, and Julian McCreary are cheerfully acknowledged.

The interannual Pacific Ocean study would have been impossible without the efforts provided by the many persons involved in the wind data analysis. I am indebted to Dr. Kensuke Takeuchi for his assistance rendered in extending this calculation for 1971-1978, and data analysis. I am indebted to Dr. Kensuke Takeuchi for his assistance rendered in extending this calculation for 1971-1978, and for his input and program development used in analyzing the central

and western Pacific variability. Chapter II will form the basis for a joint contribution with K. Takeuchi and J. J. O'Brien to the proceedings of the 14<sup>th</sup> Liège Colloquium on Ocean Hydrodynamics.

To Dr. Joël Picaut I wish to express my sincere appreciation for sharing his knowledge of the tropical Atlantic Ocean and for reviewing this manuscript. His analyses of the wind data graciously provided by Dr. Stefan Hastenrath and the dynamic height data kindly provided by Dr. Jacques Merle and Mlle Sabine Arnault were vital to this study. I will always be grateful for his help with the SALOPE calculation, the many hours of heated discussions (sans un extincteur), and midnight walks in Pigalle. I also would like to thank Dr. Dennis Moore for the opportunity to visit JIMAR, which led to the beginning of the Atlantic study. Special thanks to Dr. Roger Lukas and Ms. Sharon Yokogawa for the many hours of assistance at JIMAR. Chapter III will provide the basis for a joint publication with Joël Picaut.

I am very appreciative of the manuscript preparation provided by Pat Teaf. Valuable comments on the manuscript were kindly provided by Dr. Benoit Cushman-Roisin. I would like to acknowledge the aid provided by James Merritt, Ruth Pryor, Dewey Rudd, and Roberta Scott.

Finally, the patience, love, and support of my parents and my wife, Connie will never be forgotten. I owe them my sincerest, heart-felt thanks.

TABLE OF CONTENTS

|  | Page |
|--|------|
| ABSTRACT . . . . .   | ii   |
| ACKNOWLEDGMENTS . . . . .  | iv   |
| TABLE OF CONTENTS . . . . .  | vi   |
| LIST OF FIGURES . . . . .  | vii  |
| I. INTRODUCTION . . . . .  | 1    |
| II. ON THE INTERANNUAL WIND-DRIVEN RESPONSE OF THE TROPICAL<br>PACIFIC OCEAN . . . . . | 5    |
| A. The Model and Wind Data . . . . .   | 8    |
| B. Eastern Pacific Response . . . . .  | 10   |
| C. Western Pacific Response . . . . .  | 30   |
| D. Central Equatorial Response . . . . .   | 47   |
| III. SEASONAL VARIABILITY FROM A MODEL OF THE TROPICAL<br>ATLANTIC OCEAN . . . . .     | 56   |
| A. The Numerical Model . . . . .   | 62   |
| B. The Wind Field . . . . .  | 65   |
| C. Tropical Atlantic Response to the Seasonal<br>Wind Field . . . . .                  | 71   |
| 1. basin-wide response . . . . .   | 72   |
| 2. western tropical response . . . . .   | 83   |
| 3. equatorial response . . . . .   | 92   |
| 4. eastern tropical response . . . . .   | 100  |
| IV. SUMMARY . . . . .  | 113  |
| V. DISCUSSIONS AND CONCLUSIONS . . . . .   | 125  |
| REFERENCES . . . . .   | 132  |
| REFERENCES . . . . .   | 132  |

## LIST OF FIGURES

| Figure  | Page |
|---|------|
| 1. Comparison of the model geometry with the tropical Pacific Ocean. The model basin extends from 18°N to 12°S and 126°E to 77°W. The dashed line represents an open boundary; all remaining boundaries are solid walls. Sea level data from the island stations indicated provide details of the interannual variability in different regions of the Pacific. . . . .  | 6    |
| 2. Time series of departures from the long-term monthly mean shore temperatures at Talara, Peru, from 1961-1978, inclusive. Anomalously warm periods are shaded black. . . . .  | 11   |
| 3. Time series of observed sea level at the Galapagos Islands from 1961-1977, inclusive. Data for 1978 are not available. Periods when the mean monthly sea level is higher than the long-term annual mean are shaded black. . . . .  | 12   |
| 4. Model pycnocline height anomaly (PHA) at the Galapagos Islands. Periods when the pycnocline is deeper than the 18-year mean are shaded black. . . . .  | 15   |
| 5. Comparison of the model pycnocline height anomaly (solid) and observed sea level (dashed) at the Galapagos Islands filtered by a 12-month running-mean. The pycnocline displacement scale is in meters and sea level changes are expressed in cm. . . . .  | 18   |
| 6. Model pycnocline height anomaly at a location corresponding to Talara, Peru. . . . .   | 20   |
| 7. Contours of lagged cross correlation between the pycnocline variability at the equatorial eastern boundary and all points west. The slope of the solid line indicates an eastward propagation representative of equatorially trapped Kelvin waves. The solid line represents the westward propagation of Rossby waves excited at the boundary. . . . .   | 21   |
| 8. An X-T section along the equator for the upper-layer thickness (ULT) during 1964-65. The phase speed of the downwelling Kelvin wave responsible for triggering the 1965 El Nino in the model is indicated by the slope of an imaginary line connecting a point at the western boundary for November, 1964, with a point at the eastern boundary for downwelling Kelvin wave responsible for triggering the 1965 El Nino in the model is indicated by the slope of an imaginary line connecting a point at the western boundary for November, 1964, with a point at the eastern boundary for February, 1965. Such a line also indicates the end of the equatorial downwelling associated with the passage of the Kelvin wave. . . . . | 24   |

|     |   |    |
|-----|---|----|
| 9.  | Zonal wind stress along the equator from 1971-1978. White areas indicate westerly flow. Time periods in which the stress is greater than $1.0 \text{ dynes cm}^{-2}$ are shaded the darkest. Contour interval is $.2 \text{ dynes cm}^{-2}$ . . . . .   | 27 |
| 10. | Time series of observed sea level at Truk Island from 1961-1978, inclusive. . . . .   | 31 |
| 11. | Model pycnocline height anomaly at a location corresponding to Truk Island. . . . .   | 33 |
| 12. | The change in upper layer thickness from October, 1975 to October, 1976 in the western portion of the model domain. The stipled regions indicate where the pycnocline was shallower in October, 1976. Contour interval is 10 m. . . .   | 34 |
| 13. | A Y-T section of the pycnocline height anomaly (PHA) along $160^{\circ}\text{E}$ for 1971 to 1978. White regions indicate the model pycnocline is shallower than the 18-year mean. Contour interval is 15 m. . . . .  | 36 |
| 14. | Contours of lagged cross correlation between the model pycnocline variability at Truk Island and all points east and west along $7.5^{\circ}\text{N}$ . . . . .   | 38 |
| 15. | A Y-T diagram of the zonal wind stress averaged over $160^{\circ}\text{E}$ - $140^{\circ}\text{W}$ for 1971 to 1978. White regions indicate the easterlies are weaker (westerly anomaly) than the long-term annual mean. Contour interval is $.25 \text{ dynes cm}^{-2}$ . . . . .  | 41 |
| 16. | Idealized model of the response of the tropical ocean to the westerly wind stress anomaly confined within two meridians $30^{\circ}$ apart. a) Y-T diagram of the wind stress forcing function. Contour interval is $.2 \text{ dynes cm}^{-2}$ . b) Y-T diagram of the pycnocline response along the western edge of the forcing region. Contour interval is 10 m. . . .  | 42 |
| 17. | Same as Fig. 16 except the forcing is shifted northward by $3^{\circ}$ . . . . .  | 44 |
| 18. | Similar to Figure 16 but the forcing function is now preceded by an equatorial relaxation sequence and followed by an intensification of the trades (stipled) late in the year. . . . .   | 46 |
| 19. | Kelvin and first-mode equatorial Rossby wave components (solid) of the model pycnocline signal (dashed) at Canton Island for 1964 to 1966. a) Kelvin plus first-mode Rossby wave compared with the pycnocline signal. b) Kelvin wave compared with the pycnocline signal. c) First-mode Rossby (solid) of the model pycnocline signal (dashed) at Canton Island for 1964 to 1966. a) Kelvin plus first-mode Rossby wave compared with the pycnocline signal. b) Kelvin wave compared with the pycnocline signal. c) First-mode Rossby wave compared with the pycnocline signal. . . . . | 50 |



|     |   |       |
|-----|---|-------|
| 20. | Same as Fig. 19 except at Christmas Island. . . . .   | 51    |
| 21. | Same as Fig. 19 except from 1971-1973. . . . .  | 53    |
| 22. | Comparison of the model geometry with the tropical Atlantic Ocean basin. The dashed line represents an open boundary; all remaining boundaries are solid walls. . . . .   | 64    |
| 23. | Mean, amplitude distribution for the first harmonic, and amplitude distribution of the second harmonic for a) the zonal wind stress and b) the meridional wind stress in dynes $\text{cm}^{-2}$ . . . . .   | 69,70 |
| 24. | Annual mean perturbation (meters) to the upper layer thickness. Shaded regions indicate where the pycnocline is shallower than the initial state of no motion. . . . .  | 73    |
| 25. | Annual mean of dynamic height (dyn. cm) at 0/300 db. . . . .  | 75    |
| 26. | Annual variability of the model pycnocline depth, a) amplitude (meters) and b) phase (degrees). The phase map indicates when the pycnocline is deepest. . . . .   | 77    |
| 27. | Annual variability of dynamic height at the surface relative to 300 db, a) amplitude (dyn. cm.) and b) phase (degrees). . . . .   | 78    |
| 28. | Semiannual amplitudes of a) dynamic height (0/300db) and b) model pycnocline depth. . . . .   | 79    |
| 29. | Amplitude distributions for the pycnocline response to a) annual $\tau^x$ forcing and b) semiannual $\tau^x$ forcing. The differences from Fig. 26 and 28 indicate the influence of $\tau^y$ forcing. . . . .   | 82    |
| 30. | Seasonal pycnocline displacements for $2^\circ$ squares centered at $10^\circ\text{N}$ , $48^\circ\text{W}$ (dashed line) and $3^\circ\text{N}$ , $43^\circ\text{W}$ (solid line). These variations are indicative of a north-south tilting about a pivot line which separates the two areas. Negative values indicate the pycnocline is deeper than the annual mean. . . . . | 85    |
| 31. | Amplitude distributions for the pycnocline response to<br>a) annual $\tau^x$ forcing west of $25^\circ\text{W}$<br>b) annual $\tau^x$ forcing east of $25^\circ\text{W}$<br>c) semiannual $\tau^x$ forcing west of $25^\circ\text{W}$<br>d) semiannual $\tau^x$ forcing east of $25^\circ\text{W}$ . . . . .  | 86,87 |
| 32. | Comparison of $\frac{\partial h}{\partial t}$ (solid) and Ekman pumping contribution<br>d) semiannual $\tau^x$ forcing east of $25^\circ\text{W}$ . . . . .   | 86,87 |
| 32. | Comparison of $\frac{\partial h}{\partial t}$ (solid) and Ekman pumping contribution (dashed) at $10^\circ\text{N}$ , $48^\circ\text{W}$ . Positive values indicate the pycnocline is deepening. . . . .  | 89    |

|     |   |         |
|-----|---|---------|
| 33. | Comparison at 3°N, 43°W of  |         |
|     | a) $\frac{\partial h}{\partial t}$ (solid), Ekman pumping (dash-dot), and Rossby wave (dashed) contributions  |         |
|     | b) $\frac{\partial h}{\partial t}$ (solid), $-\frac{1}{\beta y} \frac{\partial^2 U}{\partial y \partial t}$ (dash-dot) and $\frac{1}{\beta y z} \frac{\partial U}{\partial t}$ (dashed) contributions to Eq. (2)  | 90      |
| 34. | Zonal velocity corresponding to a simulated North Equatorial Countercurrent averaged between 3°N-9°N and 30°W-42°W.   | 93      |
| 35. | Temporal variability of the model pycnocline (meters) along the equator. a) Shaded regions indicate the pycnocline is shallower than the initial state of no motion. The annual mean east-west pycnocline tilt is included in this plot. b) The annual mean east-west pycnocline tilt has been removed. Shaded regions indicate the pycnocline is shallower than the annual mean. | 94      |
| 36. | Temporal variability of the zonal wind stress (dynes cm <sup>-2</sup> ) along the equator. a) The annual mean has been included. Shaded regions indicate easterly wind stress. b) The annual mean has been removed. Shaded regions indicate an easterly wind stress perturbation.   | 96      |
| 37. | Seasonal pycnocline displacements (meters) north and south along the eastern boundary. Shaded regions indicate the pycnocline is shallower than the annual mean. The zonal coast in the Guinea Gulf extends from +500 km to +2800 km.   | 103     |
| 38. | Comparison of a) dynamic height for 0/300 db and b) model pycnocline depth at Abidjan (dashed) and Pt. Noire (solid). Negative values indicate the pycnocline is deeper than the annual mean.   | 104     |
| 39. | Zonal velocity corresponding to a simulated Guinea current averaged along the coast between 4°E and 11°W.   | 107     |
| 40. | Amplitude distributions for the pycnocline response to  |         |
|     | a) annual $\tau^x$ forcing west of 10°W   |         |
|     | b) annual $\tau^x$ forcing east of 10°W   |         |
|     | c) semiannual $\tau^x$ forcing west of 10°W   |         |
|     | d) semiannual $\tau^x$ forcing east of 10°W   | 111,112 |

## I. INTRODUCTION

The wind-driven variability of the tropical Pacific and Atlantic Oceans provide an interesting contrast between the interannual and seasonal responses of two tropical oceans. Important differences in the overlying wind fields and the size and shape of the ocean basins are key elements of the different observed oceanic responses. These features result in the tropical Pacific being more conducive to a study of the interannual variability of a tropical ocean while the tropical Atlantic is better suited for a study of the seasonal response of a tropical ocean. This should not be construed to mean the interannual variability of the tropical Atlantic is unimportant. Philander (1979) has drawn from theory and observations to discuss the different characteristics of the three tropical oceans.

The equatorial Pacific encompasses more than 40% of the circumference of the globe. Year to year fluctuations of the ocean-atmosphere system across this expanse are as large or larger than the seasonal signal (Wyrtki, 1975; Hickey, 1975). Significant interannual events known as El Niño dominate the variability of the thermal structure in the eastern tropical Pacific. The cause and effect of this phenomenon may have wide-reaching climatic implications. The largest seasonal changes to the equatorial wind field occur in the central Pacific but interannual fluctuations are more pronounced. Interannual perturbations to the wind field in the central and western Pacific are much larger interannual fluctuations are more pronounced. Interannual perturbations to the wind field in the central and western Pacific are much larger

than in the eastern Pacific. These periods of anomalous wind are often prior to and during an El Niño year. The response time to such wind changes in the equatorial Pacific, owing to the large extent of the basin, is on the order of one year (Cane and Sarachik, 1977). Since there are important wind changes from one year to the next the response of the tropical Pacific may not be in seasonal equilibrium with the wind field.

In contrast, the tropical Atlantic is characterized by a strong seasonal signal (Merle, 1980a; Merle et al., 1980). Observations of the wind field, dynamic height, sea level, and sea surface temperature indicate that annual and semiannual fluctuations dominate the variability. However, interannual perturbations to the seasonal signal do exist (Hisard, 1980; Merle, 1980b). A strong summer upwelling and a secondary winter upwelling are representative of the seasonal cycle in the Gulf of Guinea. The local winds do not exhibit a strong seasonal signal. Significant seasonal wind changes are found in the western Atlantic. The amplitude of which is several times larger than the seasonal wind field for the equatorial Pacific. Observations of the zonal pressure gradient and zonal wind field along the equator demonstrate that the oceanic response may be in equilibrium with the seasonal wind field (Katz et al., 1977). Since the width of the equatorial Atlantic basin is one-third the size of the Pacific the ocean can adjust to wind changes on a time scale of several months.

The linear, wind-driven response of the two oceans will be examined using a numerical model incorporating a single baroclinic

The linear, wind-driven response of the two oceans will be examined using a numerical model incorporating a single baroclinic mode, realistic coastline geometry, and a forcing function derived

from ship-board estimates of the surface wind field. A similar model was used successfully by Busalacchi and O'Brien (1980) to study the seasonal response of the tropical Pacific Ocean. In their analysis, the spatial and temporal variations of the model pycnocline at several locations throughout the Pacific basin were compared with observations. It was demonstrated that given a reasonable estimate of the wind field, selected features of the seasonal response could be described by linear, wind-driven processes.

The dynamic, interannual response to the tropical Pacific wind field for a span of 18 years is analyzed first. The model results are compared with sea level records at different points in the basin for 1961-1978. The dense spatial and temporal resolution of the model is used to determine the processes responsible for dramatic, out-of-phase sea level/pycnocline changes in the eastern and western tropical Pacific during simulated Los Niños. Internal, equatorially trapped Kelvin waves excited by zonal wind changes in the western and central equatorial Pacific are shown to be responsible for elevated sea level along the eastern boundary during El Niño. Westward-propagating Rossby waves excited by associated wind changes result in a rapid drop in sea level in the western Pacific.

The dynamic response to the seasonally varying wind field over the tropical Atlantic is studied next. The forced periodic response consists of a spatially dependent superposition of a locally forced response, Kelvin waves, Rossby waves, and multiple wave reflections. The phase and amplitude distributions of the seasonal signal is compared with Kelvin waves, Rossby waves, and multiple wave reflections. The phase and amplitude distributions of the seasonal signal is compared with

observed dynamic height. The relative importance between local and remote forcing effects in different parts of the basin is investigated. It is shown that the annual, wind-induced signal in the Gulf of Guinea is a response to annual zonal wind stress fluctuations west of the gulf. In the western equatorial and northernmost parts of the basin the response is primarily local.

## II. ON THE INTERANNUAL WIND-DRIVEN RESPONSE OF THE TROPICAL PACIFIC OCEAN

The importance of the interannual variability of the tropical Pacific lies in its relationship with the El Niño phenomena. In the strictest sense, El Niño is a term used presently to represent the anomalous occurrence and persistence of high sea surface temperatures (SST) along the coast of Ecuador and Peru. It is used more loosely to represent anomalous high sea level and deep thermocline periods in the eastern Pacific consistent and coincident with the SST changes. An El Niño occurrence is not an isolated phenomenon, rather it is one facet of global-wide climate anomalies characterized by changes in the Southern Oscillation Index (Kidson, 1975). With respect to the tropical Pacific Ocean, one might expect that large perturbations to the mean state are not unique to the eastern boundary region. Fortunately, there are several island stations in key areas of the tropical Pacific (Fig. 1) from which sea level time series can be used to monitor the interannual variability.

In the eastern Pacific, sea level changes at the Galapagos Islands are representative of the non-seasonal fluctuations at the equator and along the eastern boundary (Wyrтки, 1975; Hickey, 1975). In the western tropical Pacific, there is a drastic decrease in sea level and shoaling of the thermocline during the El Niño year (Hickey, 1975; Wyrтки, 1975, 1977, 1979; Meyers, 1982). The largest drop in sea level shoaling of the thermocline during the El Niño year (Hickey, 1975; Wyrтки, 1975, 1977, 1979; Meyers, 1982). The largest drop in sea level occurs north of the equator. The sea level record at Truk Island is

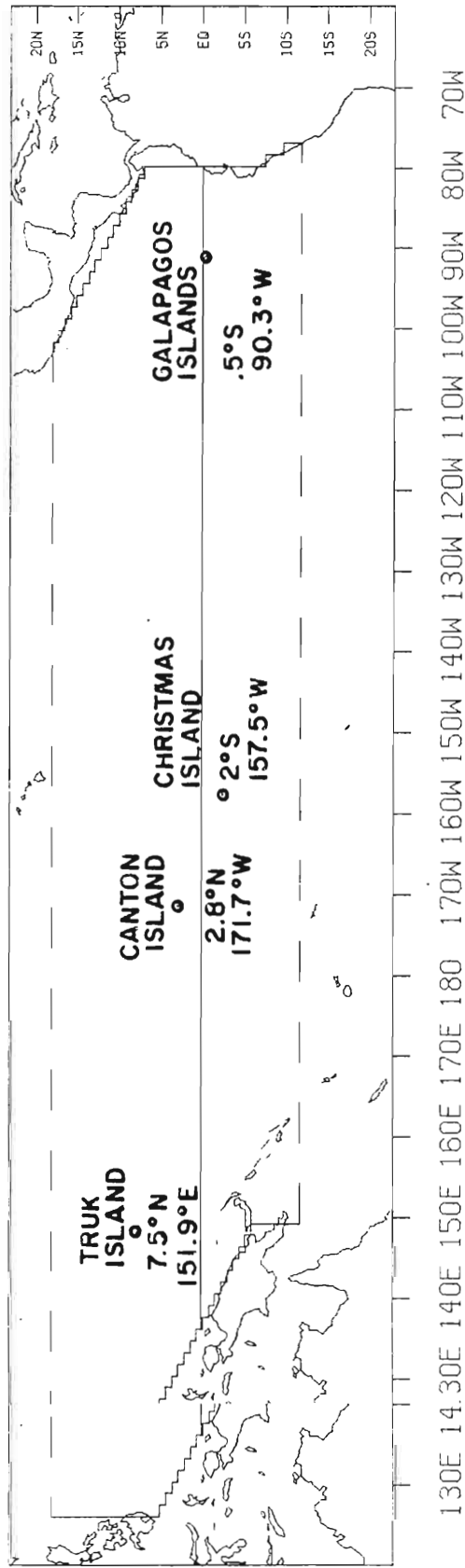


Fig. 1 Fig. 1. Comparison of the model geometry with the tropical Pacific Ocean. The model basin extends from 18°N to 12°S and 126°E to 77°W. The dashed line represents an open boundary; all remaining binning boundaries are solid walls. Sea level data from the island stations indicated provide details of the interannual variability in different regions of the Pacific.



representative of the variability in this region and is one of the longest time series available. A lagged cross correlation analysis (Hickey, 1975) indicates a maximum negative correlation of sea level between the eastern and western Pacific occurs when the eastern Pacific leads by several months. In the central equatorial Pacific, sea level data from Canton Island and Christmas Island indicate an anomalous rise in sea level during the latter half of the El Niño year. The processes responsible for the phase relations between the eastern, central equatorial, and western Pacific are not understood.

Wyrtki (1975) has attributed El Niño to the excitation of Kelvin waves due to the interannual fluctuations of the southeast trade winds over the central equatorial Pacific. A statistical analysis by Barnett (1977) linked the variability of the zonal component of the southeast trades west of the dateline with sea level changes across the Pacific basin. Numerical and analytical models by Hurlburt et al., (1976) and McCreary (1976) simulated the excitation of an equatorially trapped internal Kelvin wave in response to changes in the zonal component of the wind stress. Upon impingement with the eastern boundary, the incoming Kelvin wave excited westward-propagating internal Rossby waves and poleward-propagating coastal trapped Kelvin waves. This is consistent with the theoretical work of Moore (1968) and Moore and Philander (1977). Kindle (1979) demonstrated that the magnitude, duration, and timing of changes in the southeast trades over the central and western Pacific were important in determining the character of a simulated El Niño response. O'Brien et al. (1981) discussed these and western Pacific were important in determining the character of a simulated El Niño response. O'Brien et al., (1981) discussed these

aspects of Kelvin waves and El Niño in a simpler physical context.

This study uses the results of a linear numerical model to analyze the interannual variability of the tropical Pacific Ocean. The model of Busalacchi and O'Brien (1980) is forced by monthly estimates of the surface wind field based on ship-board observations over the tropical Pacific for 1961-1978. The dense time and space coverage provided by such a model will be used to provide insight into the causality of the wind-driven response in different parts of the basin. Regions of important wind stress fluctuations will be identified and the relevance to sea level/pycnocline responses in the eastern, central equatorial, and western Pacific will be addressed. Since the model is simple, the wind induced variability can be interpreted easily in physical terms. If the model results compare favorably with observations, physical interpretation of the model response can be applied to the observed oceanic response.

#### A. The Model and Wind Data

The model utilized by Busalacchi and O'Brien (1980) is a  $1\frac{1}{2}$  layer reduced-gravity, linear transport model on an equatorial  $\beta$ -plane. The model geometry is an idealization of the tropical Pacific from  $18^\circ\text{N}$  to  $12^\circ\text{S}$  (Fig. 1). Open boundary conditions at the northern and southern boundaries allow coastal Kelvin waves to propagate freely out of the model domain. A complete discussion of the model and its equations are included in the author's previous work.

For the present study, we will focus on the vertical displacements included in the author's previous work.

For the present study, we will focus on the vertical displacements of the model pycnocline. From this point on, all discussions of

pycnocline variability refer to the model results. The initial upper-layer thickness,  $H$ , is taken to be 300 m. This depth is sufficient to prevent any surfacing of the density interface during an 18-year integration. The corresponding first baroclinic phase speed is  $2.45 \text{ m s}^{-1}$ . This speed is the only dynamically important free parameter in the model. The Laplacian friction coefficient only cosmetically smooths the very high wave number numerical noise.

Details of the wind stress data base and a spectral analysis of that data for 1961-1970 were discussed by Goldenberg and O'Brien (1981). Monthly estimates of the surface wind stress based on ship observations over the tropical Pacific from January, 1961, to December, 1978, were subjectively analyzed onto a  $2^\circ$  by  $2^\circ$  mesh. The resulting data set, continuous in time and space, was input as a body force into the momentum equations of the model. Though the approach used in collecting and preparing the wind data is not the ultimate methodology for monitoring the wind field over the tropical Pacific Ocean, it has resulted in the only data set available with spatial and temporal resolution suitable for interannual modelling studies.

A new open-boundary condition is implemented for this 18-year simulation. After 7 years of integration, the variant of the Hurlburt (1974) open-boundary condition used in the previous study becomes unstable. The boundary condition at the northern and southern boundaries is replaced with an open-boundary condition developed by Camerlengo and O'Brien (1980). This modification of the Orlandi (1976) open-boundary treatment allows the model to be integrated for the full Camerlengo and O'Brien (1980). This modification of the Orlandi (1976) open-boundary treatment allows the model to be integrated for the full

18 years. Prior to the onset of any instability, calculations with the Hurlburt open-boundary condition and those with the Camerlengo and O'Brien open-boundary condition render the same solutions. The model is initiated using the results from year 4 of the seasonal calculation in Busalacchi and O'Brien (1980). Thus, spin-up transients are confined essentially to the first year of integration.

#### B. Eastern Pacific Response

The 18-year period of this numerical simulation encompasses several notable eastern Pacific events of varying intensity. The strongest El Niño since 1957 occurred during 1972 (Quinn et al., 1978). The associated environmental changes resulted in the accelerated collapse of the Peruvian anchoveta fishery. Sea surface temperatures (SST) off the coast of Ecuador and Peru were up to 4°C higher than the climatological monthly means (Fig. 2). Sea level was at its highest point in years. The sea level record at the Galapagos Islands (Fig. 3) is a useful indicator of this interannual variability along the eastern boundary (Wyrcki, 1975; Hickey, 1975). For the 1972 event, as opposed to previous Los Niños, large anomalies were present during the middle of the year. Positive SST anomalies peaked in March and June. Sea level began to rise in late 1971 and reached a maximum in June. Consistent with several previous El Niño events another peak in SST and sea level occurred at the end of the year.

During 1965 and 1976, moderate El Niño conditions were present in the eastern tropical Pacific. Sea surface temperatures were 2°-3°C

During 1965 and 1976, moderate El Niño conditions were present in the eastern tropical Pacific. Sea surface temperatures were 2°-3°C above normal. The 1965 event was characterized by elevated SST and

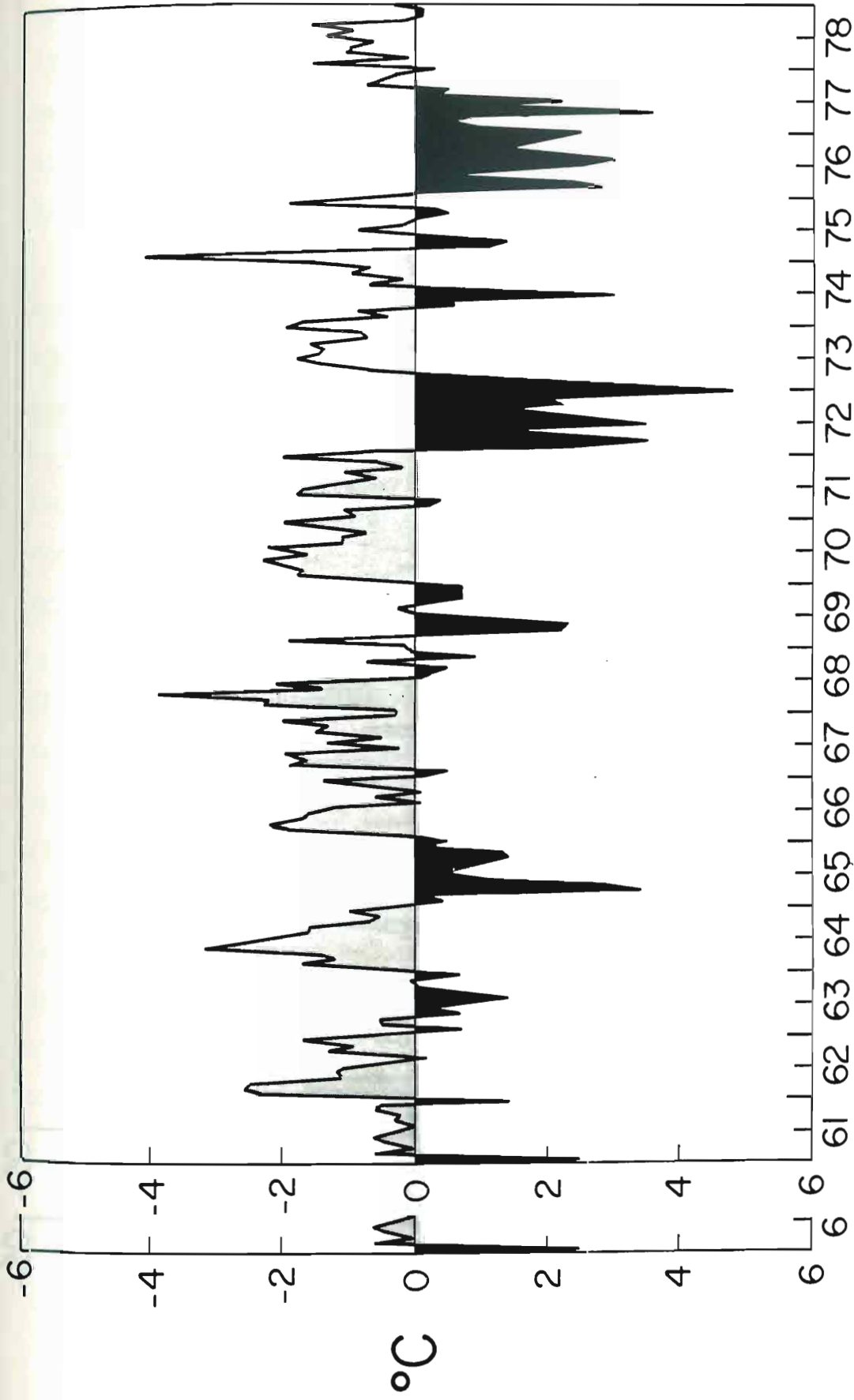


Fig. 2. Time series of departures from the long-term monthly mean shore temperatures at Talara, Peru, from 1961-1978, inclusive. Anomalously warm periods are shaded black.

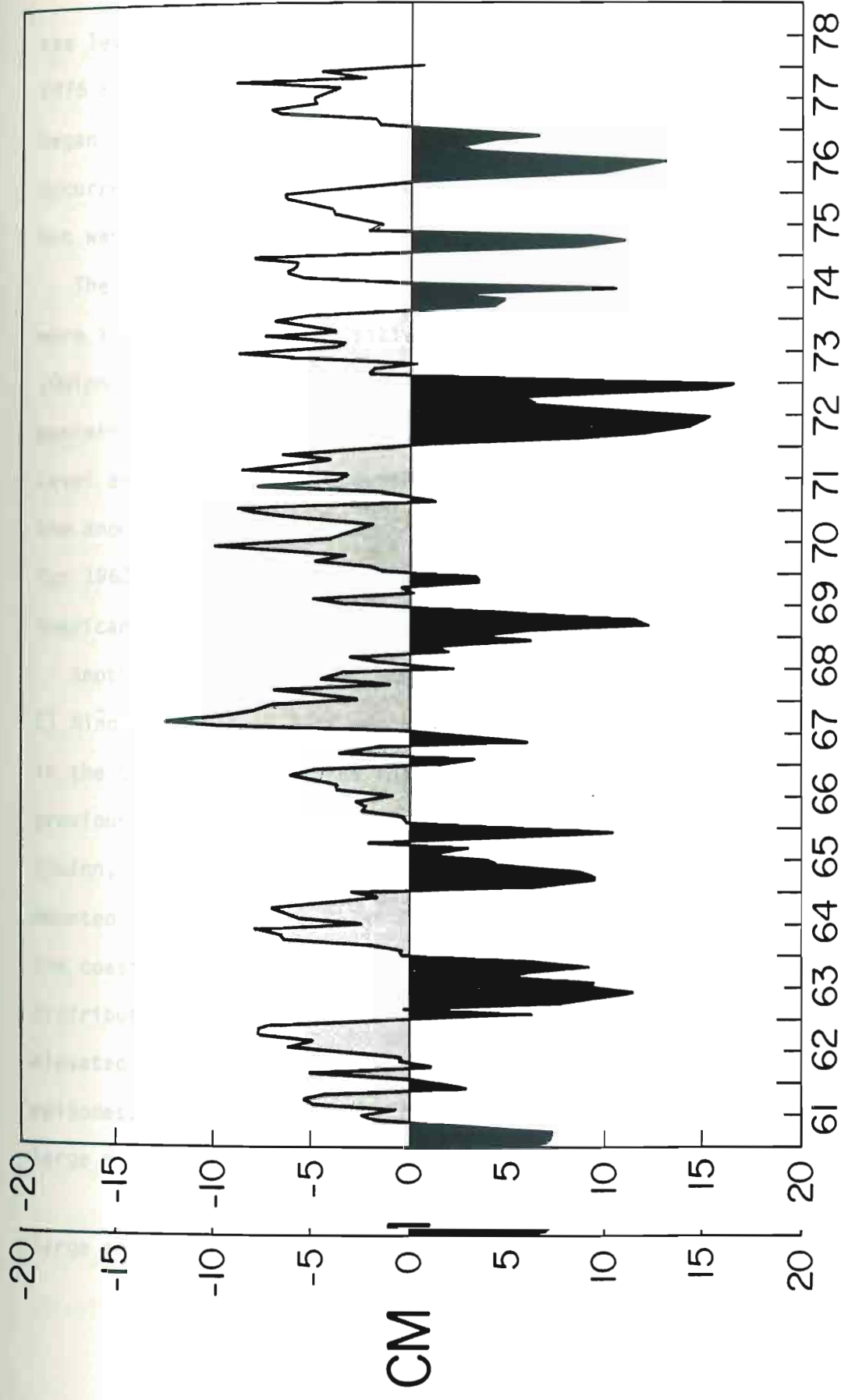


Fig. 3. Time series of observed sea level at the Galapagos Islands from 1961-1977, inclusive. Data for 1978 are not available. Periods when the mean monthly sea level is higher than the long-term annual mean are shaded black.

sea level episodes at the beginning and end of the year. For the 1976 El Niño, SST was anomalously high throughout the year. Sea level began to rise late in 1975 and peaked in June similar to the 1972 occurrence. A secondary sea level maximum was present late in the year but was much smaller relative to the first peak than in the 1972 event.

The weakest of the year-long warm events during this 18-year period were in 1963 and 1969. Positive SST anomalies were less than  $2.5^{\circ}\text{C}$  (Quinn et al. 1978). Once again sea level was elevated along the eastern boundary. However, for the very weak event in 1963 the sea level anomaly at the Galapagos Islands was not truly representative of the anomalies at coastal stations. Only at Galapagos was the sea level for 1963 higher than during the 1965 El Niño. At all the South American coastal stations monthly sea levels were higher in 1965.

Another period worthy of attention is 1975 even though it was not an El Niño year. In 1974 it was noted that there was an ongoing decrease in the Southern Oscillation Index (Wyrtki et al., 1976). Based on previous studies linking a low Southern Oscillation Index with El Niño (Quinn, 1974), a weak El Niño was predicted for 1975. An expedition mounted to observe this event found anomalous conditions present off the coast of Ecuador and Peru in February and March of 1975. The distribution of positive SST anomalies, changes in thermocline depth, and elevated sea levels were similar to the onset phase of previous El Niño episodes. These conditions did not persist long enough and were not large enough in magnitude for 1975 to be recognized as an El Niño year.

large enough in magnitude for 1975 to be recognized as an El Niño year.

By April and May the development of the warm episode had been aborted, and conditions were returning to normal.

Interspersed among the El Niño episodes were periods of low SST and depressed sea level. In this study of the linear wind-driven Pacific response the dynamics responsible for pycnocline and sea level changes during El Niño will be the same as in these non-El Niño events. Most of the following discussion of the model results will focus on the El Niño incidents since they often dominate the interannual variability, have important climatic implications, and have been the subject of previous observational and theoretical studies.

The sea surface and pycnocline fluctuate  $180^\circ$  out of phase in the model formulation used. Meyers (1979) has shown, using sea level and interfacial depth profiles, that the central and eastern Pacific act in a manner compatible with the dynamics implicit in this reduced-gravity approach. Since the model does not contain thermodynamics the results cannot give a direct indication of SST change. In general, there is no linear relation between upper-layer thickness, sea level, or thermocline depth and SST. Yet, in the eastern tropical Pacific, high (low) SST anomalies are significantly correlated with elevated (depressed) sea level (Barnett, 1977; Enfield and Allen, 1980). Modelling efforts including mixed-layer physics will provide much needed information on such relations between thermocline depth, vertical velocity, and SST.

A time series of the pycnocline height anomaly (PHA) at a location representing the Galapagos Islands (Fig. 4) depicts the vertical displacement of the model pycnocline throughout the 18-year



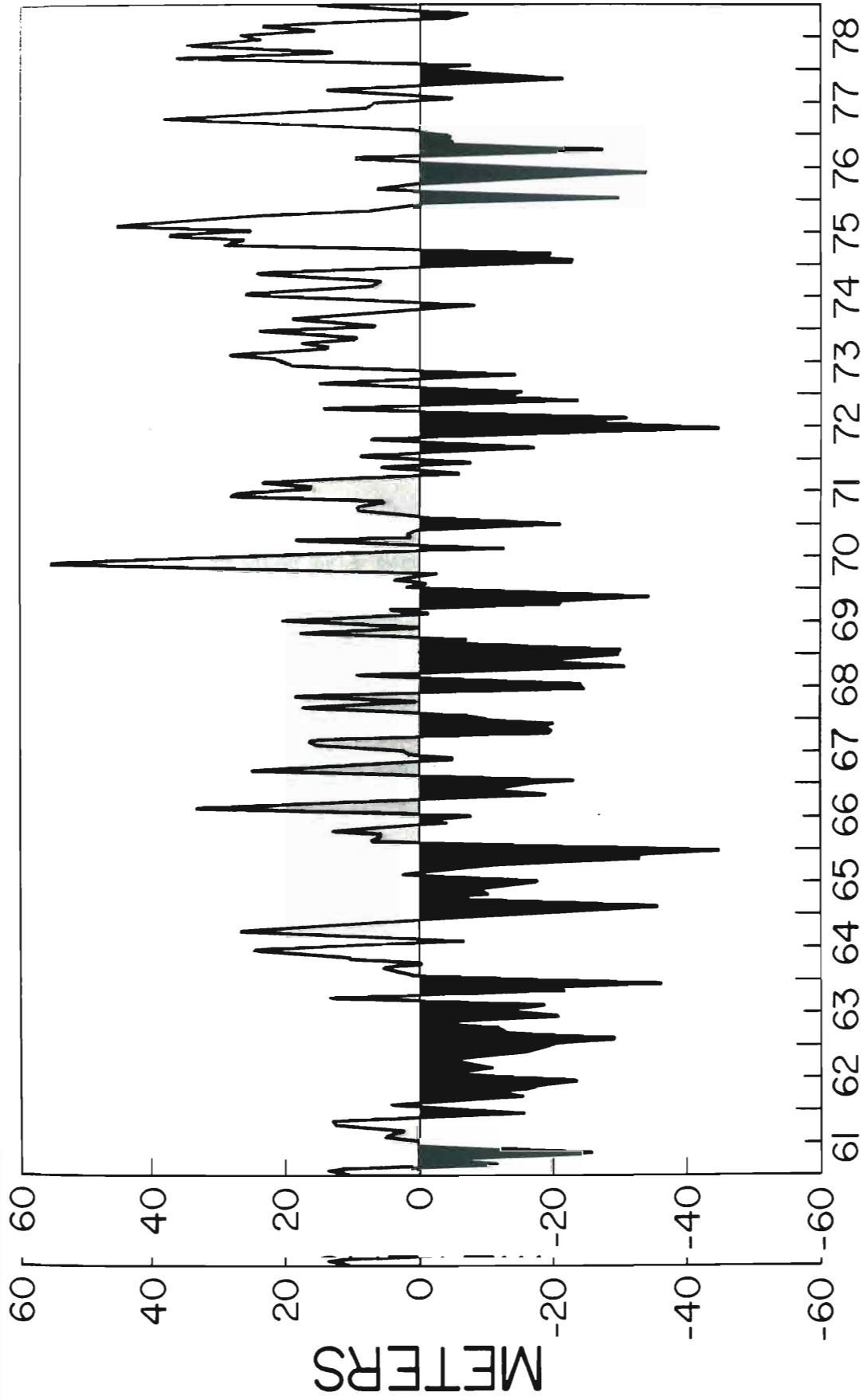


Fig. 4. Model pycnocline height anomaly (PHA) at the Galapagos Islands. Periods when the pycnocline is deeper than the 18-year mean are shaded black.

integration. The linear trend, resulting from a mean background wind stress, has been removed. Upwelling and downwelling bursts of relatively short duration constitute the variability in the entire record. The model pycnocline is the deepest during 1963, 1965, 1969, 1972, and 1976; the five El Niño years. The double-peak El Niño signature found in the sea level record (Fig. 3) is present in the model results for 1965 and 1969. During these years the upper layer becomes deepest at the beginning and end of the El Niño year. The onset of the 1972 El Niño is preceded by a deepening of the pycnocline during the second half of 1971. The pycnocline reaches its maximum depth in June followed by a secondary maximum at the end of the El Niño year. The 1976 El Niño is characterized by downwelling from mid-1975 to early 1976, maximum pycnocline depths in June, and a deep pycnocline again in the latter half of the year. The weak event of 1975 is represented by a downwelled pycnocline at the beginning of the year followed by a rapid upwelling leaving a shallow pycnocline for the remainder of the year. Even though there are periods when the relative amplitude of observed sea level change and pycnocline displacement do not agree, the timing of major upwelling and downwelling events is similar. The cross correlation of pycnocline variability and observed sea level less the seasonal signals is maximum at zero lag with a correlation of 0.52 which is significant at the 99% level. The degrees of freedom used in the significance test were determined by dividing the total record length by the integral time period needed to obtain two independent realizations (Davis, 1976). The number of equivalent

degrees of freedom was 51. Changing the phase speed of the model by  $\pm 30\%$  changes the phase of the eastern boundary response by less than one month. When comparing with monthly mean observations this shift in phase is not significant.

A major difference between the model pycnocline fluctuations and observed sea level is the presence of more high frequency variability in the pycnocline time series. This is to be expected since the temporal resolution of the model pycnocline time series is much greater than the monthly sea level record. Furthermore, in this single mode calculation the time scales of the upwelling and downwelling episodes in the east are indicative of the time and spatial scales of the wind changes to the west. The addition of slower higher-order vertical modes may lead to longer duration events. Another possible reason for this discrepancy may be that the wind estimates used have more power at high frequencies than the actual wind field.

The observed sea level and model pycnocline time series for the Galapagos Islands have been subjected to a 12-month, running-mean filter (Fig. 5). This provides a more graphic representation of the low frequency variability during the 18-year period. The similarities and differences between the model and observations are clearly displayed. The filtered data indicate a tendency for the sea level and the model pycnocline to be elevated or depressed for spans of 10-30 months. Discrepancies between the model and observations include the phase of the response from mid-1961 through 1962, the relative amplitudes of the response from late-1967 to early-1968, and the phase of the response from mid-1961 through 1962, the relative amplitudes of the response from late-1967 to early-1968, and the

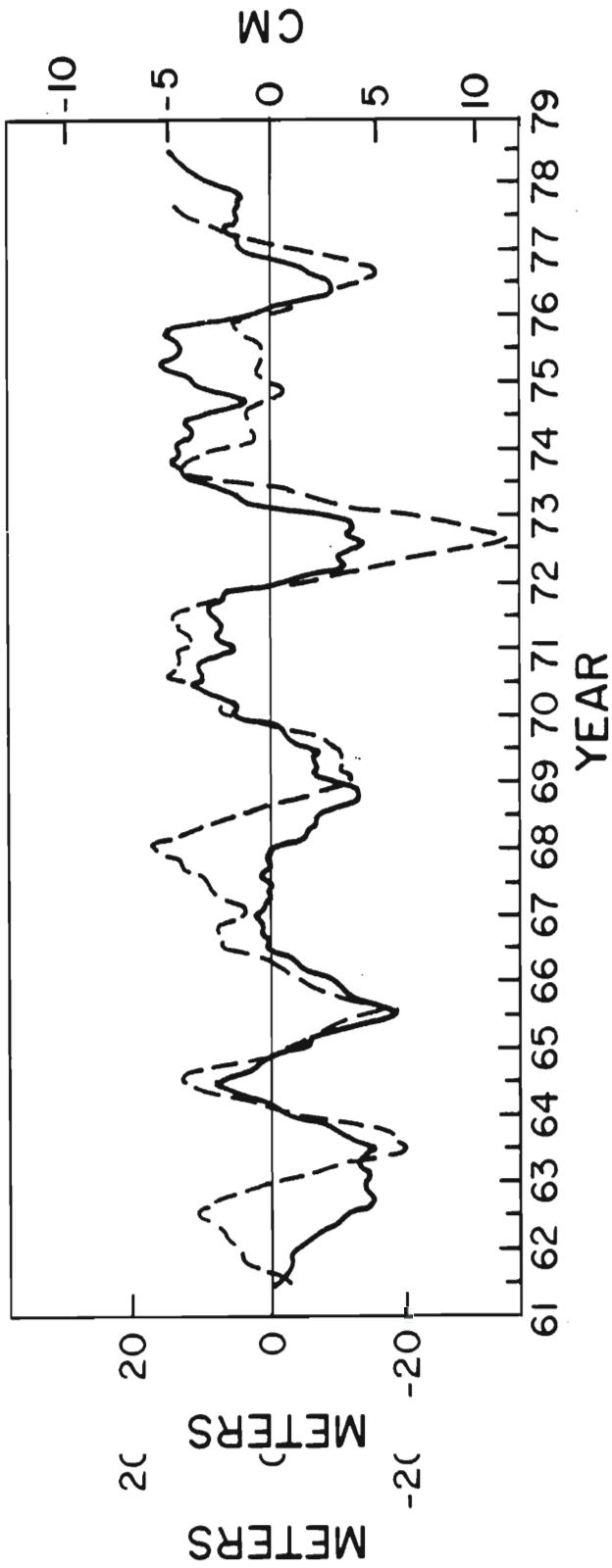


Fig. 5. Comparison of the model pycnocline height anomaly (solid) and observed sea level (dashed) at the Galapagos Islands filtered by a 12-month running-mean. The pycnocline displacement scale is in meters and sea level changes are expressed in cm.

amplitude in 1972. The cross correlation between these two filtered time series is .61.

The model pycnocline variability at the location of Talara, Peru (Fig. 6) is very similar to that at the Galapagos Islands, except the maximum cross correlation ( $r = .98$ , significant at 99% level) occurs when the signal at Talara lags Galapagos by 1-3 days. This lag increases when time series further poleward along the coast are cross correlated with the Galapagos time series. For example, the pycnocline time series at the location of Callao, Peru ( $12^{\circ}\text{S}$ ) lags Galapagos by approximately one week and is highly correlated. The great degree of similarity between these time series attests to the large areal extent of the variability near the eastern boundary. The poleward increase in lag indicates a poleward propagation of information. Smith (1978), Enfield and Allen (1980), and Romea and Smith (1982) have reported on an observed poleward propagation along the coast.

The pycnocline variability at the Galapagos Islands and Talara consists of discrete upwelling and downwelling events with a duration of several months. What is the mechanism responsible for these changes in depth of the pycnocline? A cross correlation of the pycnocline variability at the equatorial eastern boundary with all points west along the equator implies that the effects of internal Kelvin and Rossby waves are important. The lag structure of the pycnocline variability along the equator is illustrated in Fig. 7. The most striking aspect is the linear increase in lag away from the eastern boundary for high correlations. The solid line represents an eastward phase speed of  $2.45 \text{ m s}^{-1}$ , corresponding to the phase speed for an

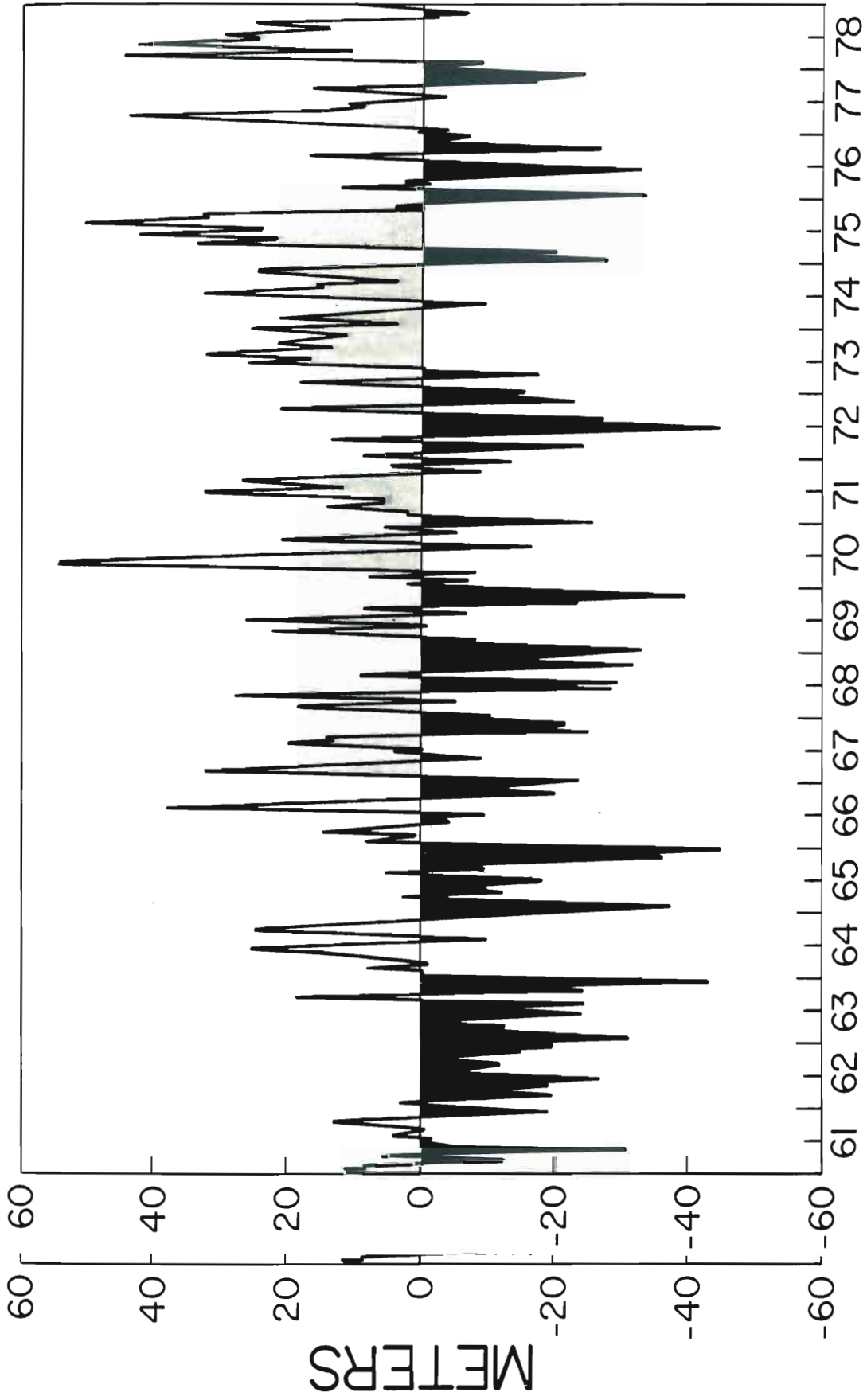


Fig. 6. Model pycnocline height anomaly at a location corresponding to Talara, Peru.

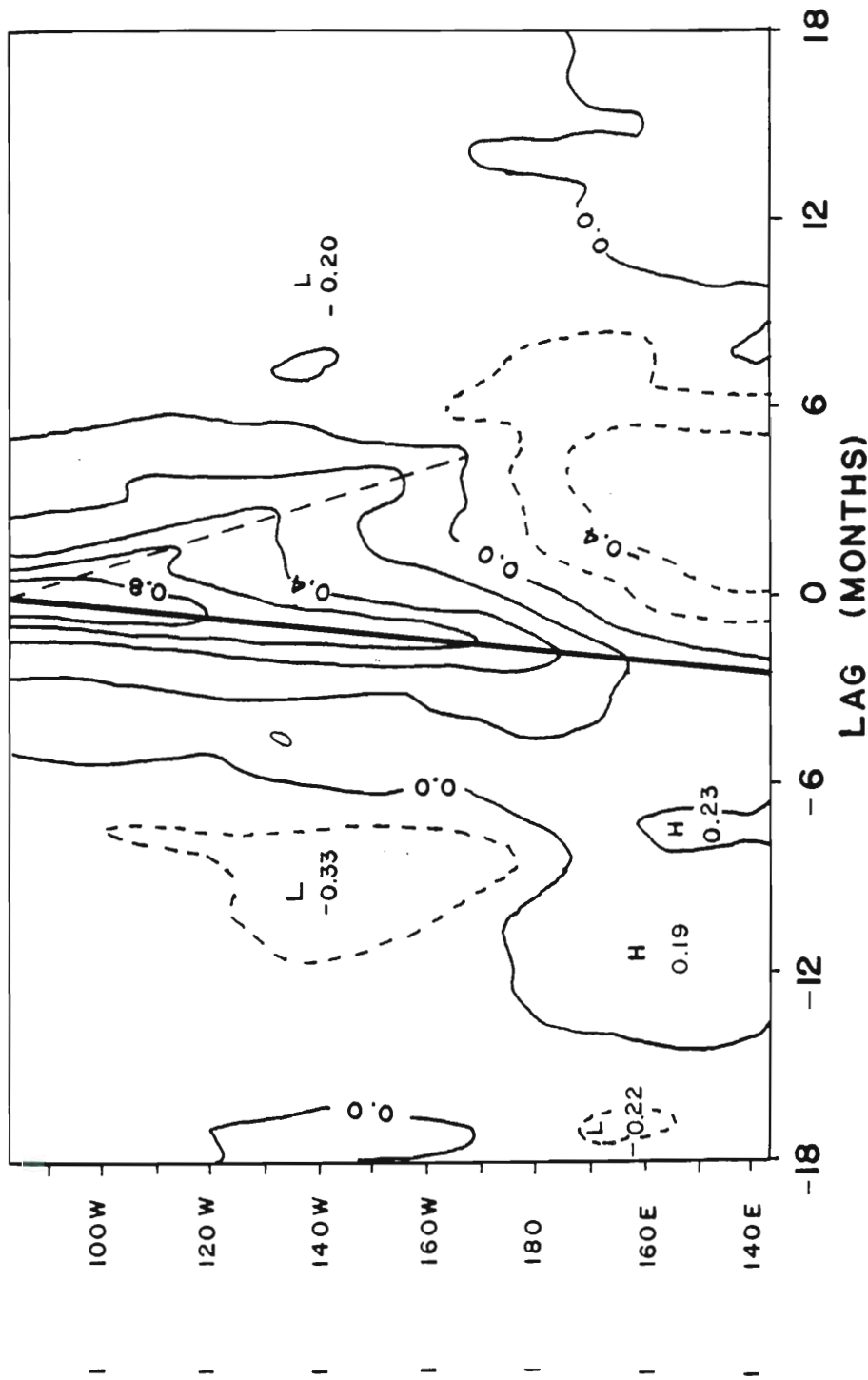


Fig. 7. Contours of lagged cross correlation between the pycnocline variability at the equatorial eastern boundary and all points west. The slope of the solid line indicates an eastward propagation representative of equatorially trapped Kelvin waves. The solid line represents the westward propagation of Rossby waves excited at the boundary.

internal, equatorially trapped Kelvin wave in this model. As a result, 50% of the variability at the eastern boundary is accounted for by the variability along the Kelvin wave characteristic in the central Pacific. Knox and Halpern (1982) have observed eastward propagation along the equator from 152°W to 91°W.

The linear increase in lead away from the eastern boundary (dashed line) represents the westward propagation of the lowest order Rossby waves excited at the coast. The slope of the dashed line represents a phase speed of  $.82 \text{ m s}^{-1}$ , one-third the speed of the Kelvin wave. These waves were excited by the impingement of Kelvin waves or local changes in the wind stress. These waves have a noticeable effect on the pycnocline variability westward to 160°W. There is also a notable negative correlation when the eastern boundary leads the western boundary by several months.

Away from the boundaries an equatorial Kelvin wave can only be generated by the equatorial divergence caused by temporal fluctuations of the symmetric component of the zonal wind stress at the equator. A test calculation was performed in which the model was only driven by the zonal wind stress for the period mid-1973 through 1977. This was intended to test the premise that the interannual events in the eastern part of the basin are remotely forced by Kelvin waves. The time interval was chosen because it contained several large changes in depth of the pycnocline. The resulting pycnocline response along the eastern boundary was essentially the same as the total response to zonal and meridional winds. The cross correlation between the zonal wind stress solution and the total forced case was .99 at zero lag. The



pycnocline variability at the eastern boundary of this linear model is the integrated response to the zonal equatorial wind stress fluctuations to the west. The evolution of significant events, e.g., El Niño occurrences, can be traced back in time and space along the Kelvin wave characteristics. The location of the forcing responsible for each event has been identified in this manner.

We now describe the character of El Niño events from 1961-1978 depicted in this model as periods when the pycnocline was persistently deep. The period 1964-1965 is a good time frame within which to study the transformation from a non-El Niño regime to an El Niño regime. The semiannual pycnocline variability at the eastern boundary previously discussed by others (Meyers, 1979; Kindle, 1979; Busalacchi and O'Brien, 1980) has been associated with Kelvin wave signals excited between  $180^\circ$  and  $120^\circ\text{W}$ . Evidence for this seasonal cycle is seen throughout the model integration (Figs. 4,6). The semiannual variability is typical of a non-El Niño year in the 1960's. From January, 1964, to April, 1964, the pycnocline in the eastern two-thirds of the equatorial Pacific is being upwelled (Fig. 8). This is a result of an upwelling Kelvin wave front excited during an October, 1963 to March, 1964 intensification of the easterlies between  $180^\circ$ - $160^\circ\text{W}$ . The downwelling at the western boundary through June, 1964, is caused by a downwelling Rossby wave front excited by the same intensification of the easterlies between  $180^\circ$ - $160^\circ\text{W}$ . Another large amplitude upwelling Kelvin wave front is excited in the interior from July through September. Towards the end of a non-El Niño year a downwelling Kelvin wave front is excited in the interior from July through September. Towards the end of a non-El Niño year a downwelling Kelvin

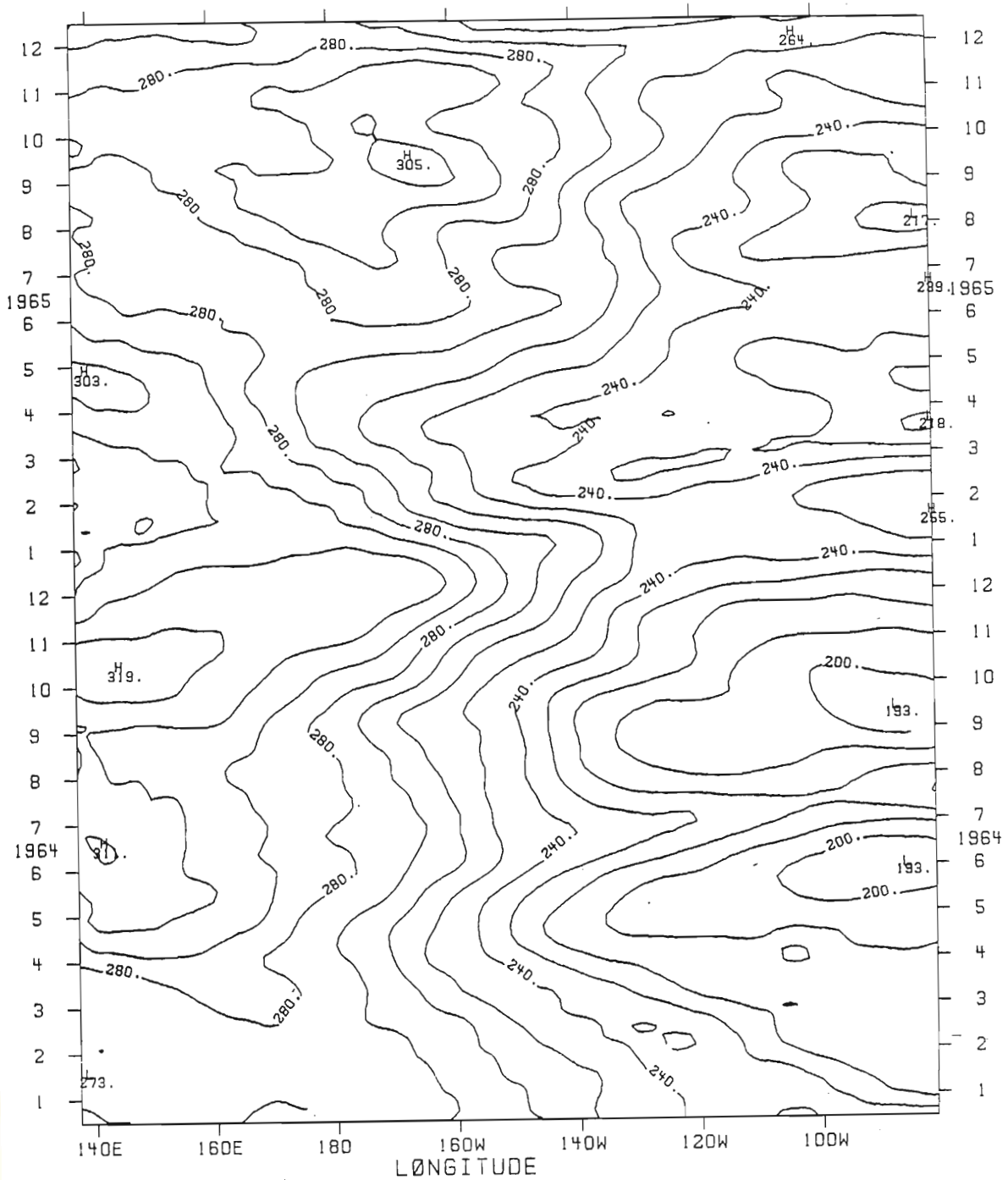


Fig. 8. An X-T section along the equator for the upper-layer thickness (ULT) during 1964-65. The phase speed of the downwelling Kelvin wave responsible for triggering the 1965 El Niño in the model is indicated by the slope of an imaginary line connecting a point at the western boundary for November, 1964, with a point at the eastern boundary for February, 1965. The downwelling Kelvin wave responsible for triggering the 1965 El Niño in the model is indicated by the slope of an imaginary line connecting a point at the western boundary for November, 1964, with a point at the eastern boundary for February, 1965. Such a line also indicates the end of the equatorial downwelling associated with the passage of the Kelvin wave.

wave front is excited in the central equatorial Pacific. A simulated seasonal El Niño along the eastern boundary is associated with this downwelling Kelvin wave front. Though the amplitude and precise timing of these upwelling signals may vary amongst non-El Niño years, there is often an upwelling of the pycnocline early in the year. The upwelling is important because it causes the pycnocline to be upwelled following the seasonal downwelling of the pycnocline during the austral summer.

The changes in pycnocline depth that typify the 1965 El Niño event have their roots in the western Pacific during the latter half of 1964. A  $0.4 \text{ dynes cm}^{-2}$  relaxation of the easterly wind stress between the western boundary and the dateline from August–November, 1964, excites a downwelling Kelvin wave front. The slope of the downwelling signal in Fig. 8 represents the inverse phase speed of an internal Kelvin wave. The equatorial pycnocline is depressed as the wave front propagates eastward; terminating at the eastern boundary in January, 1965. The timing of this wave is such that it greatly enhances the normal seasonal downwelling during the Southern Hemispheric summer. The same sequence of events precedes the 1969 El Niño.

In addition to the downwelling Kelvin wave excited near the western boundary, the semiannual upwelling signals of 1965 are much weaker than those of non-El Niño years. As a result, there is no mechanism to raise the deeper than normal downwelled pycnocline present in early 1965. The upwelling signals are weaker than non-El Niño years because the intensification of the interior easterlies is not as strong. This cessation of the normal semiannual variability of the zonal wind stress

also occurs during 1969. Therefore, over a one-year period of time the pycnocline is deeper than the long term mean.

Towards the end of 1965 (Fig. 8), the seasonal relaxation of the interior easterlies excites a downwelling Kelvin wave front. This downwelling Kelvin wave is the cause of the downwelling at the eastern boundary at the beginning of 1966. Though this Kelvin wave is associated with the seasonal signal, it is atypical in the sense that it was excited at a time when the pycnocline was deeper than normal. Hence, there is a double-peak downwelling signature during 1965.

The excitation of a large amplitude downwelling Kelvin wave west of the dateline, which then enhances the normal seasonal downwelling, and the concomitant cessation of the semiannual interior zonal wind stress is the scenario that describes the 1965 and 1969 El Niño events. The minor El Niño of 1963 is solely due to weakened seasonally varying zonal wind stress over the central equatorial Pacific. There were not any large amplitude downwelling Kelvin waves excited during late 1962.

The events of the 1970's were somewhat different than in the previous decade. Beginning in October 1971, there was a relaxation or weakening of the trade winds west of the dateline (Fig. 9). This band of wind relaxation progressed eastward (Wyrtki, 1977) to 160°W during the entire El Niño year. Concurrent with the initial weakening in the west there was an intensification of the central equatorial easterlies, 130°W-170°W, from mid-October until the end of 1971. The combined effect of weakening winds in the west and intensifying winds in the central Pacific yielded average pycnocline depths in the east at the

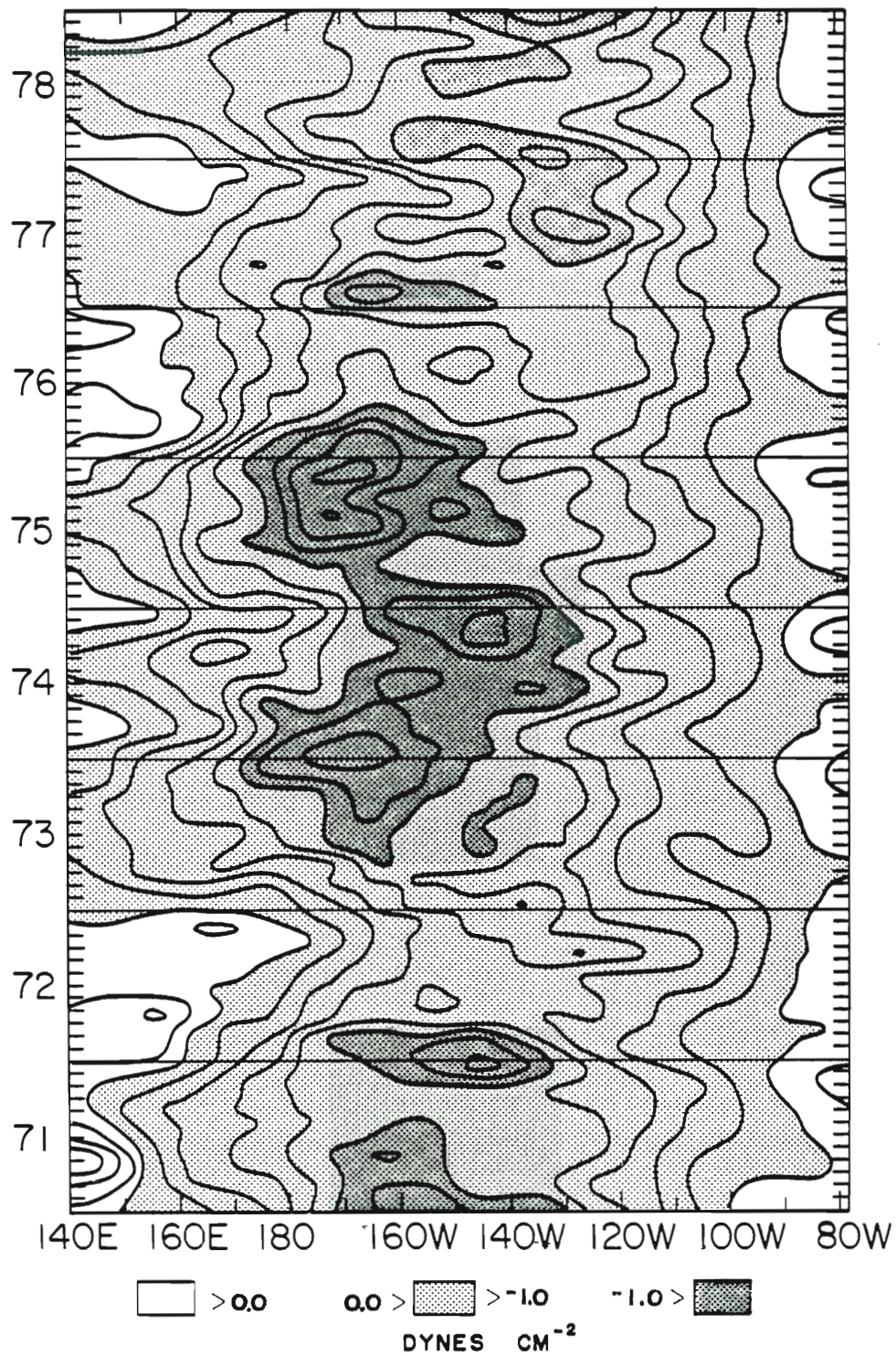


Fig. 9. Zonal wind stress along the equator from 1971-1978. White areas indicate westerly flow. Time periods in which the stress is greater than 1.0 dynes cm<sup>-2</sup> are shaded the darkest. Contour interval is .2 dynes cm<sup>-2</sup>.

Fig. 9. Zonal wind stress along the equator from 1971-1978. White areas indicate westerly flow. Time periods in which the stress is greater than 1.0 dynes cm<sup>-2</sup> are shaded the darkest. Contour interval is .2 dynes cm<sup>-2</sup>.

beginning of 1972 (Fig. 4). From January through April, at  $120^{\circ}\text{W}$ - $180^{\circ}$ , there was a decrease in the zonal wind stress of more than  $.6 \text{ dynes cm}^{-2}$ . Thereafter, the winds in the central equatorial Pacific remained weak. This weakening of the easterlies excited a downwelling Kelvin wave front responsible for the deep model pycnocline (Fig. 4) corresponding with observed elevated sea level (Fig. 3) along the eastern boundary in June. During the latter half of the year an intensification-relaxation sequence at  $100^{\circ}\text{W}$ - $140^{\circ}\text{W}$  was responsible for the second downwelling peak at the end of 1972. Recovery from the 1972 El Niño began with strengthening trades in January of 1973.

In September of 1974 the trade winds west of the dateline began decreasing and continued until January, 1975. The winds in the central Pacific did not change appreciably. The resulting downwelling Kelvin wave front induced the deep pycnocline in the east at the beginning of 1975. As opposed to 1972, the trades in the western and central Pacific did not continue to weaken. An intensification of the easterlies beginning west of the dateline in January and east of the dateline in March produced a rapid recovery from the downwelling at the beginning of the year. A persistently deep pycnocline was not present at the eastern boundary in 1975. Consistent with observations, the event in early 1975 never matured into an El Niño.

The onset of the 1976 El Niño began when the winds west of  $160^{\circ}\text{E}$  started decreasing in October of 1975. An eastward progression of this weakening transpired similar to the wind changes in 1972. A more rapid decrease in the trades between  $140^{\circ}\text{W}$  and the dateline during the first weakening transpired similar to the wind changes in 1972. A more rapid decrease in the trades between  $140^{\circ}\text{W}$  and the dateline during the first

four months of 1976 was once again responsible for the large downwelling peak in June of the El Niño year. Continued weakening between  $160^{\circ}\text{W}$  and  $140^{\circ}\text{W}$  produced the last downwelling pulse of the El Niño year. The zonal wind stress remained weak up until December. Recovery from the 1976 El Niño began with a short period of intensified easterlies between  $140^{\circ}\text{W}$  and  $180^{\circ}$  (Wyrski, 1979). The subsequent upwelling Kelvin wave front produced shallow pycnocline depths along the eastern boundary during the first half of 1977.

Comparisons of the simulated El Niño events of 1972 and 1976 with those of 1965 and 1969 yield an important difference. The model pycnocline variability during Los Niños of the 1960's were comprised of pycnocline depth maxima at the beginning and end of the El Niño year. In the middle of the El Niño year the pycnocline was not significantly deep. On the contrary, during the 1972 and 1976 El Niño events the maximum pycnocline depth was attained in June. The reasons for this difference bear out the uniqueness of each El Niño.

The central equatorial easterlies during the 1970's had a significantly greater impact on the eastern boundary variability than in 1965 or 1969. The downwelling pulses at the beginning of 1965 and 1969 were due to weakening trades in the western Pacific during the four preceding months. During this same period the winds in the central Pacific did not intensify. Similar conditions were present at the beginning of 1975 and 1976; years in which the pycnocline was deep in January. A deep pycnocline did not exist at the beginning of 1972 in January. A deep pycnocline did not exist at the beginning of 1972

because the easterlies in the central Pacific intensified in late 1971 while the winds west of the dateline were changing from easterly to westerly. From January to April of 1972 and 1976 the central equatorial easterlies decreased markedly. This resulted in the deep pycnocline along the eastern boundary in June. During the first four months of 1965 and 1969 the central equatorial trade winds did not weaken noticeably. Hence, the pycnocline was not deep in mid-1965 or mid-1969. In 1975 the trade winds intensified and were anomalously strong for the entire year resulting in a rapid upwelling from an initially deep pycnocline.

#### C. Western Pacific Response

Since Wyrtki (1975) proposed a scenario of El Niño it has been thought that, due to strong easterlies, sea level in the western tropical Pacific was deserving of attention in the year preceding El Niño. However, as Meyers (1982) recently reported, and, as shown in Fig. 10, the sea level change at Truk Island is much more dramatic in El Niño years themselves. The sea level record at Truk Island is presented because it is representative of the interannual changes in the western Pacific and is one of the longest time series available.

In every year classed as an "El Niño year" for the period 1961-1978, a significant drop of the sea level is observed in the latter half of the year. Sustained significantly high sea levels are not necessarily observed in the year previous to every El Niño. The decreases in sea level at Truk during El Niño years have a common necessarily observed in the year previous to every El Niño. The decreases in sea level at Truk during El Niño years have a common



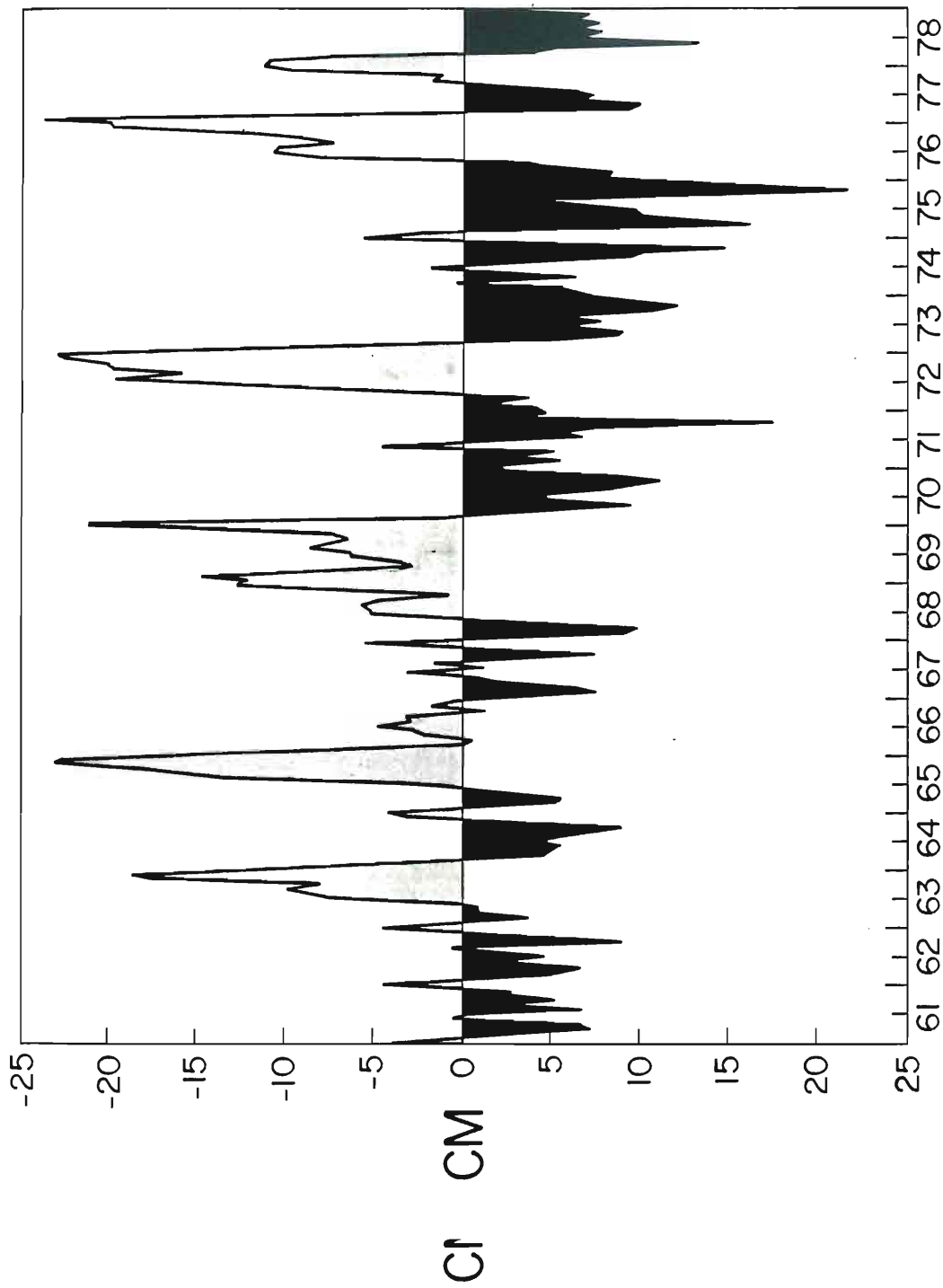


Fig. 10. Time series of observed sea level at Truk Island from 1961-1978, inclusive.

pattern. They begin in late winter or spring (February-May) and in most cases (1963, 1969, 1972, and 1976) an initial sea level minimum is attained in the middle of the year (June-September). The lowest sea level, as low as 20 cm below the annual average, is reached at the end of the year. This is followed by a rapid recovery within the next few months, usually from January to April of the following year.

Wyrтки (1979) examined the sea levels at widely scattered islands in the western Pacific Ocean for the 1976 El Niño event. Widespread low sea levels were evident in the western tropical Pacific for the second half of the year. The maximum sea level decrease was within a zonal band at 5°N-10°N. This indicates that Truk Island is located in an advantageous position to monitor the sea level change during El Niño years. The sea level excursions in the Southern Hemisphere are much smaller.

The time series of the model pycnocline displacement at the location of Truk Island is depicted in Fig. 11. The time series is characterized by several shallow pycnocline events. Except for 1966, these events occur during the latter half of an El Niño year and correspond well to the sea level time series at Truk (Fig. 10). Note again a shallow pycnocline (positive PHA) corresponds to low sea level. As expected from this comparison, the correlation between the observed sea level and the model pycnocline at Truk has a maximum as high as 0.76 at zero lag.

The spatial distribution of the anomalous model pycnocline depths in an El Niño year is also in agreement with the observations. Fig. 12

The spatial distribution of the anomalous model pycnocline depths in an El Niño year is also in agreement with the observations. Fig. 12

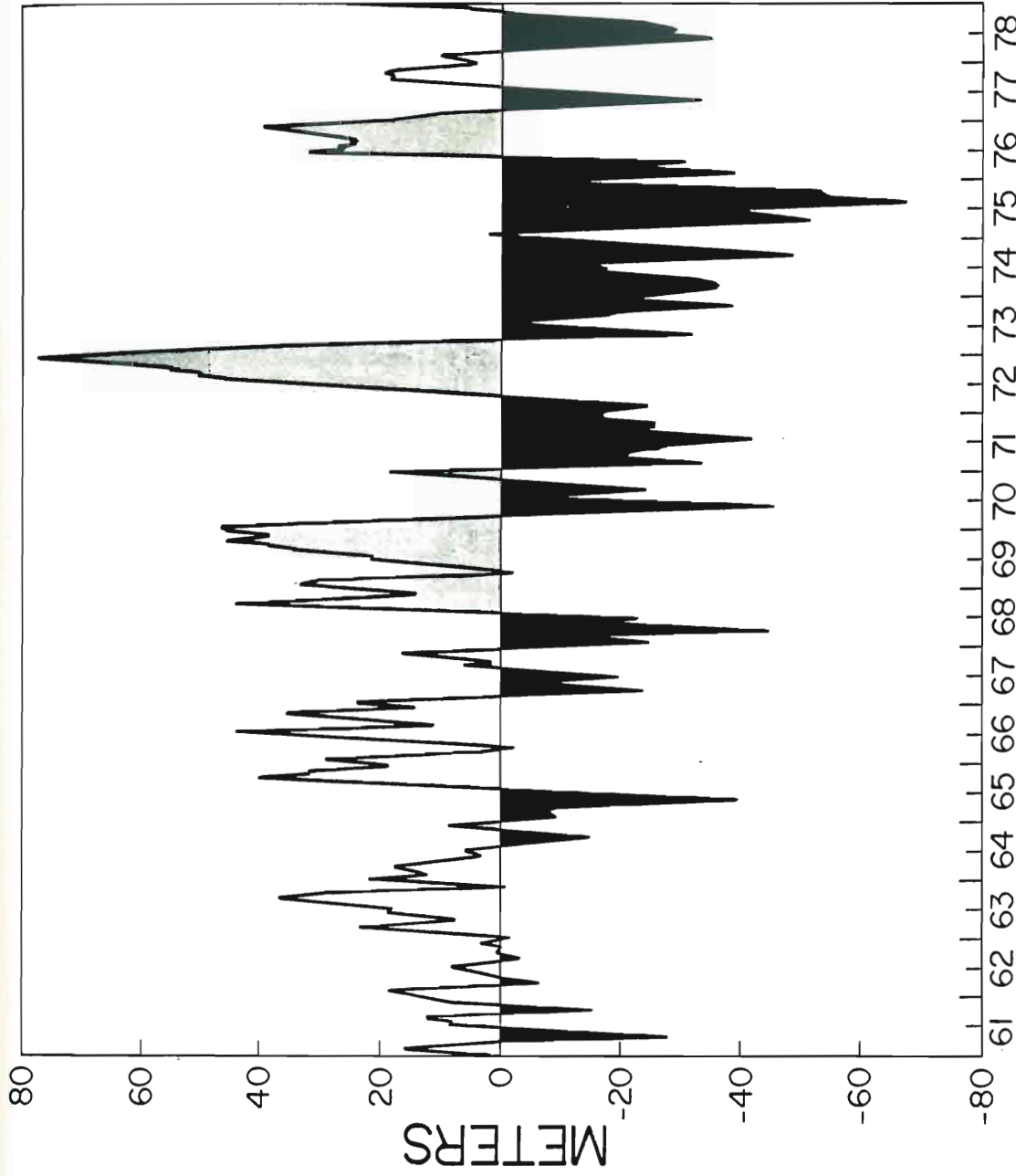


Fig. 11. Model pycnocline height anomaly at a location corresponding to Truk Island.

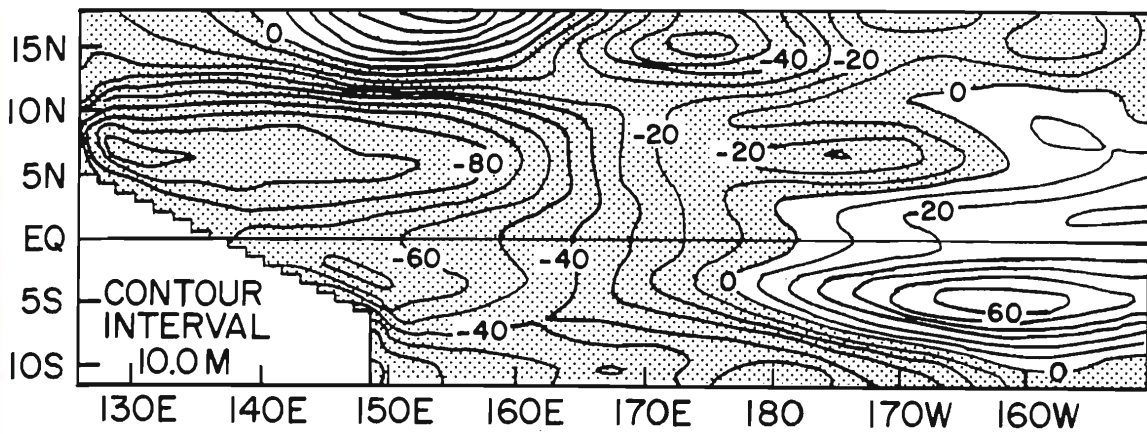


Fig. 12. The change in upper layer thickness from October, 1975 to October, 1976 in the western portion of the model domain. The stippled regions indicate where the pycnocline was shallower in October, 1976. Contour interval is 10 m.

shows the difference in depth of the model pycnocline for the western Pacific between October, 1976 and October, 1975. The spatial structure of the change in pycnocline depth agrees with the observations shown by Wyrтки (1979, Fig. 7) except for the region close to the northern open boundary of the model. The maximum pycnocline rise is also found around  $5^{\circ}\text{N}$ - $10^{\circ}\text{N}$ . A smaller maximum is found in the Southern Hemisphere near the western boundary.

A Y-T diagram of the model pycnocline at  $160^{\circ}\text{E}$  for the period 1971 to 1977 (Fig. 13) is convenient for examining the meridional distribution of the shallow pycnocline during El Niño years. The longitude  $160^{\circ}\text{E}$  is selected to avoid the effects of the western boundary in the Southern Hemisphere. It is not considered inadequate to choose  $160^{\circ}\text{E}$  as being representative of the western tropical Pacific since the model pycnocline variability at  $7.5^{\circ}\text{N}$ ,  $160^{\circ}\text{E}$ , has a similar time series to that of Truk Island.

In both the 1972 and 1976 cases the maximum positive pycnocline anomalies take place around  $7^{\circ}\text{N}$ . Anomalies in the Southern Hemisphere are smaller for both El Niño events. Also common to both events are smaller positive anomalies found in both hemispheres 3-4 months prior to the main peaks. The latitudes of the smaller anomalies are  $4^{\circ}$  to  $6^{\circ}$  from the equator depending on the event and the hemisphere but always closer to the equator than the maximum anomalies. These earlier periods of shallow pycnocline depth are more symmetric to the equator than the latter ones and represent the initial shallowing of the pycnocline at Truk Island. The maximum positive anomaly at  $7^{\circ}\text{N}$

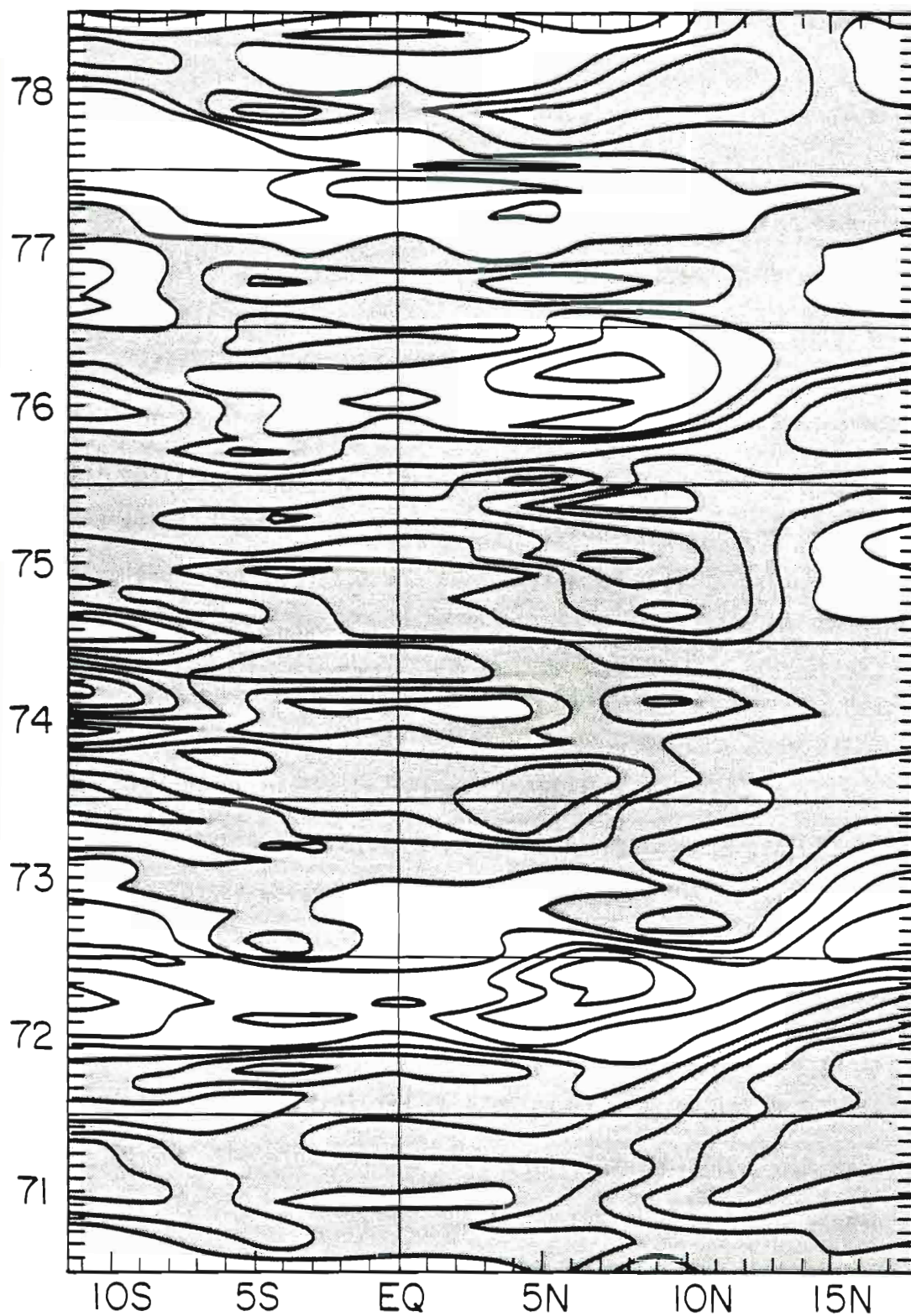


Fig. 13. A Y-T section of the pycnocline height anomaly (PHA) along 160°E for 1971 to 1978. White regions indicate the model pycnocline is shallower than the 18-year mean. Contour interval is 15 m.

Fig. 13. A Y-T section of the pycnocline height anomaly (PHA) along 160°E for 1971 to 1978. White regions indicate the model pycnocline is shallower than the 18-year mean. Contour interval is 15 m.

corresponds to the period when the pycnocline is shallow at Truk near the end of the El Niño year. This pattern of pycnocline depth change is not as evident in the El Niño events of the 1960's. For example, during the 1965 El Niño the maximum positive pycnocline anomalies are more symmetric to the equator. However, it can be stated that the Y-T pattern of the shallow pycnocline anomaly near 7°N late in the year is typical of an El Niño year for the 18-year record studied here.

A matrix of lagged cross correlations between Truk Island and all points along 7.5°N (Fig. 14) shows the pycnocline variability at Truk lagging that to the east. The inclination of maximum positive correlations represents a westward propagation of the pycnocline signal at approximately 40 cm s<sup>-1</sup>. This compares favorably with the 35 cm s<sup>-1</sup> phase speed for third latitudinal mode Rossby waves in this calculation. Projection of the meridional pycnocline structure onto the free modes of the system indicates the dominant response at Truk is due to third-mode Rossby waves. Depending on the event, the variability at Truk may also be influenced by first, second, and fourth-mode Rossby waves.

As discussed in the previous section, relaxation of the easterlies takes place in the central and western Pacific during El Niño. It is suspected that the wind changes that are responsible for high sea level in the eastern equatorial Pacific through the generation of equatorial Kelvin waves may also be responsible for low sea level in the western tropical Pacific through the generation of Rossby waves at the same time. McCreary (1977) showed that the onset of westerlies in the western tropical Pacific through the generation of Rossby waves at the same time. McCreary (1977) showed that the onset of westerlies, which is

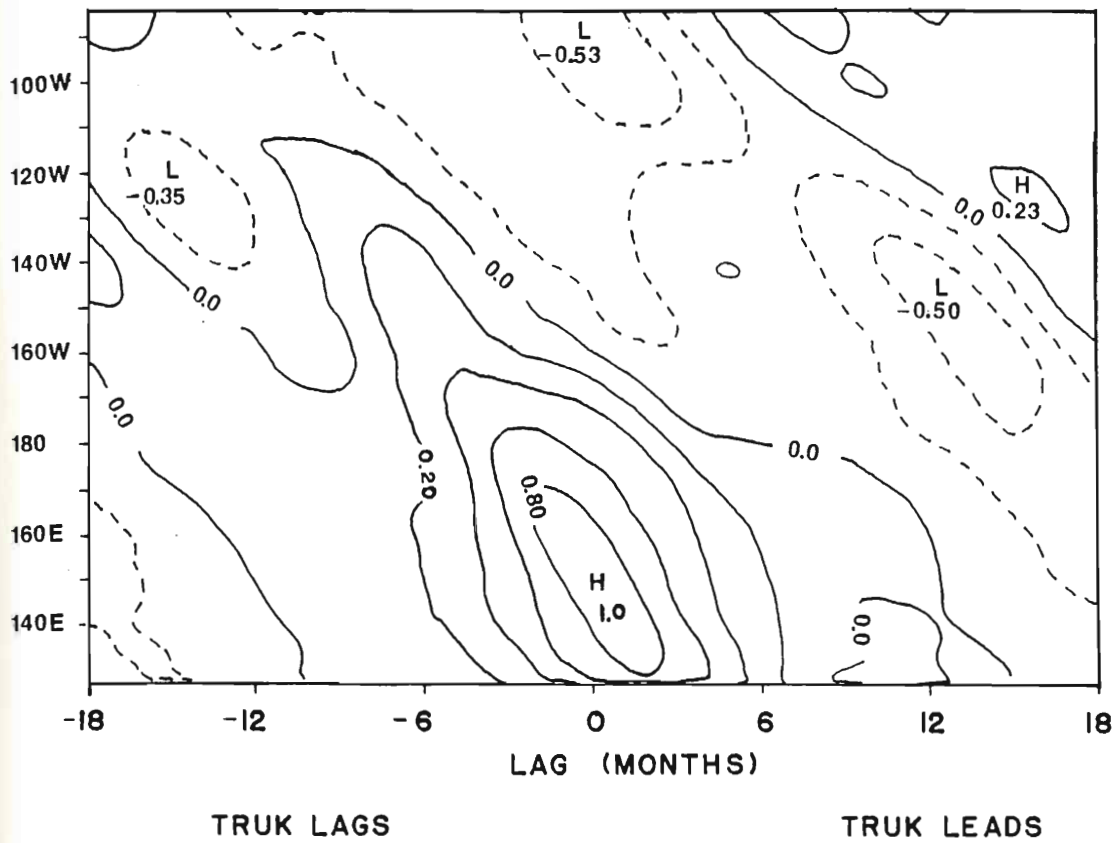


Fig. 14. Contours of lagged cross correlation between the model pycnocline variability at Truk Island and all points east and west along 7.5°N.



equivalent to the relaxation of easterlies in linear theory, generates an eastward-propagating, downwelling, equatorial Kelvin wave front and a westward-propagating, upwelling, Rossby wave front which has minimum pressure on both sides of the equator. Therefore, it seems quite reasonable to attribute the decrease of sea level in the western tropical Pacific to the relaxation of the easterlies. This would also explain the negative correlation and phase lag between the equatorial eastern boundary and western boundary variability (Fig. 7). The maximum cross correlation between the non-seasonal model pycnocline signal at Truk and Galapagos is also negative and occurs when Galapagos leads by a few months. Since the phase speed of the Kelvin wave is several times faster than the Rossby wave, the maximum pycnocline depth in the east may be expected to precede the minimum pycnocline depth in the west during El Niño.

In McCreary's study, the wind stress and the resultant sea level distributions were symmetric to the equator. The observed sea level and the model pycnocline fluctuations presented here, however, are not symmetric to the equator. This tendency for the largest sea level/pycnocline displacements to occur north of the equator suggests that the relaxation of the easterlies may not be symmetric to the equator. To judge if this is true the meridional distribution of the wind stress variability is examined next.

Only the zonal component of the wind stress is considered because it is more important in forcing low frequency motion in the equatorial ocean. This is supported by the test calculation when the model was it is more important in forcing low frequency motion in the equatorial ocean. This is supported by the test calculation when the model was forced only by the zonal wind stress for mid-1973 through 1977. At

Truk the pycnocline response to zonal forcing was very similar to that for the full model calculation forced by both zonal and meridional components. The meridional structure of the zonal wind stress variability is obtained by averaging the annual anomalies of the zonal wind stress between 160°E and 140°W for 1971 to 1978 (Fig. 15). The longitudinal range is chosen to include the major wind stress changes in the El Niño years. The width of each wind event is 30°-40° of longitude. The area west of 160°E is omitted because long Rossby waves generated there have no influence eastward.

The winds are predominantly easterly for the range 160E-140W, so positive values in Fig. 15 indicate weakened easterlies. The seasonal variations are obvious and are basically out of phase between the hemispheres; the weakest easterlies occur in the second half of each year in the Northern Hemisphere and in the earlier half of each year in the Southern Hemisphere. In 1972 and 1976, the weakening of the easterlies in the Northern Hemisphere was larger and the area of weakening (5°N-10°N) was closer to the equator. The easterlies at the equator were also weaker than usual beyond March.

Does such a distribution of decreasing easterlies cause the pressure field distribution found in Fig. 13? The response of the ocean to an idealized wind forcing event is calculated to determine this. An eastward wind stress anomaly which has a Y-T pattern shown in Fig. 16a, constant in the zonal direction between two meridians, and zero outside of it is assumed. The width of the region is taken to be 3300 km, corresponding to about 30° of longitude. This idealized forcing is a

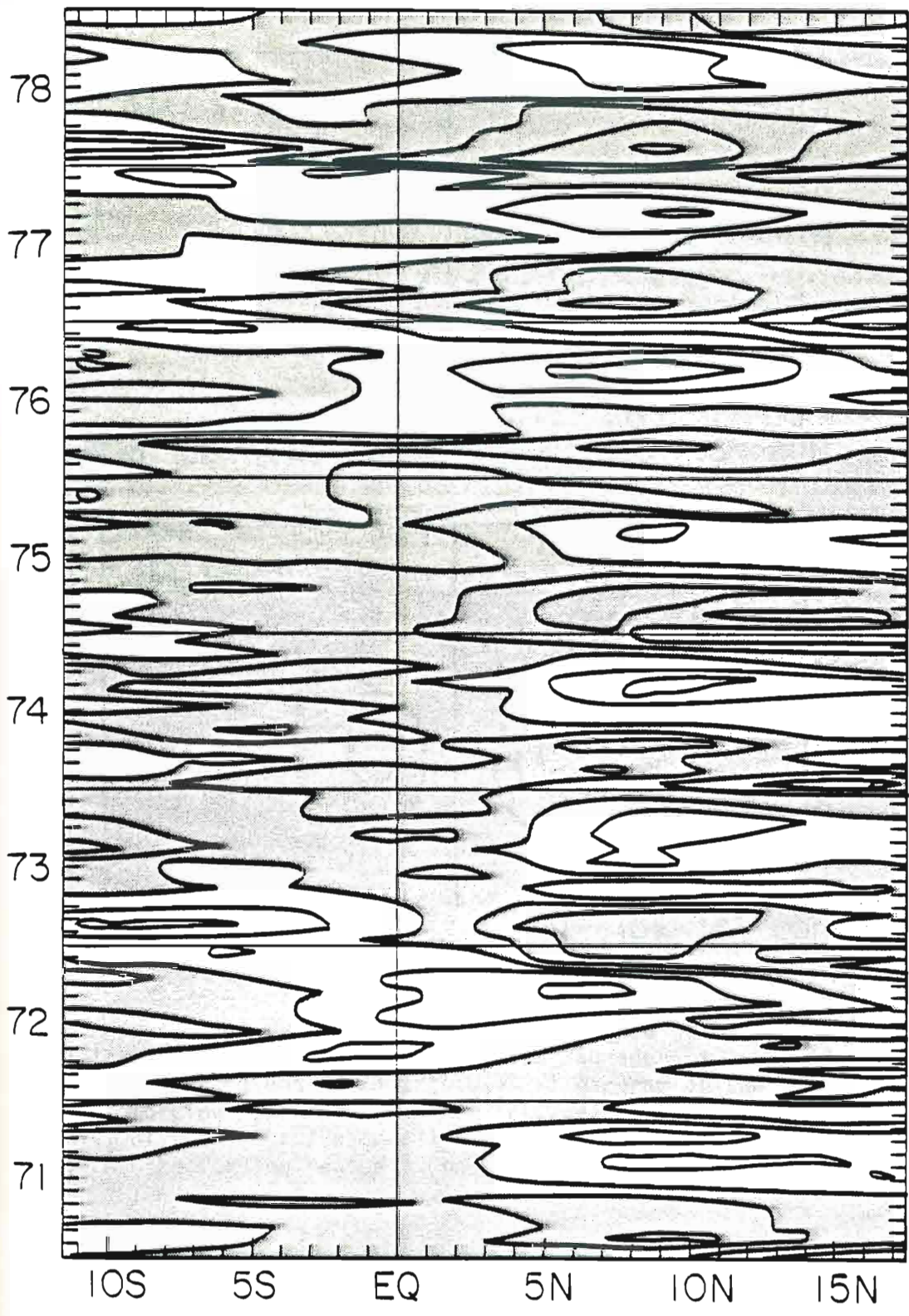


Fig. 15. A Y-T diagram of the zonal wind stress averaged over 160°E-140°W for 1971 to 1978. White regions indicate the easterlies are weaker (westerly anomaly) than the long-term annual mean. Contour interval is .25 dynes cm<sup>-2</sup>.

Fig. 15. A Y-T diagram of the zonal wind stress averaged over 160°E-140°W for 1971 to 1978. White regions indicate the easterlies are weaker (westerly anomaly) than the long-term annual mean. Contour interval is .25 dynes cm<sup>-2</sup>.

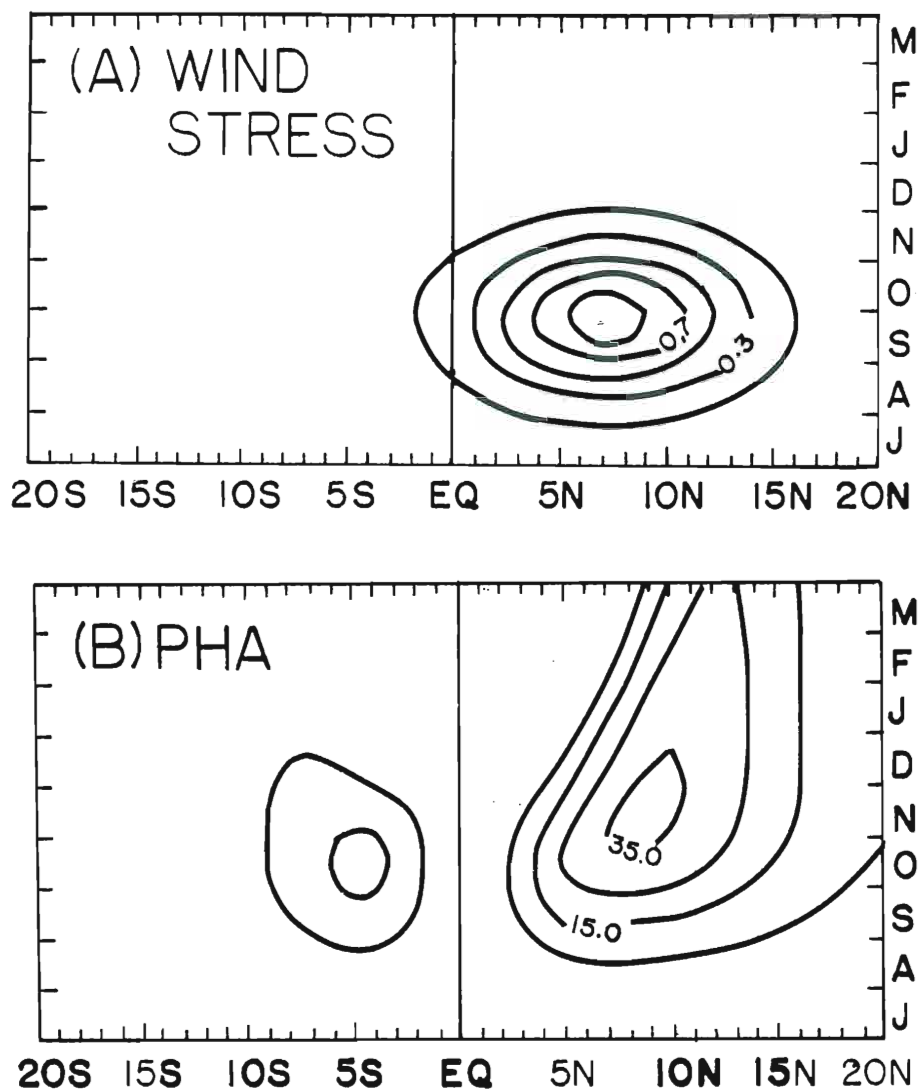


Fig. 16. Idealized model of the response of the tropical ocean to the westerly wind stress anomaly confined within two meridians 30° apart. a) Y-T diagram of the wind stress forcing function. Contour interval is .2 dynes cm<sup>-2</sup>. b) Y-T diagram of the pycnocline response along the western edge of the forcing region. Contour interval is 10 m.

crude approximation of the relaxation and recovery phase of the northeast trades during the 1972 and 1976 Los Niños. Initially the ocean is assumed to be at rest. The geostrophic balance is assumed for the zonal momentum equation. The Y-T distribution of pressure along the meridian at the west end of the forcing region is calculated and shown in Fig. 16b. Forcing functions for equatorial Rossby modes are calculated analytically and integrated numerically along the characteristics of each mode.

The response to the idealized forcing (Fig. 16b) has some similarities with the modelled response of the western tropical Pacific in El Niño years (Fig. 13). The response has a peak in each hemisphere although the wind forcing is mostly in the Northern Hemisphere. The largest response is north of the equator. The minimum pycnocline depth appears around  $7^{\circ}\text{N}$ , about 1.5 months after the wind forcing minimum. This supports the idea which attributes sea level anomalies in the western tropical Pacific in the latter half of the El Niño year to the weakening of easterlies centered north of the equator.

The response of the model ocean is fairly sensitive to the location of the wind forcing. If the center of the forcing shifts northward to around  $10^{\circ}\text{N}$ , similar to the location for the center of normal seasonal weakening, the low-latitude response becomes considerably smaller and the maximum response shifts northward more than the shift of the wind forcing (Fig. 17). In this case the forced motion is more like mid-latitude Rossby waves than equatorial Rossby waves. Also, it may explain why the relaxation of the easterlies found in the

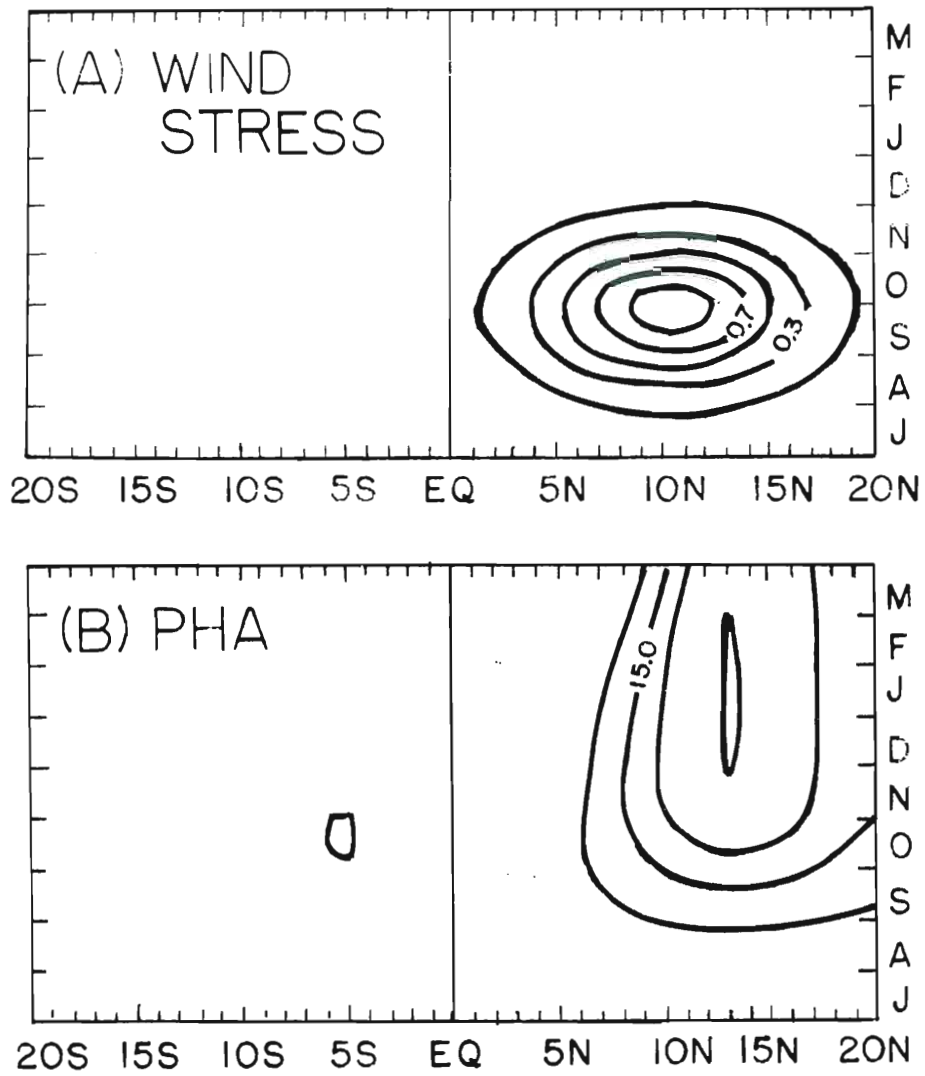


Fig. 17. Same as Fig. 16 except the forcing is shifted northward by  $3^\circ$ .

latter half of most years produces only a small response in the low latitudes of the western tropical Pacific except in El Niño years.

Four or five months prior to the main weakening of the northeast trades, weakened easterlies exist about the equator in both 1972 and 1976 (Fig. 15). Since the wind anomalies are maximum near the equator, the response of the ocean should be symmetric to the equator. Late in the El Niño year the relaxation of the northeast trades is followed by strong westward anomalies. The switch from eastward to westward anomalies takes place very rapidly. This rapid recovery of the easterlies, along with the earlier eastward anomalies near the equator, might provide a more complete description of the typical sea level change at Truk Island during an El Niño event, i.e., a two-step drop in sea level during the El Niño year with lowest sea level occurring at the end of the year followed by a rapid rising.

Another idealized forcing calculation is performed in which there are minimum easterlies at the equator in April, minimum northeast trades in September, followed by a rapid strengthening yielding anomalously strong northeast trades in the following January and February (Fig. 18a). The resulting pycnocline response (Fig. 18b) is initially symmetric about the equator with minimum pycnocline depths at  $\pm 5^\circ$  in May-June. The remainder of the response is not symmetric to the equator whereby the pycnocline depth minimum is located at  $9^\circ\text{N}$  in November. This compares favorably with the shallow pycnocline depths of the 1972 and 1976 events depicted in Fig. 13. The pycnocline response (Fig. 18b) at  $7.5^\circ\text{N}$  is also similar to that at Truk Island

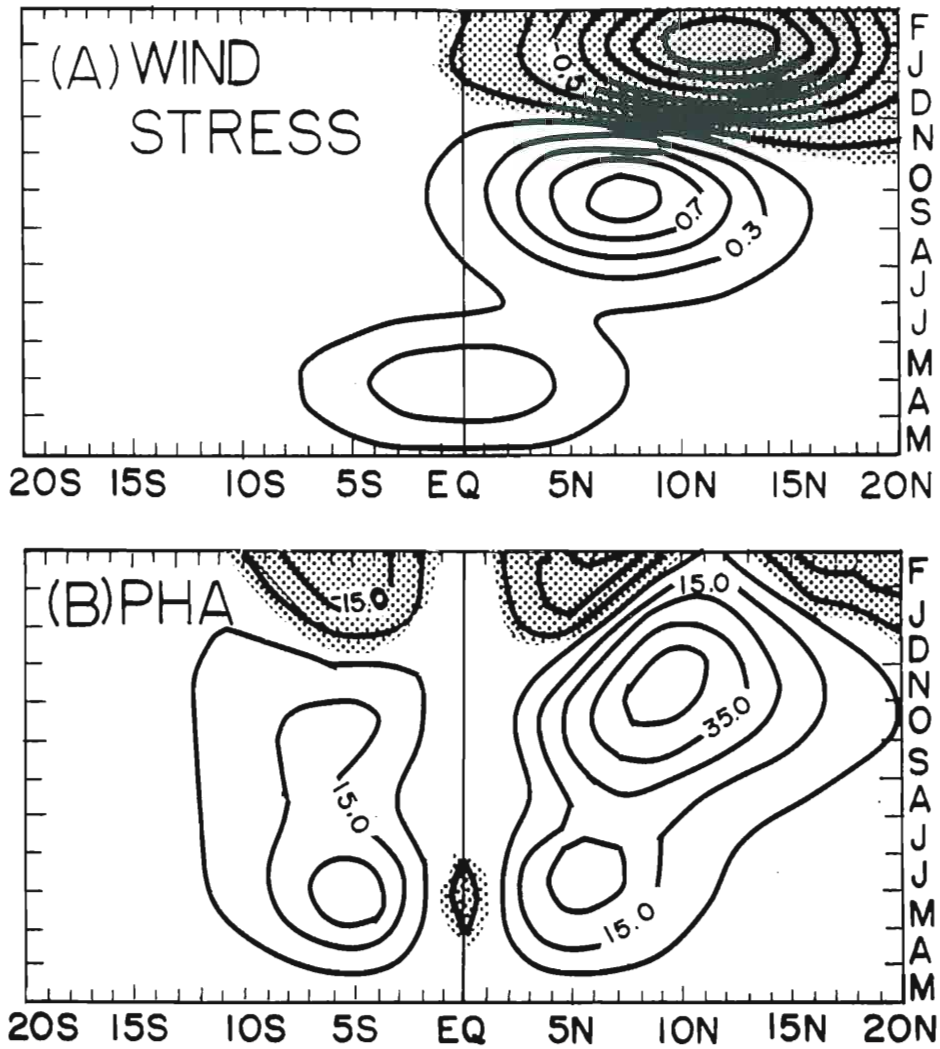


Fig. 18. Similar to Figure 16 but the forcing function is now preceded by an equatorial relaxation sequence and followed by an intensification of the trades (stipled) late in the year.



during an El Niño year (Fig. 11). There is an initial shoaling of the pycnocline from March to May, followed by a few months during which there is a slight increase in pycnocline depth, further rising of the pycnocline until October-November, and a final rapid increase in pycnocline depth.

#### D. Central Equatorial Response

The two previous sections have demonstrated that for 1961-1978 the variability in the eastern tropical Pacific may be influenced by equatorially trapped Kelvin waves and the western tropical Pacific may be influenced by westward-propagating Rossby waves. In the central equatorial Pacific there are not many long-term observations. The sea level data at Canton and Christmas Islands are among the few available. The location of these two islands are important for two reasons. First, longitudinally they are in a region where there are major wind stress changes to the east and west. The sea levels at these islands may therefore be affected by both Kelvin waves generated west of the islands and Rossby waves generated east of the islands. Second, latitudinally these islands are situated where both Kelvin waves and first-mode Rossby waves have relatively high amplitudes in the pressure field.

Unfortunately, the time series from these two islands are not continuous and do not cover the entire 18 years of interest. Furthermore, data are missing during several El Niño events. Nonetheless, the most significant features are high sea levels at both islands during more, data are missing during several El Niño events. Nonetheless, the most significant features are high sea levels at both islands during the second half of an El Niño year. Smaller high sea level peaks are

often found at the beginning of an El Niño year . A lagged cross correlation with the model pycnocline time series is impossible because of the data gaps in the sea level record. A zero lag cross correlation can be performed if the sea level observations are concatenated and then correlated with the corresponding points in time for the model pycnocline record. The zero lag cross correlations are 0.40 at Canton and 0.67 at Christmas Island. Instead of comparing the observed sea level and model pycnocline variations, it is of interest to know the relationship of these variations at Christmas and Canton to those in the eastern and western Pacific discussed in the previous sections. This may aid future analyses of sea level records when complete time series become available.

For the baroclinic phase speed chosen in this study the equatorial radius of deformation is  $2^{\circ}57'$  (327 km). At the latitudes of Christmas,  $1^{\circ}59'N$ , and Canton,  $2^{\circ}48'S$ , sea level variations due to an equatorial Kelvin wave are 80% and 64% of that at the equator, respectively. At low frequencies, the first-mode equatorial Rossby wave has its maximum height field amplitude at  $\pm 3^{\circ}36'$  from the equator. The amplitude of Rossby wave sea level variations at Christmas and Canton are 80% and 95% of the maximum, respectively. Therefore, it is suggested that the sea level at these islands is strongly influenced by both Kelvin and first-mode Rossby waves. It is impossible to separate Kelvin and Rossby signals from the observed sea levels at these islands. Fortunately, the model pycnocline variability is similar at times with the observed sea level. It is possible to get some hint of the

Fortunately, the model pycnocline variability is similar at times with the observed sea level. It is possible to get some hint of the

contributions of Kelvin and Rossby waves to the sea level variations by projecting the model pycnocline structure onto the Kelvin and Rossby wave components.

In Fig. 19 and 20, Kelvin and first-mode Rossby wave components of the model pycnocline are plotted for the 1965 El Niño event at Canton and Christmas. Most of the variations of the model pycnocline at both islands are attributed to Kelvin waves and first-mode Rossby waves. The pycnocline variability at Christmas Island contains a slightly larger Kelvin wave signal than at Canton. Since Christmas Island is located closer to the equator than Canton, if the amplitudes of the Kelvin waves at the longitudes of these islands are the same, Christmas Island would experience a stronger Kelvin wave signal than would Canton. In addition, the longitudinal location of these islands can also lead to stronger Kelvin signals at Christmas since the Kelvin waves generated between the longitudes of Canton and Christmas only reach Christmas Island, which is further east. By similar reasoning, Canton Island is likely to receive larger Rossby signals than Christmas if the Rossby waves generated between the islands add constructively.

For the 1965 El Niño, the downwelling peak at the beginning of the year at both islands is primarily due to the Kelvin wave component. The shallow pycnocline in March-April is greatly influenced by the upwelling Rossby wave front discussed in the previous section. Another deep pycnocline episode occurs in the second half of the year. However, in this latter downwelling event, the first-mode Rossby wave component shares the role of depressing the pycnocline. At Christmas Island, the

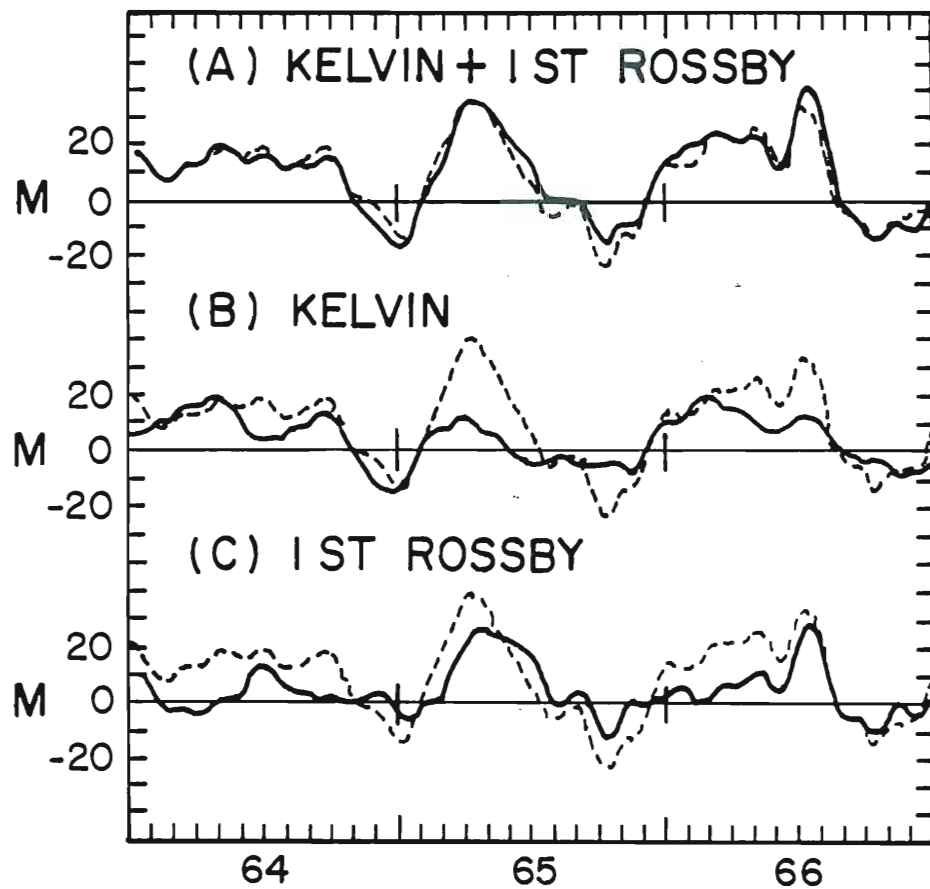


Fig. 19. Kelvin and first-mode equatorial Rossby wave components (solid) of the model pycnocline signal (dashed) at Canton Island for 1964 to 1966. a) Kelvin plus first-mode Rossby wave compared with the pycnocline signal. b) Kelvin wave compared with the pycnocline signal. c) First-mode Rossby wave compared with the pycnocline signal.

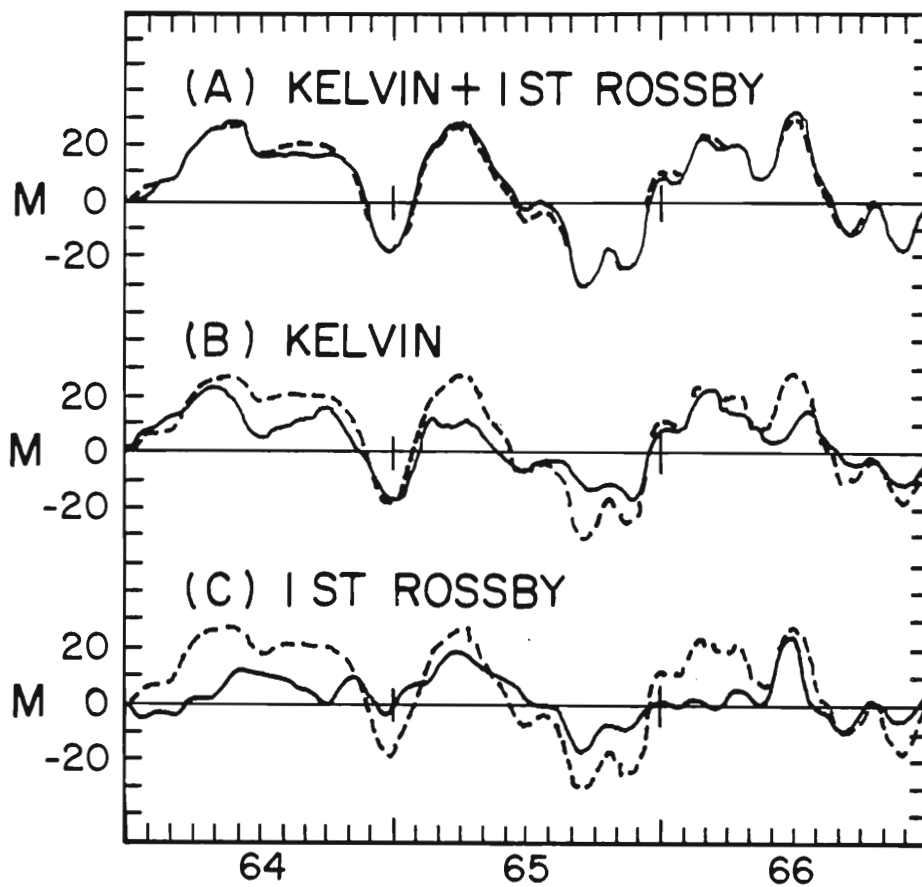


Fig. 20. Same as Fig. 19 except at Christmas Island.

downwelling peaks of the Kelvin wave component and first-mode Rossby wave component have a slight time lag and result in a double peak in the pycnocline variability. This feature is also present in the observed sea level record.

The temporal variation of the Kelvin wave component at these two islands is similar at a slight time lag. The variability at Galapagos Island is also similar at a lag of about 1.5 months. The downwelling peak of the Kelvin wave component at the beginning of the year does not change much in amplitude as it passes Canton, Christmas, and Galapagos. The peak later in the year grows in amplitude as it passes Canton, Christmas, and Galapagos. This suggests the forcing region of the Kelvin wave front responsible for the deep pycnocline in the beginning of the year is west of the forcing region for the Kelvin wave front excited later in the year. This is common among several El Niño events in this 18-year period and consistent with the previous identification of the forcing regions.

The 1972 El Niño (Fig. 21) provides another interesting example of the relationship between the effects of the Kelvin waves and the Rossby waves. In this event the Kelvin wave component exhibits two downwelling peaks: at the beginning and middle of the year. The initial downwelling Kelvin wave signal of 1972, which emanates in the west, has little influence on the pycnocline depth at Galapagos because of intensified easterlies in the central Pacific. This intensification, from mid-October until the end of 1971, is responsible for a downwelling Rossby wave response at Canton at the beginning of 1972. The from mid-October until the end of 1971, is responsible for a downwelling Rossby wave response at Canton at the beginning of 1972. The

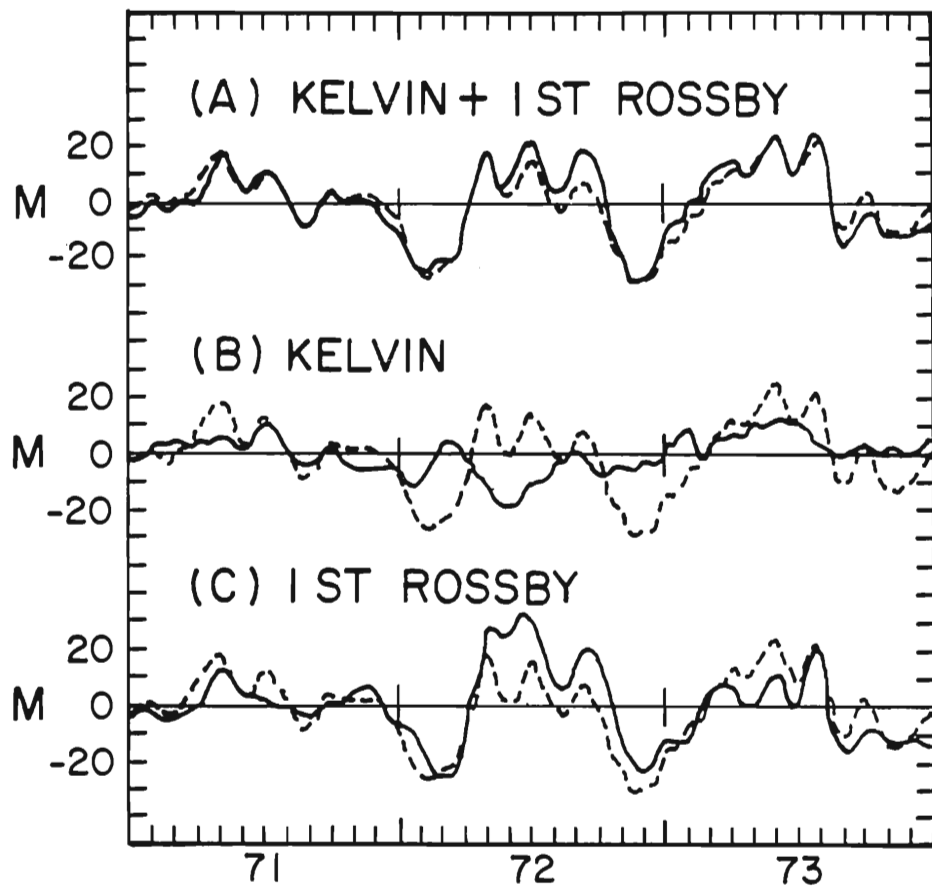


Fig. 21. Same as Fig. 19 except from 1971-1973.

Kelvin wave peak later in the year is not found in the total pycnocline signal at Canton because the Kelvin wave component is canceled out by an upwelling first-mode Rossby wave contribution excited to the east. At Galapagos, this second Kelvin wave signal is no longer affected by a Rossby wave and thereby contributes to a deep pycnocline in June. The large downwelling at the end of 1972 is mainly a Rossby wave response.

It appears there may be great difficulty in interpreting the sea level data at Canton and Christmas Islands due to the interplay between Kelvin waves and Rossby waves from one event to the next. This is also evident if the 18-year pycnocline records for all points along a longitude representative of Canton or Christmas Island are correlated with the model pycnocline variability at Galapagos. At  $2^{\circ}$ - $3^{\circ}$  from the equator the influence of the Kelvin waves have been reduced enough that the resulting maximum positive correlation when the central Pacific leads Galapagos is comparable to the maximum negative correlation due to Rossby waves when the central Pacific variability lags Galapagos. At times the sea level data of these islands can be used to discuss the passage of Kelvin waves. However, the present study suggests a strong influence of the first-mode equatorial Rossby waves at these islands. In order to fully understand the processes responsible for the observed sea level variability at these islands, it is necessary to know the sea level and wind stress variability to the east and west or the meridional structure of the sea level variability.

This study of the variability of the tropical Pacific from 1961-1978 has shown that a combination of simple dynamics, realistic

This study of the variability of the tropical Pacific from 1961-1978 has shown that a combination of simple dynamics, realistic coastline geometry, and a detailed description of the wind field can be



used to interpret the interannual, wind-driven, oceanic response. Kelvin waves excited by zonal wind stress changes in the central and western equatorial Pacific are responsible for depressing the pycnocline at the eastern boundary during El Niño. Associated wind stress fluctuations generate upwelling Rossby waves which affect the western tropical Pacific during El Niño. In the central equatorial Pacific both types of waves combine to determine the variability.

### III. SEASONAL VARIABILITY FROM A MODEL OF THE TROPICAL ATLANTIC OCEAN

In the upper tropical Atlantic Ocean the seasonal variations of heat content are approximately ten times larger than the seasonal variations of the heat gain from the atmosphere through the surface (Merle, 1980a). This annual cycle of the heat content is caused mainly by the horizontal redistribution of heat associated with wind induced changes in the topography of the thermocline. Therefore, understanding the dynamic response of the upper tropical Atlantic to the seasonal surface winds is fundamental, and this would be the first step toward the development of sophisticated, thermodynamic and coupled tropical ocean-atmosphere models.

The Atlantic Ocean is a prime region to study the seasonal response of a tropical ocean because of the strong seasonal cycle present. Merle et al. (1980) determined that the annual sea surface temperature (SST) signal in the Gulf of Guinea was several times greater than the interannual variability. Katz et al. (1977) and Lass et al. (1982) have shown that the zonal pressure gradient in the western and central equatorial Atlantic varies almost in phase with the seasonally varying winds. These findings are in contrast to the tropical Pacific where interannual fluctuations often associated with El Niño dominate (Wyrski, 1975; Hickey, 1975). Studying the seasonal variability may also help in understanding nonseasonal events since interannual changes are frequently perturbations to the seasonal cycle. variability may also help in understanding nonseasonal events since interannual changes are frequently perturbations to the seasonal cycle.

The Gulf of Guinea is characterized by a shallow thermocline due to the eastward shoaling of the thermal structure at low latitudes. Thus, this is the region of the tropical Atlantic where the seasonal variability of SST has the largest amplitude ( $5^{\circ}$ - $7^{\circ}\text{C}$  compared to  $1^{\circ}$ - $2^{\circ}\text{C}$  further west). Anomalous SST variability in this area has been linked with extreme climatic events such as droughts and excessive rainfall along the coast of the Gulf of Guinea, in Sub-Sahara Africa, and possibly in northeastern Brazil (Hastenrath, 1976; Markham and McLain, 1977; Lamb, 1978; Bakun, 1978). The presence of abnormal SST in the tropical Atlantic may also have an important effect on cyclogenesis (Namias, 1969). Moreover, this surface and associated subsurface variability appear to have a significant effect on the coastal and pelagic fisheries (Hisard and Piton, 1981).

The seasonal equatorial and coastal upwelling that produce cold water outbreaks in this region have never been convincingly explained by forcing due to the local winds or local currents (Houghton, 1976; Berrit, 1976; Bakun, 1978; Voituriez, 1981a,b). Moore et al. (1978) suggested that a strong upwelling signal, generated by a significant increase of the easterlies in the western Atlantic, can be transmitted to the eastern Atlantic as an equatorially trapped Kelvin wave. When this disturbance reaches the African coast part of the energy splits poleward as coastal Kelvin waves and the remainder is reflected westward as equatorial Rossby waves. Following this idea, Servain et al. (1982) found that the nonseasonal variability of SST in the Gulf of Guinea is highly correlated with the nonseasonal variability of the al. (1982) found that the nonseasonal variability of SST in the Gulf of Guinea is highly correlated with the nonseasonal variability of the zonal wind stress in the western equatorial Atlantic. The correlation

between the local wind stress anomaly and SST anomaly in the Gulf of Guinea was also considerably smaller. In a study of the seasonal SST signal, Picaut (1982) found poleward propagation of the mean seasonal coastal upwelling. Thus, there is a need to understand the relation between the equatorial wind forcing and this upwelling in the Gulf of Guinea. For a more detailed review of this Gulf-of-Guinea problem see Picaut (1982).

Other prominent features of the subsurface thermal structure in the eastern tropical Atlantic are the shallow thermocline regions of the Guinea and Angola Domes (Mazeika, 1967; Voituriez, 1981c). Although observations and modelling studies have been used to provide an understanding of the Costa Rica Dome in the eastern tropical Pacific Ocean (Wyrtki, 1964; Hofmann et al., 1981), little is known about the counterparts in the tropical Atlantic.

The northwestern part of the equatorial Atlantic is characterized by a north-south tilting of the thermocline near the mean position of the Inter-Tropical Convergence Zone (ITCZ) (Merle, 1982). This pivot line is situated where equatorial waves and Ekman pumping may play an important role in determining the variability. Due to the location, the presence of this feature may influence the variability of the North Equatorial Current and Countercurrent. Hence, an explanation is desired for such an important oscillation.

Modelling efforts would substantially increase our applied knowledge of the tropical Atlantic Ocean. This region is also interesting from a purely theoretical point of view. For example, the knowledge of the tropical Atlantic Ocean. This region is also interesting from a purely theoretical point of view. For example, the presence of a zonal coast north of the equator in the Gulf of Guinea

might induce a combination of Kelvin and Rossby wave modes which could not exist in the other oceans (Hickie, 1977; Philander, 1977). In addition, there is a considerable difference in the adjustment time of equatorial regions and mid-latitudes. According to theory, the oceanic adjustment time scale for a change in wind conditions is on the order of one year or less in the equatorial oceans and can be greater than a decade at mid-latitudes (Philander, 1979). Modelling the seasonal cycle of the equatorial Atlantic in relation to one entire year of intensive measurements, e.g., the SEQUAL (Seasonal Equatorial Atlantic) and FOCAL (Francais-Ocean-Climate-Atlantique-Equatorial) experiments would be invaluable in the study of this process.

Within the last five years some progress has been made in modelling the equatorial Atlantic Ocean. O'Brien et al. (1978) and Adamec and O'Brien (1978) demonstrated the remote forcing mechanism of Moore et al. (1978) with a linear, 1 1/2-layer model, in which the wind in the western part of the basin was switched on impulsively. Cane and Sarachik (1981) examined the linear, inviscid, response of a meridionally infinite but zonally bounded equatorial basin to periodic zonal forcings, with some implications for the Atlantic Ocean. Philander and Pacanowski (1981a, b), with a three-dimensional, nonlinear model, studied the response to various x-independent and y-independent periodic wind forcings in a rectangular basin comparable to the width of the equatorial Atlantic. In all of these studies the wind forcing and the coastline geometry had limited resemblance to those of the tropical Atlantic.

McCreary et al. (1982) detailed the effect of remote forcing and vertical propagation of energy in the eastern tropical Atlantic with a three-dimensional, linear model forced by an annual periodic wind. Despite the fact that the coastal geometry was an approximation of the Brazilian and African coasts and the wind stress forcing was a simple representation of the annual zonal wind stress west of  $20^{\circ}\text{W}$ , this model succeeded in simulating several important features of the vertical structure in the Gulf of Guinea, e.g. the annual variation of the equatorial and coastal undercurrents and the upward phase propagation of the upwelling signal. Another three-dimensional numerical calculation has been performed by Anderson (1979) with realistic mean seasonal winds and coastlines. The variability of the resultant current fields were compared with the few observations available. The discussion of upwelling features was limited by constraints imposed by the surface boundary condition. Patton (1981) used a single baroclinic model to study the seasonal cycle in the Gulf of Guinea. The model was forced by an analytical approximation of the real wind field. The influence of the winds in the eastern and western halves of the basin was examined. A subsequent extension of this calculation with the Atlantic wind data of Hellerman (1980) simulated rather well the mean seasonal sea level variation in the Gulf of Guinea (M. Cane personal communication, 1982). Both these studies represent the Brazil coast by a north-south boundary at  $50^{\circ}\text{W}$ .

In the present work a more detailed calculation is used to simulate more realistically the seasonal cycle in the tropical Atlantic.

Three-dimensional models have been suggested for this but they give

results that are very difficult to interpret and are often sensitive to the value of the eddy coefficients used. Furthermore, despite the measurements in the tropical Atlantic, little is known about the three-dimensional variability of this ocean. However, the historical measurements are numerous enough to provide a good indication of the seasonal variability of SST (Hastenrath and Lamb, 1977) and dynamic height for an average year (Merle and Arnault, 1982). The historical seasonal wind stress is also reasonably well known (Hastenrath and Lamb, 1977; Hellerman, 1980). As demonstrated by Schopf and Harrison (1982), perturbations to the dynamic height field respond in a linear manner to the gravest vertical modes of the system. Therefore, a single-mode linear model of the tropical Atlantic, with realistic coastline geometry, forced by the mean seasonal wind stress, is amenable to comparison with the mean surface dynamic height field available. The success of a similar calculation for the tropical Pacific Ocean (Busalacchi and O'Brien, 1980) indicates such a study may provide useful information pertaining to the seasonal Atlantic Ocean response.

A description of the tropical Atlantic model is presented next. This is followed by a discussion of the climatological wind stress data which is used to form a periodic forcing function for the model. The basin-wide response to the seasonal forcing is then compared with the available dynamic height data. The important seasonal responses in the western tropical, equatorial, and eastern tropical Atlantic are subsequently analyzed in more detail.

subsequently analyzed in more detail.

### A. The Numerical Model

A linear, single baroclinic mode, numerical model on an equatorial  $\beta$ -plane will be used to study the oceanic response to an applied wind stress forcing. A similar approach was used by Busalacchi and O'Brien (1980) to study the wind-driven seasonal variability of the tropical Pacific Ocean. The linear governing equations for the horizontal dependency of a single baroclinic mode on an equatorial  $\beta$ -plane are as follows:

$$\frac{\partial \vec{V}}{\partial t} = -\beta y \hat{k} \times \vec{V} - c^2 \nabla h + \frac{\vec{\tau}}{\rho} + A \nabla^2 \vec{V} \quad (1a)$$

$$\frac{\partial h}{\partial t} = -\nabla \cdot \vec{V} \quad (1b)$$

$$\vec{V} = U \hat{i} + V \hat{j} \quad (1c)$$

$$U = uH, \quad V = vH, \quad (1d)$$

where  $U$ ,  $V$  are the respective  $x$ ,  $y$  components of the horizontal transport,  $c$  is the baroclinic phase speed taken to be  $1.37 \text{ m s}^{-1}$ , and the wind stress  $\tau$  is included as a body force. The pycnocline depth anomaly is denoted by  $h$ . The initial depth of the pycnocline is  $H$ . When computing current velocities a mean depth of 75 m is used. The diffusive terms are included to bring the horizontal flow to zero along closed boundaries. Bottom topography, thermohaline, and thermodynamic effects have been neglected in the present model. These model equations are the same as those used in the Pacific Ocean study but with a different value for  $c$ .

different value for  $c$ .



Philander and Pacanowski (1980) pointed out that the presence of a shallow tropical thermocline in a continuously stratified ocean will result in the largest projection of the surface wind stress onto the second baroclinic mode. McCreary et al. (1982) found that the second baroclinic mode provided the dominant sea level response in a linear, three-dimensional model of remote forcing in the Gulf of Guinea. The vertical structure for their model was based on many observed density profiles at the equator. The mean equatorial density profile implied a  $1.34 \text{ m s}^{-1}$  (18.3 cm equivalent depth) phase speed for the second baroclinic mode. An equivalent depth of 20 cm was suggested by Moore and Philander (1977) as being typical of the second baroclinic mode in the equatorial Atlantic. The phase speed chosen for the single baroclinic mode of the model presented here corresponds to a 19 cm equivalent depth. Parameter tests indicate the qualitative character of the modelled oceanic response is relatively insensitive to changes in the phase speed of  $\pm 0.35 \text{ m s}^{-1}$ .

The model basin extends from  $20^{\circ}\text{N}$  to  $20^{\circ}\text{S}$  and  $61^{\circ}\text{W}$  to  $12^{\circ}\text{E}$ . It is important that the model basin approximate the coastline geometry of the Atlantic Ocean since the wind stress forcing is derived from wind observations over the Atlantic. No regions of the wind field will be ignored nor will the ocean wind field be extended over the continents as in studies with rectangular-type geometries. Boundary effects present in the wind field will also influence the ocean in a corresponding location. The coastline idealization chosen is shown in Fig. 22. Meridional boundaries are taken to be solid walls. An open boundary condition (Camerlengo and O'Brien, 1980) is applied at the

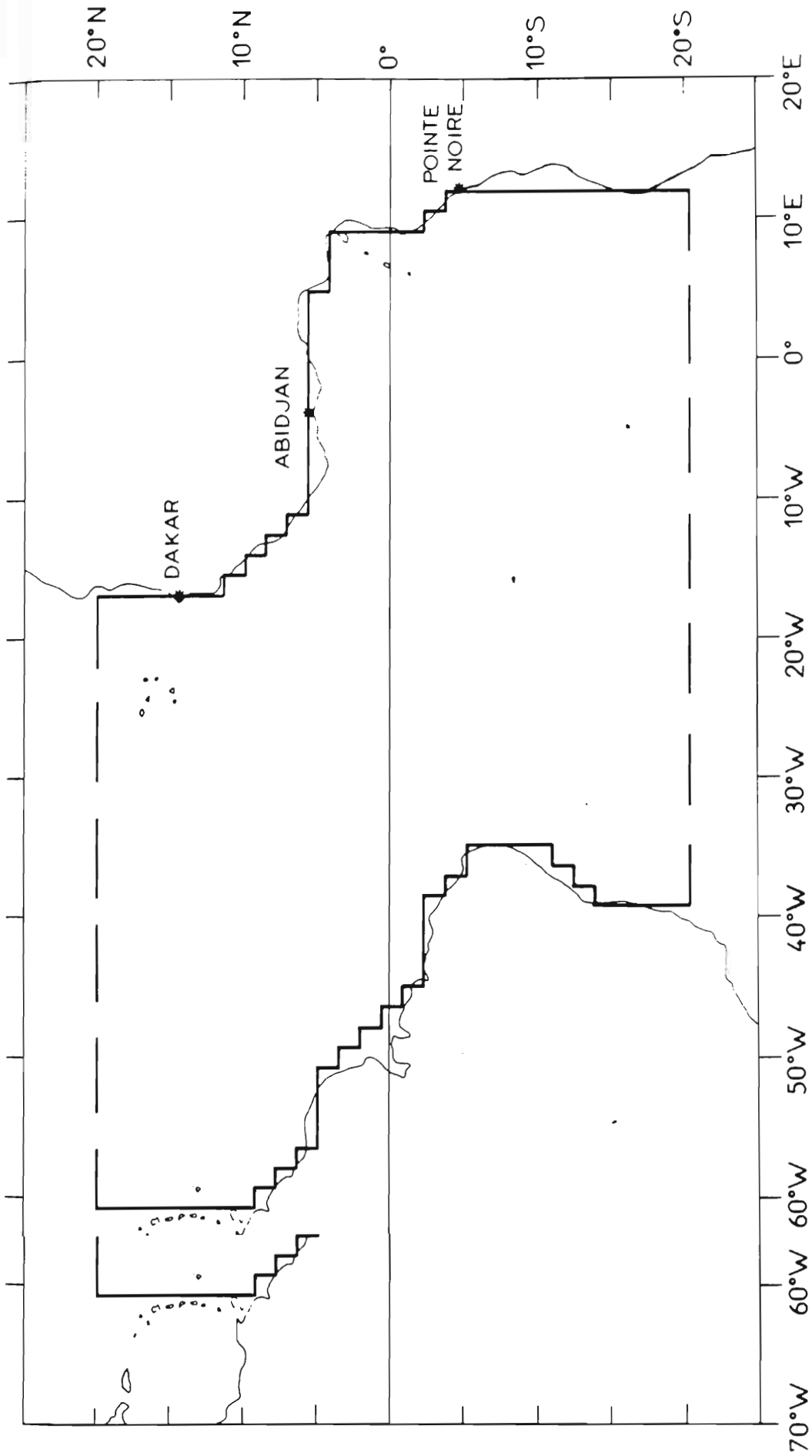


Fig. 22. Comparison of the model geometry with the tropical Atlantic Ocean. The dashed line represents an open boundary; all remaining boundaries are solid walls.

northern and southern boundaries permitting the passage of coastal Kelvin waves, thus preventing contamination of the interior solution.

A staggered grid with 40 km spacing in both x and y is employed to reduce computer storage. A 2 hour time step is incorporated for the integration of the model equations over five years. This provides sufficient time for the initial transients to die out and for a seasonal signal to develop. All the results to be presented are from the fifth year of integration. Hereafter, all references to pycnocline variability pertain to the model results.

#### B. The Wind Field

The seasonal forcing for this study is based on monthly mean ship-board estimates of the surface wind field compiled by Hastenrath and Lamb (1977) for a climatological atlas of the tropical Atlantic. The observations for each calendar month were averaged in time from 1911 to 1970 and averaged in space within a  $1^\circ$  square. Conspicuously incorrect observations were deleted. The area of interest,  $20^\circ\text{N}$ - $20^\circ\text{S}$ , is covered by a substantial number of ship tracks. Despite the high density of observations ( $\sim 2$  million) there are still a few  $1^\circ$  squares with little or no data for a particular month. Regions with the lowest number of observations are along the southern limit of the model basin.

Each monthly mean wind estimate was converted to wind stress using the relation  $\vec{\tau} = \rho_a C_D |\vec{W}| \vec{W}$ , where  $\vec{\tau}$  is the wind stress,  $\rho_a$  the air density,  $C_D$  the drag coefficient and  $\vec{W}$  the wind velocity. When converting the monthly mean wind data to stress, Hastenrath and Lamb (1977) used a rather large value of  $C_D = 2.8 \times 10^{-3}$  to compensate for underestimating the square of the resultant wind speed. Bunker (1976)

created an alternate wind stress product in which each individual wind observation was converted to stress using a drag coefficient that was dependent on wind speed and atmospheric stability. Hellerman (1980) interpolated this irregularly spaced, coarse resolution data onto a  $1^\circ$  mesh. Comparison between the Hastenrath and Lamb monthly stress fields and those of Hellerman indicates that both analyses are similar if the drag coefficient used by Hastenrath and Lamb is reduced to  $2.0 \times 10^{-3}$  (Picaut, 1982).

For this study, as in Busalacchi and O'Brien (1980), the air density was assumed to be constant at  $1.2 \text{ kg m}^{-3}$  and a constant drag coefficient of  $1.5 \times 10^{-3}$  was chosen. The precise value of  $C_D$  is not critically important in this linear calculation since we will not focus on the absolute magnitudes of the oceanic response. The phase and relative amplitude of the response between one part of the basin and another is more important. If a different constant drag coefficient is chosen the model results would change in proportion with  $C_D$ .

The 12 monthly means at each point were decomposed into the first five Fourier harmonics in time, 12 month, 6 month, 4 month, 3 month, 2.4 month, to provide a continuous time series for the model integration. This resulted in a smoother profile of the seasonal cycle than would linear interpolating from month to month. The possibility of high frequency noise being generated in the model by rapid wind stress changes at mid-month has thus been reduced. The implementation of this harmonic forcing also allows the total ocean response at any point to be analyzed and described in terms of five harmonics of this harmonic forcing also allows the total ocean response at any point to be analyzed and described in terms of five harmonics.

Fourier decomposition of the wind stress data also helped in editing the monthly means. The wind stress amplitude fields for the five harmonics were used to locate  $1^\circ$  squares with anomalous data. The higher harmonics were very good indicators of noisy data. The monthly mean time series for each  $1^\circ$  square in question were adjusted to provide continuity in time and space. All the points needing correction were in regions where a few of the monthly means were determined by only a small number of observations. Less than 0.5% of the monthly means were corrected following this procedure. Next, the zonal and meridional wind stress monthly means were interpolated from the  $1^\circ$  grid to the finer model grid. A two-dimensional Hanning filter was used to suppress small spatial scale variability in each monthly stress field. These adjusted monthly means were once again Fourier decomposed into their final form to be used as input for the model calculation.

Representation of the climatological seasonal cycle by five harmonics provides a reasonable fit with climatological daily mean data (Picaut, 1982). This is primarily due to the large influence of the lower harmonics. Spectral analysis and Fourier decomposition of wind time series of up to 15 years at 10 coastal stations in the Gulf of Guinea and at St. Helena Island ( $16^\circ\text{S}$ ,  $6^\circ\text{W}$ ) indicate that the annual and semiannual harmonics dominate the seasonal cycle with some contribution from the third harmonic (Picaut et al., 1978). This is confirmed for the entire tropical Atlantic by the Fourier decomposition of the wind stress data in this study. Basin-wide, the largest harmonic amplitudes are for the annual and semiannual signals.

The spatial distribution of the annual mean, annual harmonic amplitudes, and semiannual harmonic amplitudes for the zonal and meridional wind stress are depicted in Fig. 23. The mean stress field is characterized by the northeast and southeast trade wind systems associated with the Azores and St. Helena anticyclones. The trade systems flow toward South America and converge north of the equator to form the ITCZ. West of the Gulf of Guinea the mean zonal wind stress (Fig. 23a) is easterly and maximum near the Brazil Coast. Since the ITCZ is located north of the equator the low-latitude meridional wind field (Fig. 23b) is predominantly southerly. In the Gulf of Guinea there is an eastward veering of the southerly wind towards the low pressure of the Sahara. This forms the basis for the West African monsoon.

Annual variations in both stress fields (Fig. 23) are most pronounced in the western tropical Atlantic. The core regions of the northeast trades are strongest from January to March and the southeast trades are strongest from July to September. This is also reflected in the seasonal excursion of the ITCZ which is near the equator in March and reaches its northernmost extent in August. The semiannual variability of the trades, particularly in the west, is much smaller than the annual. Strong semiannual wind variability has been detected in the Caribbean Sea by Hellerman (1980) and Cochrane (personal communication, 1981) but this is northwest of our area of interest. The effect of semiannual forcing must not be dismissed. Studies of sea level (Verstraete et al., 1980) and subsurface thermal structure (Merle and LeFloch, 1978) in the Gulf of Guinea indicate the semiannual

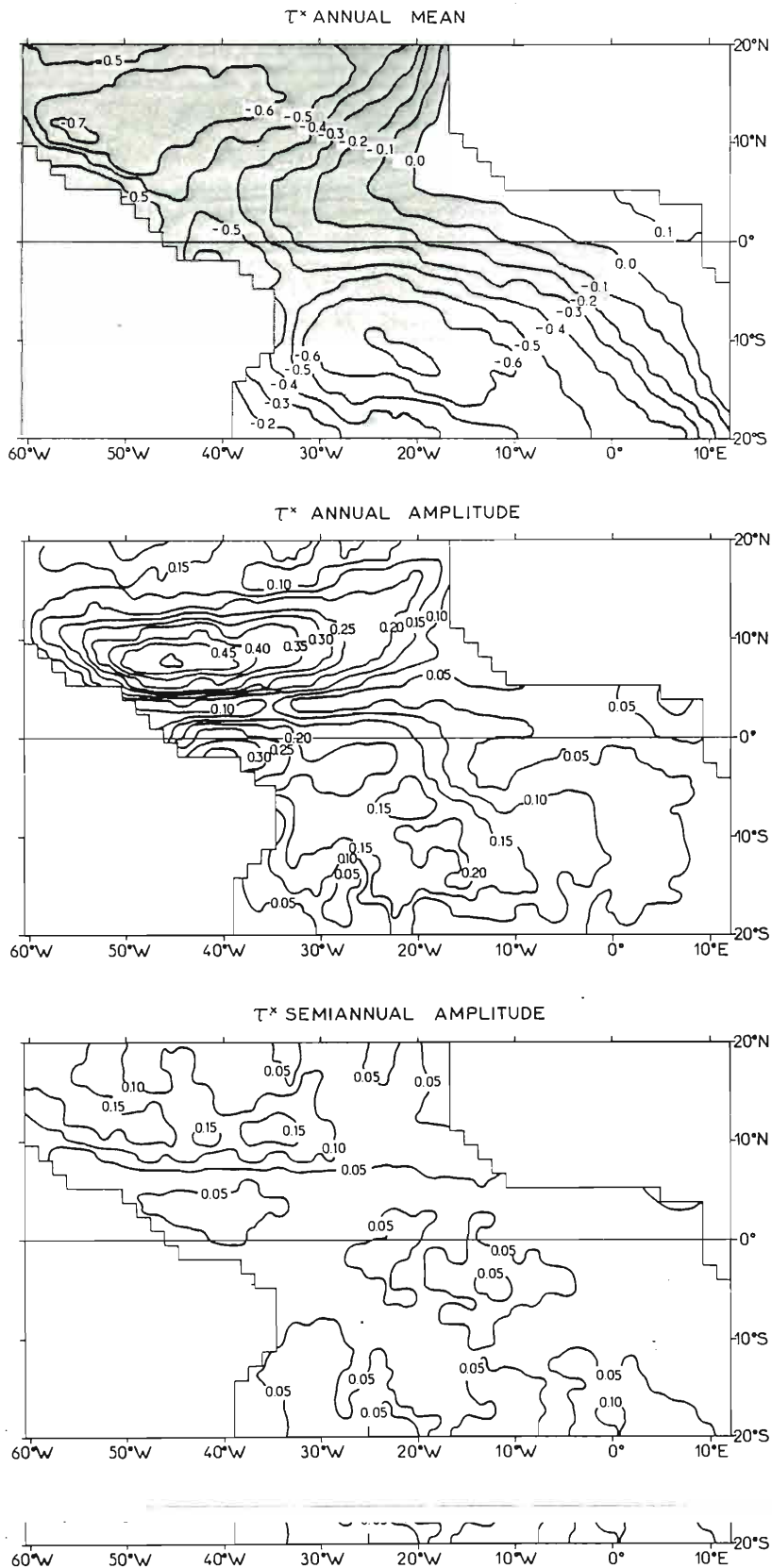


Fig. 23a. Mean, amplitude distribution for the first harmonic, and amplitude distribution of the second harmonic for the zonal wind stress in dynes cm<sup>-2</sup>.

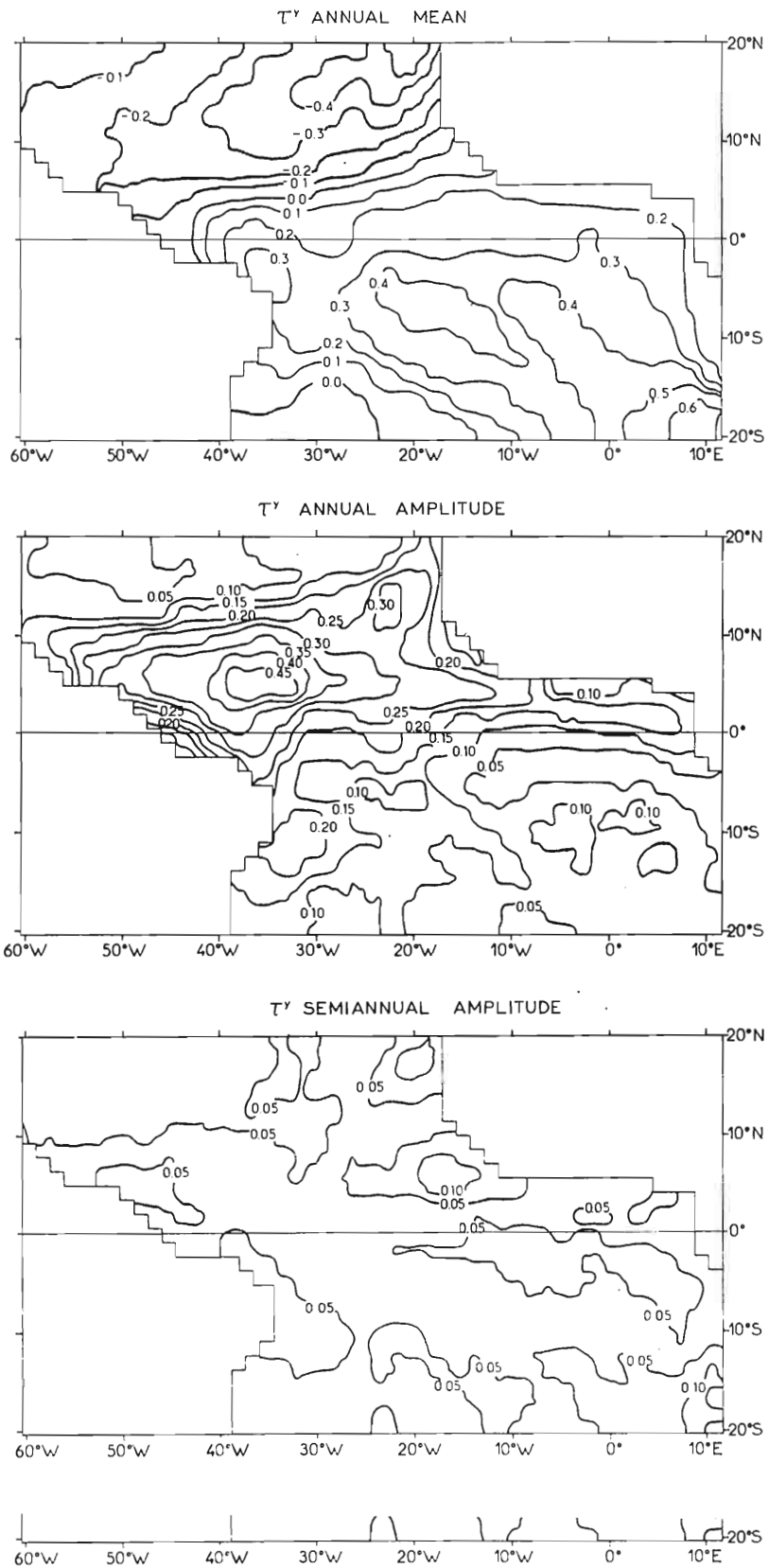


Fig. 23b. Mean, amplitude distribution for the first harmonic, and amplitude distribution for the second harmonic of the meridional wind stress in dynes cm<sup>-2</sup>.



variability is almost as large as the annual signal. A four month sea level oscillation was also detected by Verstraete et al. (1980). At the four month period the amplitude of the tropical Atlantic wind stress is still notable (roughly half that of the semiannual) but the physical meaning, if any, of such an atmospheric oscillation is unclear. The higher harmonics of the wind stress decomposition probably have no physical basis, rather they are mathematical artifacts accounting for small differences between the monthly means and the low-order harmonics.

### C. Tropical Atlantic Response to the Seasonal Wind Field

The seasonal variability of the model height field will be our primary concern in this study. The model results will be examined in terms of deviations about the local mean depth of the pycnocline. Analysis of the height field variability will provide some insight into the processes responsible for observed fluctuations in sea level and dynamic height since these quantities are influenced by the gravest baroclinic modes. The effect of wind stress curl, alongshore wind, zonal equatorial wind, and remotely forced Kelvin waves and Rossby waves at various points in the basin will be addressed. Analysis of the current variability is of lesser importance since the current fields are determined by only a single mode and nonlinear influences have been neglected.

An overview of the pycnocline response to the tropical Atlantic wind field will be presented first. This will consist of a discussion of the mean and seasonal fluctuations of the pycnocline topography for wind field will be presented first. This will consist of a discussion of the mean and seasonal fluctuations of the pycnocline topography for the whole basin. Comparison with observed variations of dynamic height

will be provided. A closer scrutiny of the response in the western Atlantic, along the equator, and in the eastern Atlantic will follow.

#### 1) basin-wide response

The model pycnocline response to the mean wind field over the tropical Atlantic is presented in Fig. 24 as the mean displacement of the pycnocline from a level surface. In this linear calculation the mean undisturbed upper-layer thickness,  $\bar{H}$ , was taken to be 75 m. The mean depth chosen is relatively unimportant when discussing the height field variability (not so for current magnitudes). The magnitude of  $c^2$  is of importance for pycnocline variations since  $\bar{H}$  and the density contrast across the pycnocline can be changed while keeping  $c^2$  or the equivalent depth constant. Hence, we will only consider fluctuations about the mean depth of the pycnocline, not the change in upper-layer thickness.

The mean height field is characterized by a shallow pycnocline in the east and a deep pycnocline in the west. Superimposed upon this east-west gradient are a zonal equatorial trough and a low-latitude ridge in each hemisphere terminating at an upwelled, dome-like feature. The zonal slope at the equator is induced by the mean zonal wind stress,  $\tau^x = c^2 h_x$ . The meridional pycnocline topography is determined by the wind-stress curl distribution, primarily  $\frac{\partial \tau^x}{\partial y}$ , (see Fig. 7 of Hellerman, 1980) and the influence of cross-equatorial winds. The shallow region in the northeastern part of the basin is in the vicinity of the Guinea Dome. This formation is well defined by observations and has been described by Rossignol and Meyrueis (1964) and Mazeika (1967). of the Guinea Dome. This formation is well defined by observations and has been described by Rossignol and Meyrueis (1964) and Mazeika (1967). The Angola Dome in the Southern Hemisphere is not clearly defined.

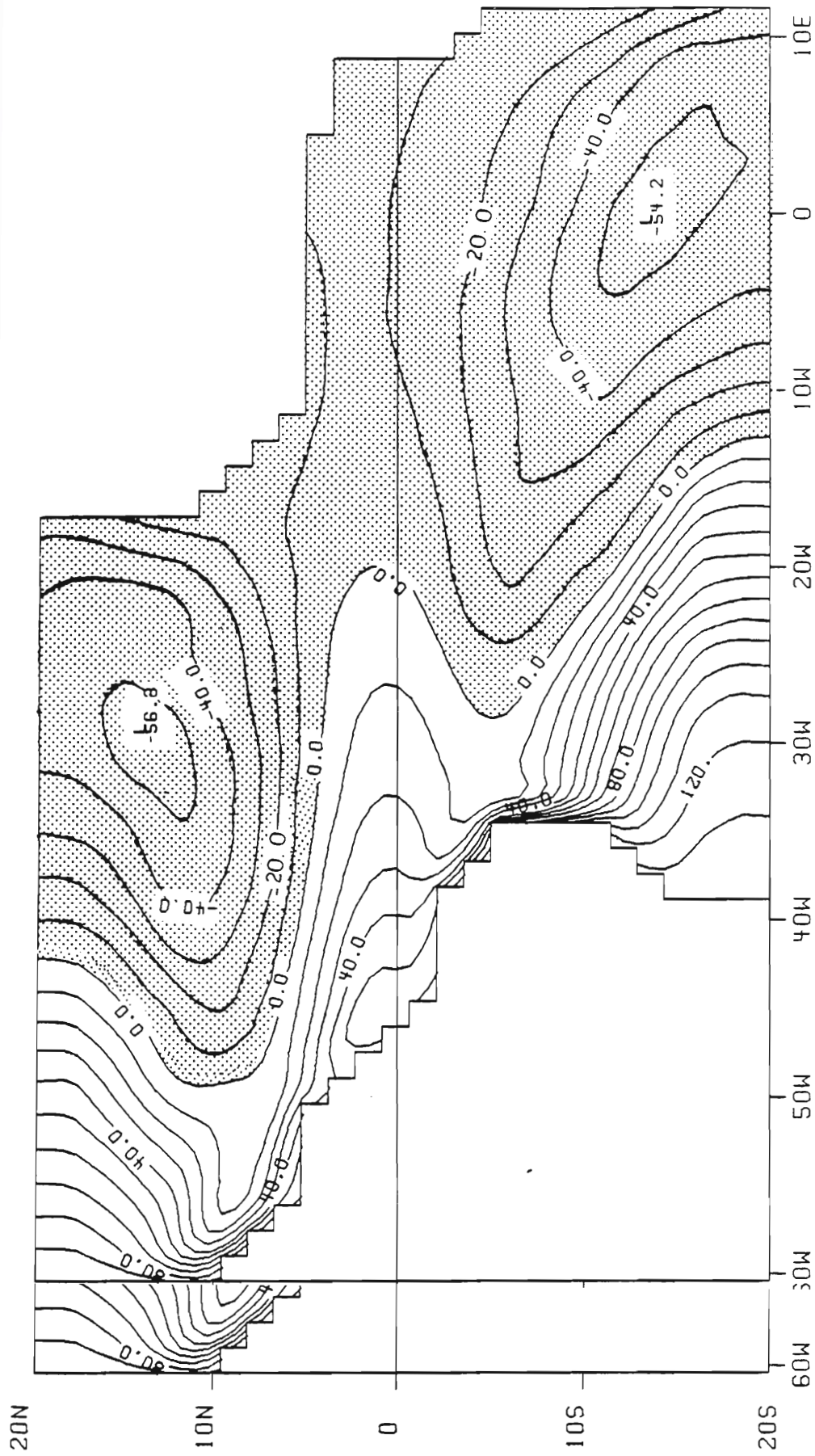


Fig. 24. Annual mean perturbation (meters) to the upper layer thickness. Shaded regions indicate where the pycnocline is shallower than the initial state of no motion.

Mazeika (1967) noted the existence of a subsurface dome structure located near  $10^{\circ}\text{S}$ ,  $9^{\circ}\text{E}$  during the austral summer but Bogorov et al. (1973) described a larger cyclonic vortex centered at  $13^{\circ}\text{S}$ ,  $3^{\circ}\text{E}$ .

All historical Nansen, CTD, MBT, and XBT data available have recently been used by Merle and Arnault (1982) to update a computation of the mean dynamic height field relative to 300db for the tropical Atlantic. The MBT and XBT data were used to obtain salinity information via the T-S relation following Stommel (1947) and Emery (1975). The updated dynamic height data are more precise than the previous calculation by Merle (1978) which only included Nansen data up through 1972. The monthly mean dynamic height data (surface/300 db), generously provided by S. Arnault and J. Merle, were subjected to a weighted least squares method to extract the mean, annual harmonic, and semiannual harmonic.

The mean dynamic height field (Fig. 25) and the model pycnocline topography (Fig. 24) compare favorably. A system of troughs and ridges delineates several equatorial currents (Katz, 1981) as in the tropical Pacific (Wyrtki, 1974a,b). Based on the distribution of dynamic height, the North Equatorial Current is located between  $20^{\circ}\text{N}$  and the trough (pycnocline ridge) near  $10^{\circ}\text{N}$ . The North Equatorial Countercurrent (NECC) is bounded by the trough at  $10^{\circ}\text{N}$  and the ridge at  $3^{\circ}\text{N}$ . In the model this ridge (pycnocline trough) is closer to the equator as was the location of the Equatorial Ridge in the Pacific Ocean model by Busalacchi and O'Brien (1980). The sparse data in the Southern Hemisphere indicate a poorly defined ridge in dynamic height Ocean model by Busalacchi and O'Brien (1980). The sparse data in the Southern Hemisphere indicate a poorly defined ridge in dynamic height at  $8^{\circ}\text{S}$  which may form the northern boundary of the South Equatorial

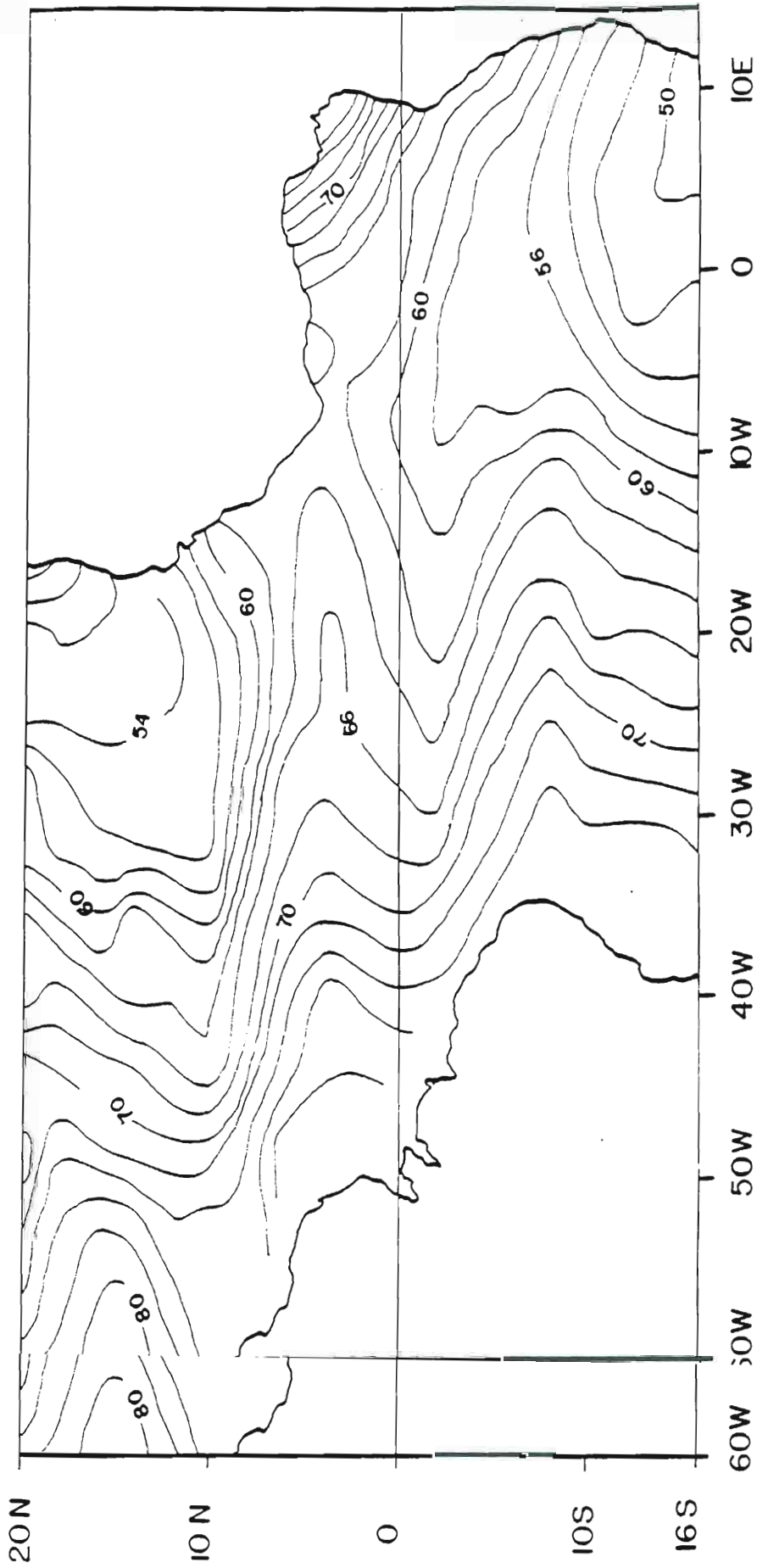


Fig. 25. Annual mean of dynamic height (dyn. cm) at 0/300 db.

Countercurrent (Merle, 1977). A corresponding feature is not present in the annual mean of the model pycnocline topography. A seasonal pycnocline trough is present south of the equator in the central and eastern sections of the model basin from June to August.

The major thrust of this study will deal with the seasonal variations about the mean state. Merle and LeFloch (1978) have shown that the seasonal cycle of the surface and subsurface thermal structure in the tropical Atlantic is mainly described by the annual and semiannual harmonics. This is also true of the wind field. Since the wind forcing the model is periodic and because the model is linear, it is justified to Fourier decompose the model results in time. This provides a straightforward method of assessing the basin-wide spatial and temporal variability. The seasonal signals of both the model pycnocline and observed dynamic height are governed by annual and semiannual fluctuations (Fig. 26-28). The phase of the response should be overlooked in regions where the amplitude is very small. Due to errors inherent in dynamic height calculations only amplitudes greater than 2 dynamic cm are significant.

The largest annual pycnocline and dynamic height changes (Figs. 26, 27) are in the western half of the basin north of the equator and south of a band of rapid phase change. This area of large amplitudes is associated with a north-south pivoting of the northern tropical Atlantic about a line roughly parallel to the ITCZ. North of the pivot line, near  $10^{\circ}\text{N}$ , a secondary amplitude maximum is present in the model. The pivot line also indicates the location of the smallest seasonal SST line, near  $10^{\circ}\text{N}$ , a secondary amplitude maximum is present in the model. The pivot line also indicates the location of the smallest seasonal SST variations for the tropical Atlantic (Merle and LeFloch, 1978). Along

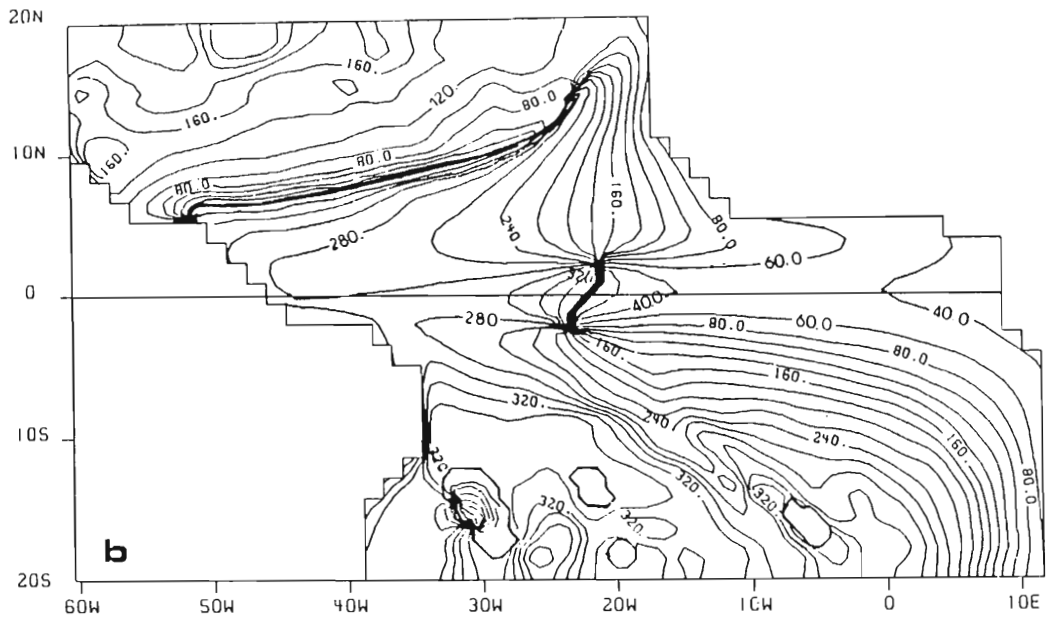
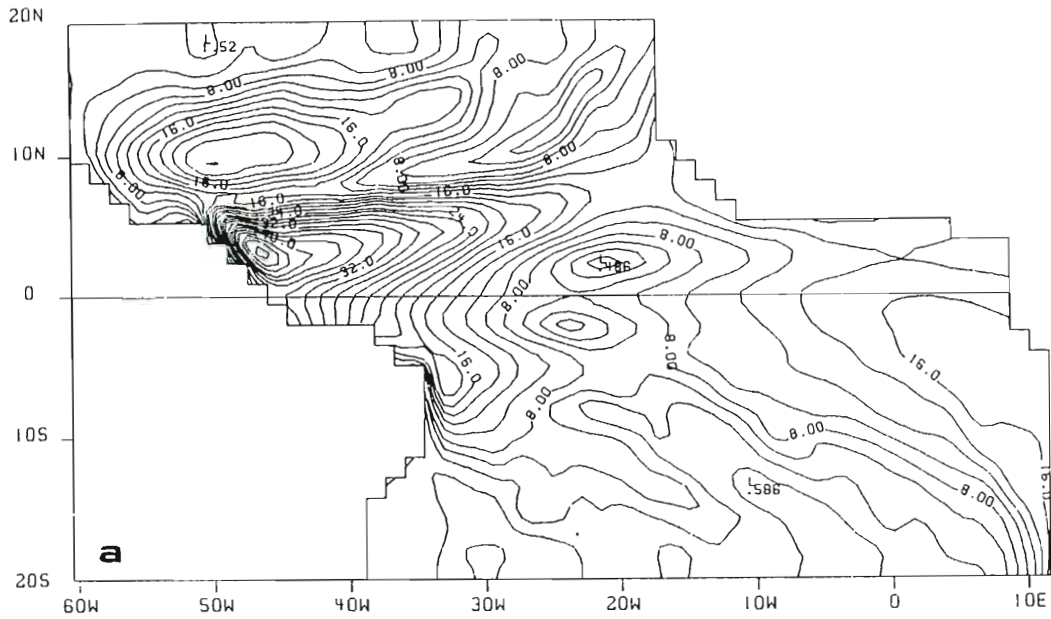


Fig. 26. Annual variability of the model pycnocline depth, a) amplitude (meters) and b) phase (degrees). The phase map indicates when the pycnocline is deepest.

depth, a) amplitude (meters) and b) phase (degrees). The phase map indicates when the pycnocline is deepest.

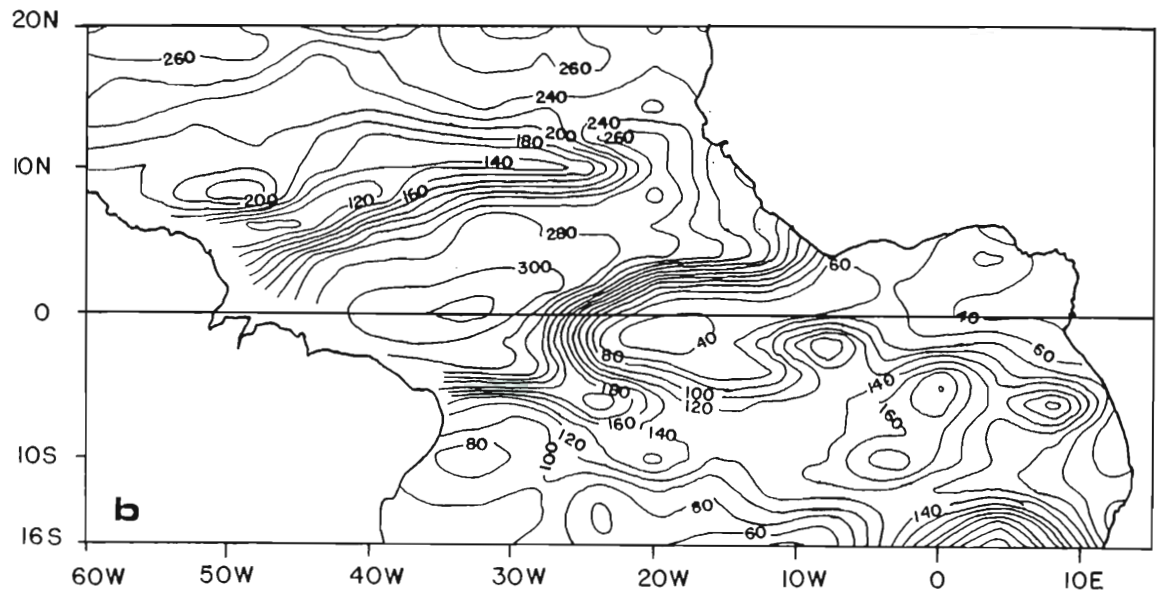
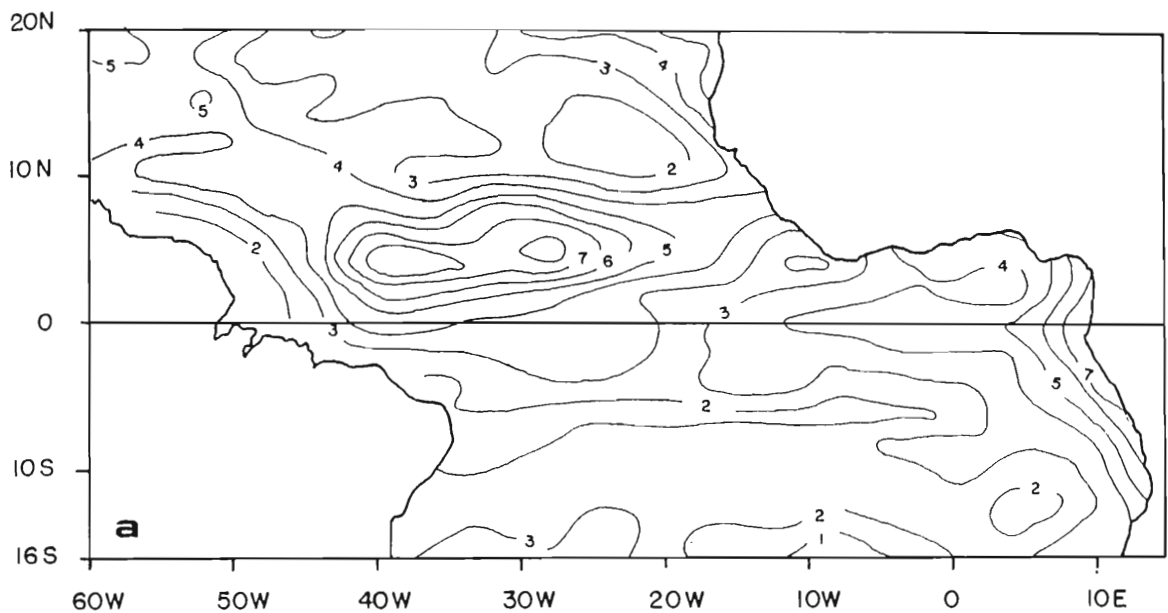


Fig. 27. Annual variability of dynamic height at the surface relative to 300 db, a) amplitude (dyn. cm.) and b) phase (degrees).

Fig. 27. Annual variability of dynamic height at the surface relative to 300 db, a) amplitude (dyn. cm.) and b) phase (degrees).



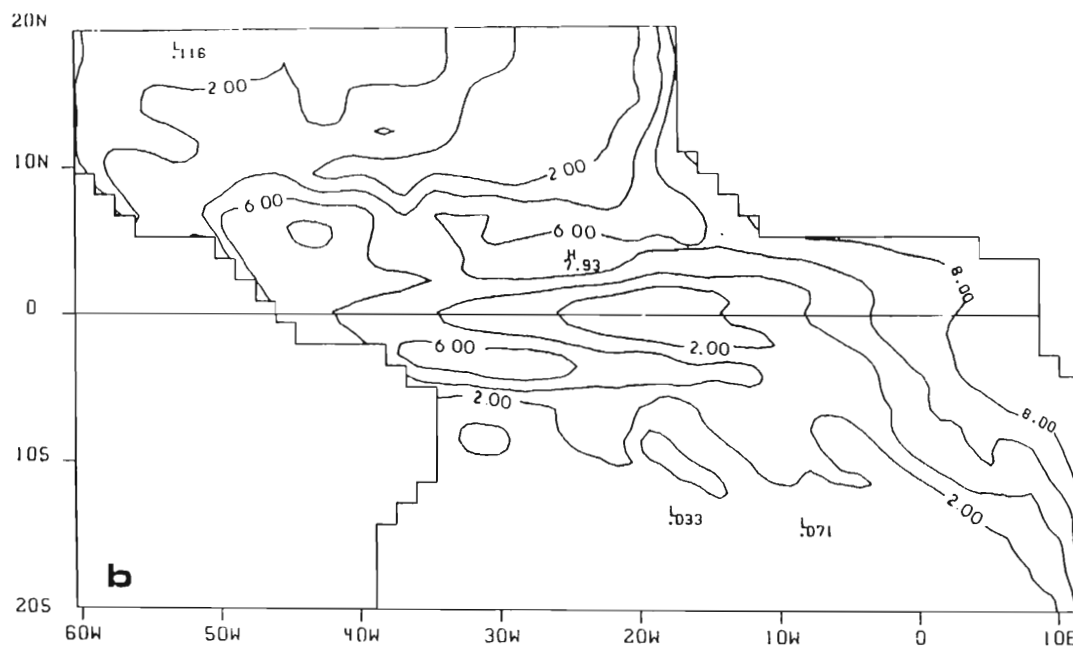
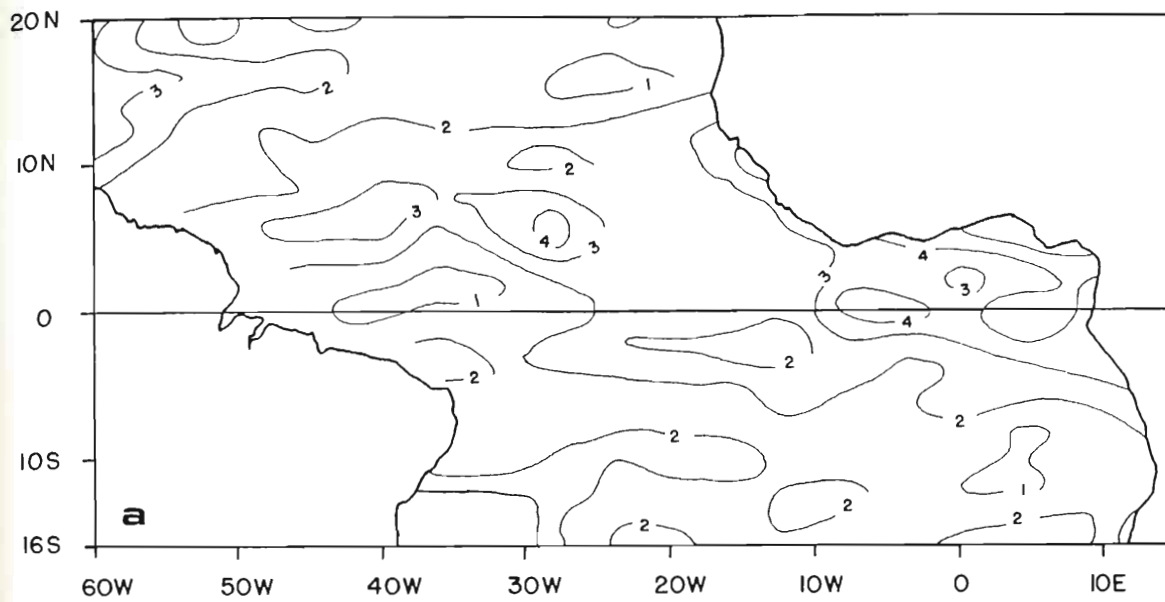


Fig. 28. Semiannual amplitudes of a) dynamic height

Fig. 28. Semiannual amplitudes of a) dynamic height (0/300 db) and b) model pycnocline depth.

the equator the largest amplitudes in the model and observations are near the eastern and western boundaries. An amplitude minimum and a large phase gradient in the central equatorial Atlantic represent a pivot point for the east-west tilting of the pycnocline along the equator (Merle, 1980a). In the eastern Atlantic, an area of notable amplitude is along the southern coast of the Gulf of Guinea extending northwestward towards the equator. The modelled and observed phase compare rather well there. Near the equator between the eastern boundary and  $4^{\circ}\text{W}$ , there is a very small westward increase in phase. Between  $4^{\circ}\text{W}$  and the pivot point the phase increases eastward. An area of major discrepancy between the model and observations is along the coasts of Mauritania and Senegal. In this region the amplitudes of dynamic height increase northward, but the model height field amplitudes decrease northward. For the remainder of the basin, near the northern and southern extremes, the modelled and observed amplitudes are small and phase lines indicate the pycnocline is deeper in the summer-fall of each hemisphere.

The distribution of the semiannual amplitudes for the model and observations are presented in Fig. 28. The major areas of variability are similar to those of the annual period. Regions of maximum amplitude are along the eastern boundary and north of the equator in the central and western Atlantic. In contrast with the annual signal, there is no significant semiannual variability near the western boundary at  $10^{\circ}\text{N}$ . At the equator in the central model basin there is little semiannual change. The phase lines (not shown) indicate this boundary at  $10^{\circ}\text{N}$ . At the equator in the central model basin there is little semiannual change. The phase lines (not shown) indicate this

area corresponds to a pivot point for a 6 month period east-west tilting of the equatorial pycnocline. The smallest dynamic height changes along the equator occur near the western boundary. An important feature of the semiannual response is that the largest amplitudes are in the east, opposite to that for the annual response. The semiannual response in the Gulf of Guinea is roughly one-half of the annual signal. Variations in subsurface thermal structure (Merle and LeFloch, 1978) and sea level (Verstraete et al. 1980) also indicate a strong semiannual component in the eastern Atlantic in agreement with Fig. 28. Inspection of the wind stress fields (Fig. 23) does not offer any explanation of these relations.

Several case studies were performed in order to understand the interesting features reproduced by the model. These entailed integrating the model equations with parametric wind distributions representing portions of the total wind stress field. The separate influences of the zonal and meridional wind stress were isolated by repeating the model calculations with only zonal wind stress forcing, i.e. the meridional wind stress was set identically equal to zero (Fig. 29). By comparing the annual and semiannual response to zonal winds with the total forcing solution (Figs. 26, 28) it is evident that the variations in the central and western parts of the model basin are due to the variability of the zonal wind stress component. The only notable influence of the meridional wind variability is along the eastern boundary. The coastal signal along Mauritania and Senegal is much larger when the alongshore winds are neglected. The tongue of eastern boundary. The coastal signal along Mauritania and Senegal is much larger when the alongshore winds are neglected. The tongue of

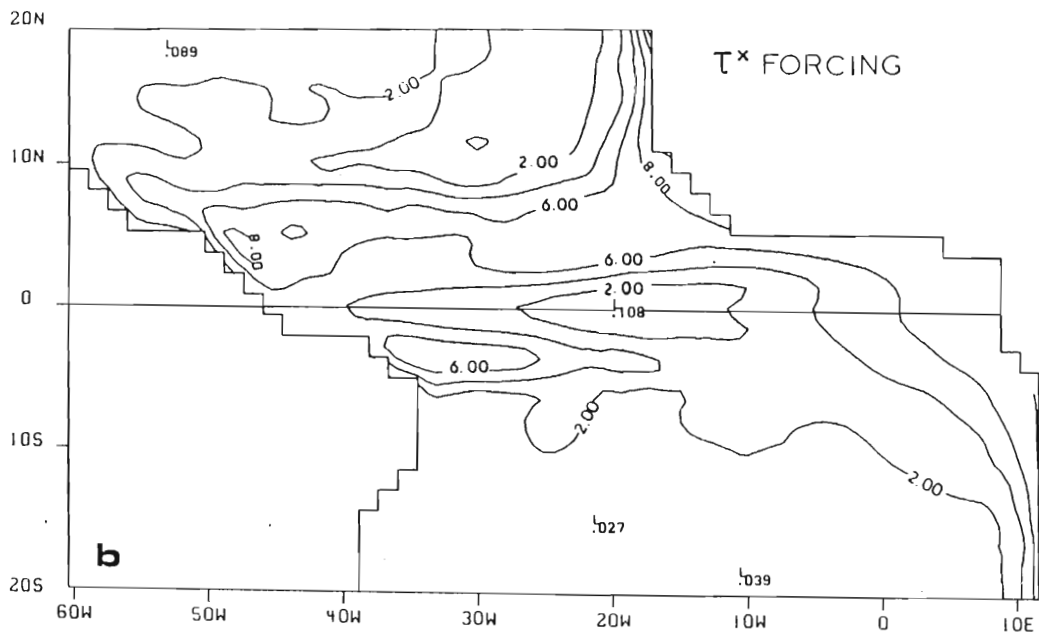
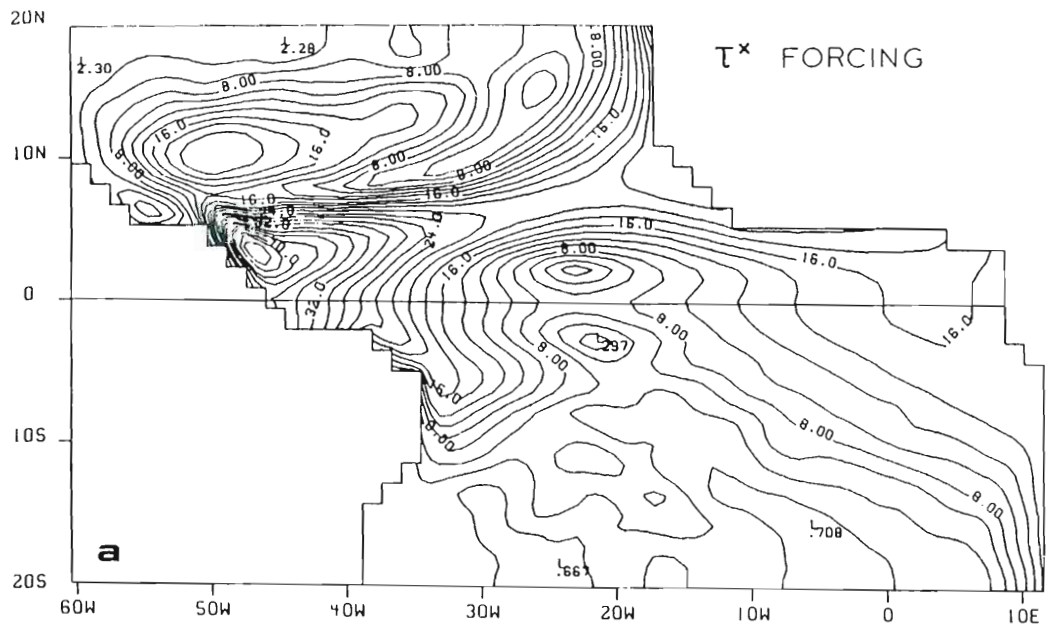


Fig. 29. Amplitude distributions for the pycnocline response to a) annual  $\tau^x$  forcing and b) semiannual  $\tau^x$  forcing. The differences from Fig. 26a and 28b indicate the influence of  $\tau^y$  forcing.

response to a) annual  $\tau^x$  forcing and b) semiannual  $\tau^x$  forcing. The differences from Fig. 26a and 28b indicate the influence of  $\tau^y$  forcing.

large pycnocline changes in the Gulf of Guinea is not well defined when annual zonal forcing is employed. The importance of meridional winds near the equator and along the southern coast have been discussed by Voituriez (1981a) and Philander and Pacanowski (1981a). In the present linear model nearly all of the annual and 75% of the semiannual pycnocline fluctuations in the Gulf of Guinea are driven by changes in the zonal component of the wind field.

Additional calculations were performed whereby the zonal wind stress was limited to being either inside or outside the Gulf of Guinea or was limited to the eastern or western sides of the basin. Since the meridional stress was neglected, no erroneous wind stress curl was produced by this fractional suppression of the wind stress. These calculations will aid in determining the processes responsible for seasonal changes in the western, equatorial, and eastern Atlantic. The results will provide a simple determination of whether the seasonal response in a particular region of the model basin is dominated by local or remote forcing.

## 2) western tropical response

The model results and observations (Figs. 26-28) demonstrate that the seasonal variability in the western tropical North Atlantic is characterized by two different annual oscillations. Close to the equator ( $2^{\circ}$ - $3^{\circ}$ ) the annual variability is due to an east-west tilting of the pycnocline. Katz et al. (1977) and Lass et al. (1982) have reported that the observed sea surface slope at the equator is governed by the zonal wind stress. This seasonal response along the equator reported that the observed sea surface slope at the equator is governed by the zonal wind stress. This seasonal response along the equator

will be discussed in the next subsection. North of the equator there is a north-south tilting of the sea surface/pycnocline topography. A pivot line extending northeastward from the western boundary at 5°N, parallel to the mean position of the ITCZ, separates two regions of large, out-of-phase variability. The seasonal displacements of the pycnocline are dominated by annual processes (Fig. 30). Semiannual fluctuations are considerably smaller as they are in the local wind field. North of the pivot line the annual signal is driven by zonal wind stress changes in the western part of the basin (Figs. 29a and 31a). In the region to the south there is a contribution from the wind stress east of 25°W (Fig. 31b) implying the influence of Rossby waves.

A convenient description of the vertical displacement of the pycnocline can be obtained by forming the vorticity equation from the inviscid version of (1a), and then substituting for the divergence and  $\beta V$  terms. The pycnocline fluctuations are then described by

$$h_t = \frac{1}{\beta y} [V_{xt} - U_{yt} + \frac{1}{y} U_t] - \nabla_x \frac{\tau}{\rho \beta y} + \frac{c^2}{\beta y^2} h_x . \quad (2)$$

The magnitudes of the terms in (2) are calculated in order to isolate the mechanisms responsible for the large amplitude variability in the western tropical Atlantic. Theory and observations indicate that at extra-equatorial latitudes Ekman pumping and Rossby waves (last two terms) may be important on seasonal time scales (Yoshida, 1955; Meyers, 1979). The acceleration terms have been included because the region south of the pivot line is close enough to the equator to be influenced by equatorial waves.

south of the pivot line is close enough to the equator to be influenced by equatorial waves.

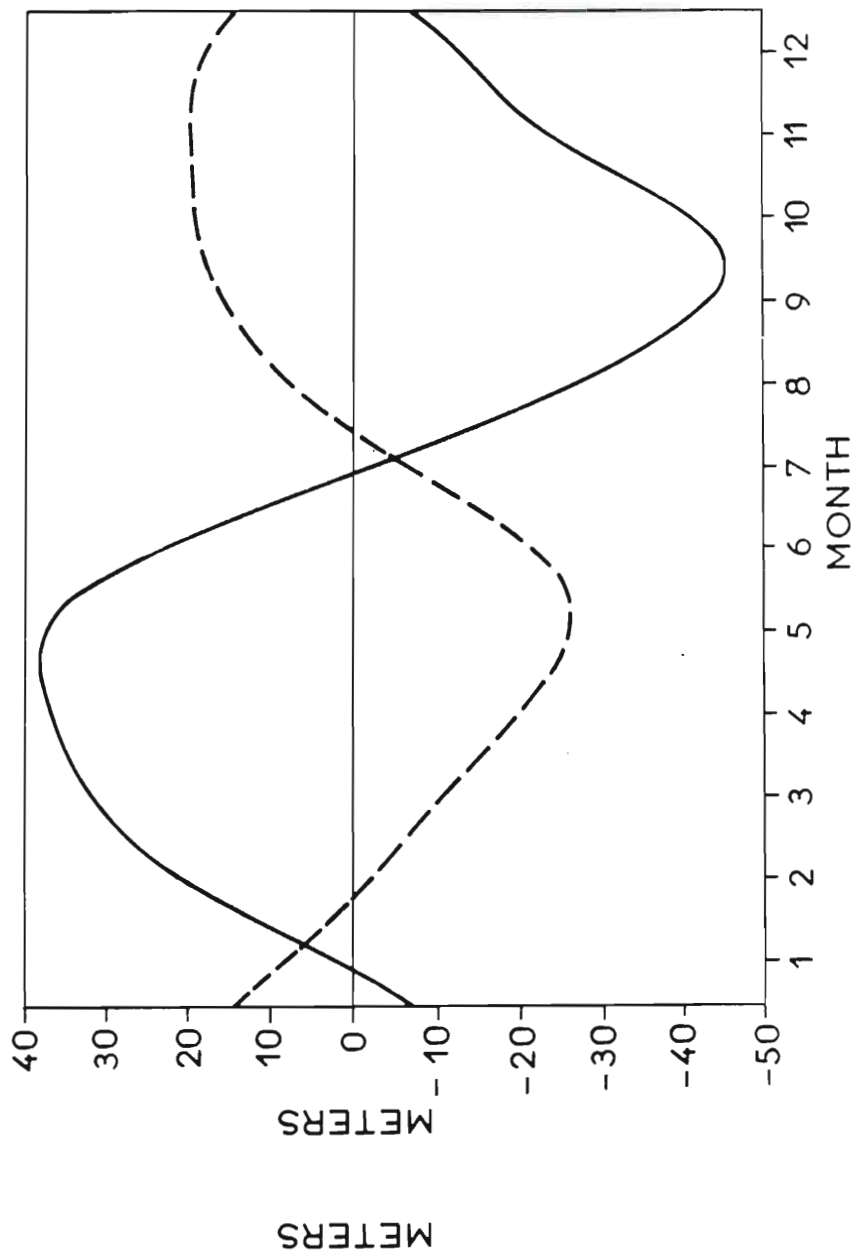


Fig. 30. Seasonal pycnocline displacements for 2° squares centered at 10°N, 48°W (dashed line) and 3°N, 43°W (solid line). These variations are indicative of a north-south tilting about a pivot line which separates the two areas. Negative values indicate the pycnocline is deeper than the annual mean.

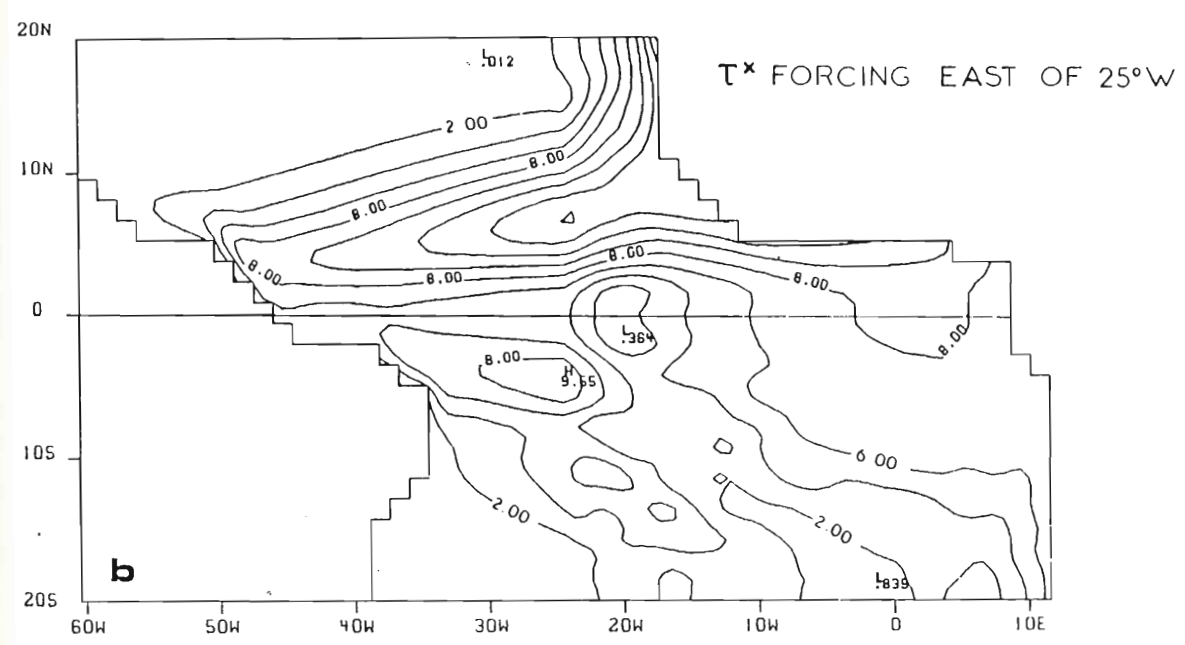
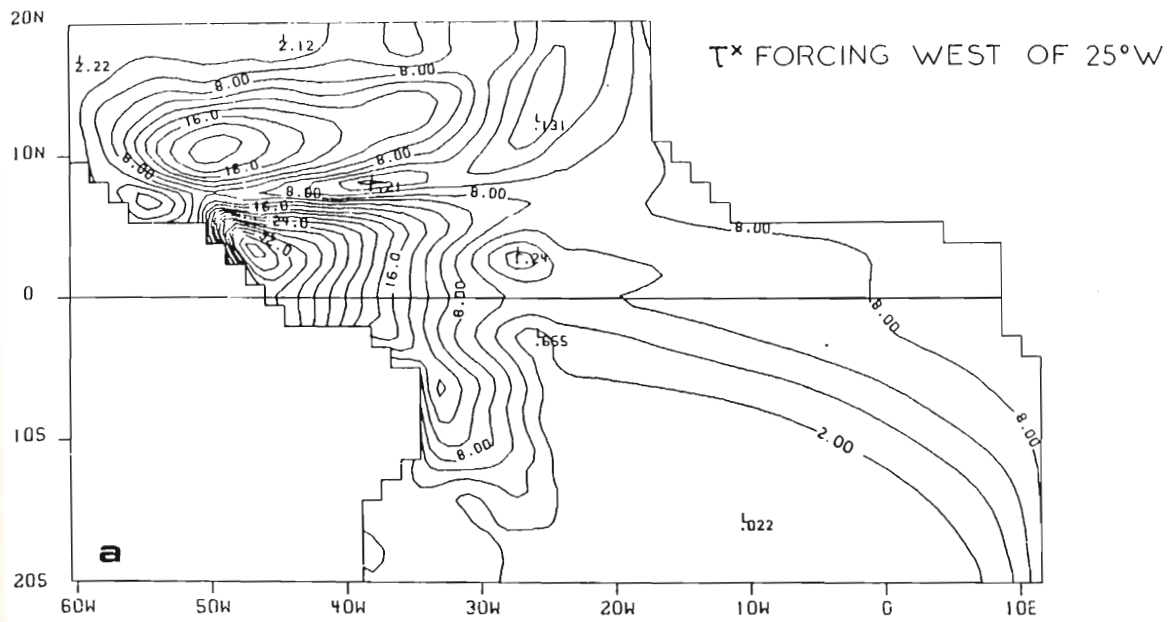


Fig. 31. Amplitude distributions for the pycnocline response to  
 a) annual  $\tau^x$  forcing west of  $25^\circ\text{W}$

Fig. 31. Amplitude distributions for the pycnocline response to  
 a) annual  $\tau^x$  forcing west of  $25^\circ\text{W}$   
 b) annual  $\tau^x$  forcing east of  $25^\circ\text{W}$



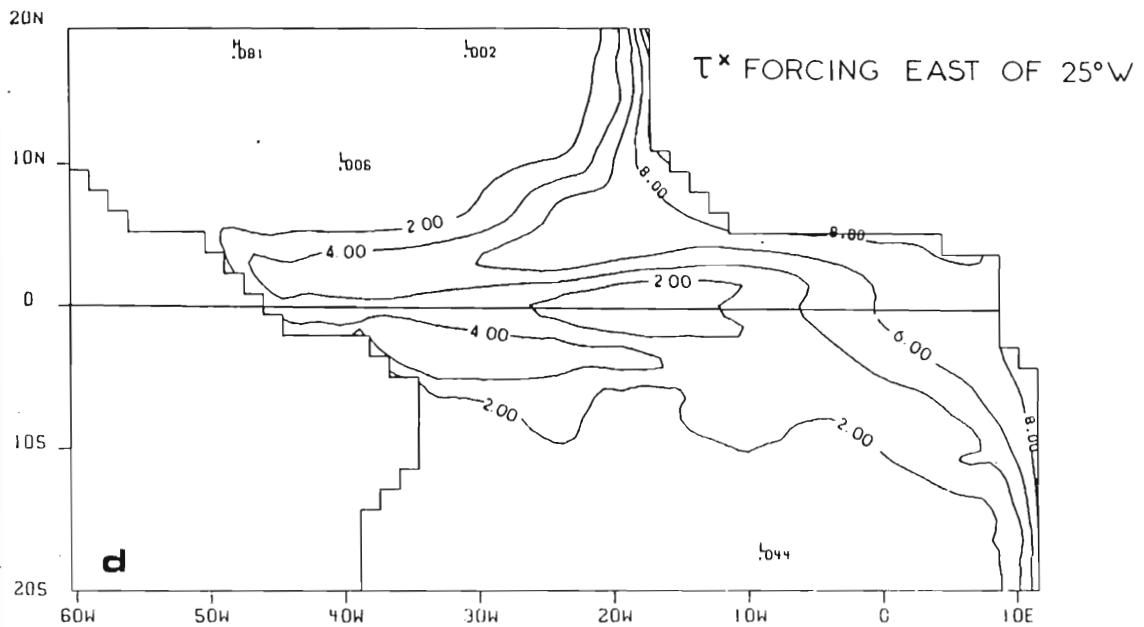
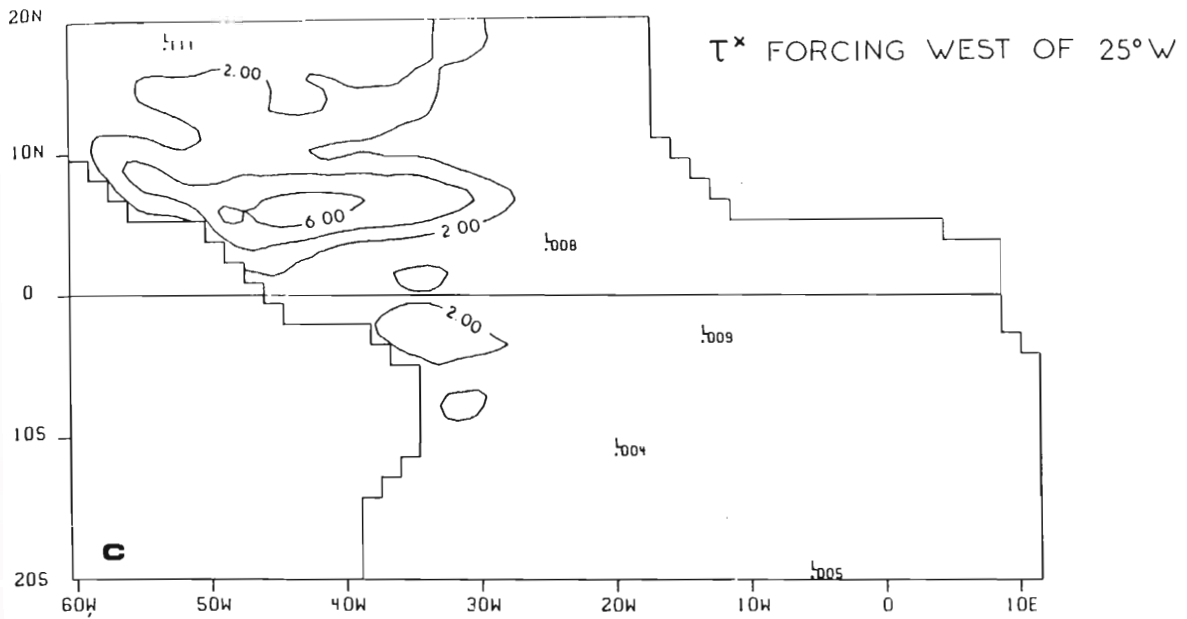


Fig. 31. Amplitude distributions for the pycnocline response to  
 c) semiannual  $\tau^x$  forcing west of  $25^\circ\text{W}$

Fig. 31. Amplitude distributions for the pycnocline response to  
 c) semiannual  $\tau^x$  forcing west of  $25^\circ\text{W}$   
 d) semiannual  $\tau^x$  forcing east of  $25^\circ\text{W}$

The major contribution in (2) representing pycnocline displacements centered at  $10^{\circ}\text{N}$ ,  $48^{\circ}\text{W}$  is Ekman pumping (Fig. 32), primarily  $\partial(\tau^x/\rho\beta y)/\partial y$ . The seasonal deepening of the pycnocline during the first half of the year is a local response to an increase in the easterly wind stress and an anticyclonic perturbation to the wind stress curl. These wind stress changes are related to the southward displacement of the ITCZ. All other terms in (2) are insignificant. This is consistent with the case studies incorporating partial forcing (Fig. 31) which demonstrate that the variability north of the pivot line is locally forced. During the parameter range tests this region north of the pivot line was the only part of the model basin in which the magnitude of the pycnocline variations was independent of the phase speed  $c$ . This also implied the relative importance of Ekman pumping with respect to the Rossby wave influence at this location.

The case studies indicate remote and local effects are present south of the pivot line (Fig. 31). Ekman pumping and Rossby waves are the dominant mechanisms (Fig. 33a). The seasonal displacement of the pycnocline is determined by the phase relation between the two processes. The effects of the acceleration terms are small but only the  $V_{xt}$  term can be ignored. The contributions from  $U_t$  and  $U_{yt}$  (Fig. 33b) are not negligible because of the proximity to the equator. Rossby waves emanating from the east are downwelling favorable from March to August. The sign of the Ekman pumping in this area is governed by the changes in the wind stress curl. From June to November the ITCZ is shifted north of its mean position. The associated influx governed by the changes in the wind stress curl. From June to November the ITCZ is shifted north of its mean position. The associated influx

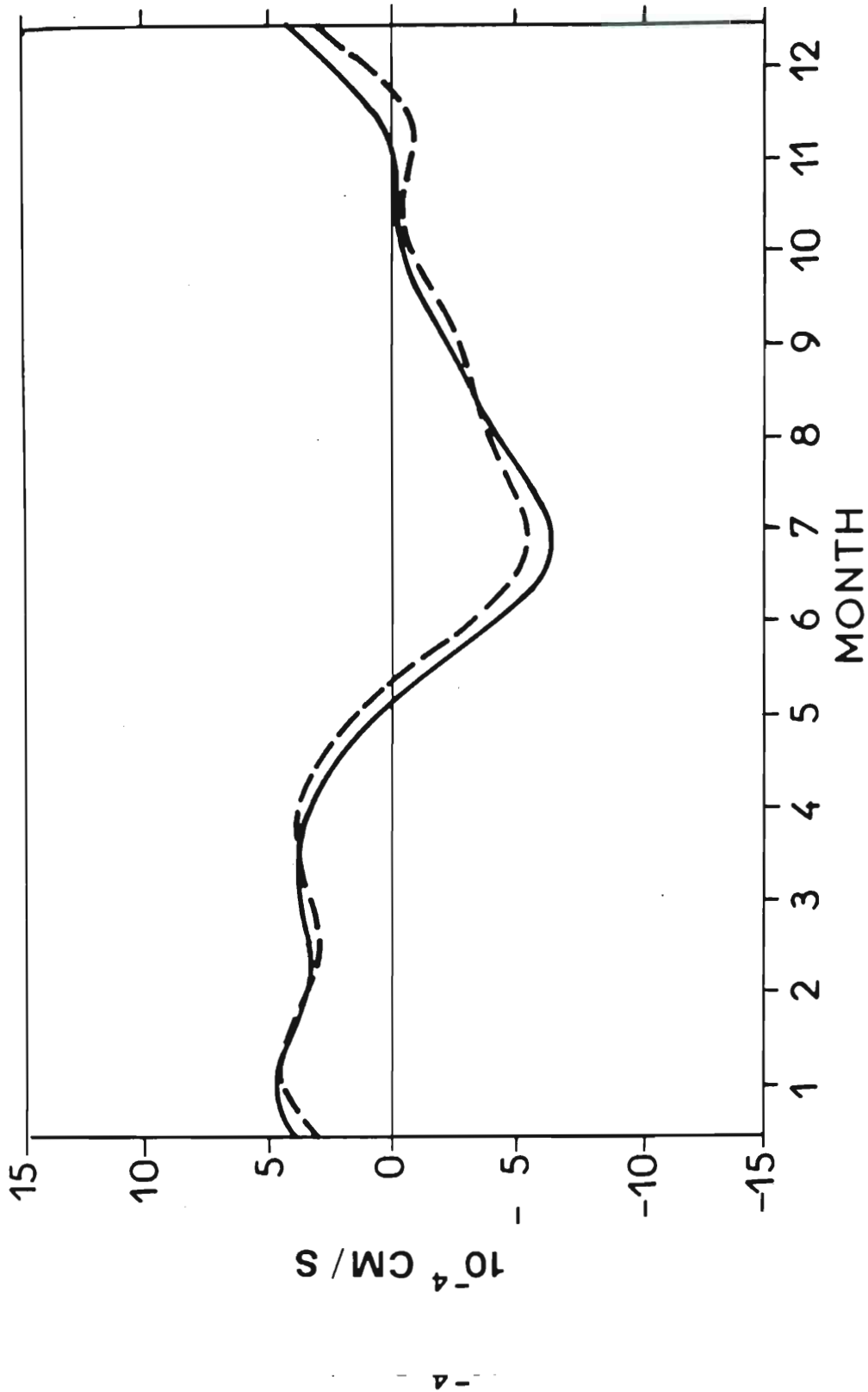


Fig. 32. Comparison of  $\frac{\partial h}{\partial t}$  (solid) and Ekman pumping contribution (dashed) at  $10^{\circ}\text{N}$ ,  $48^{\circ}\text{W}$ . Positive values indicate the pycnocline is deepening.

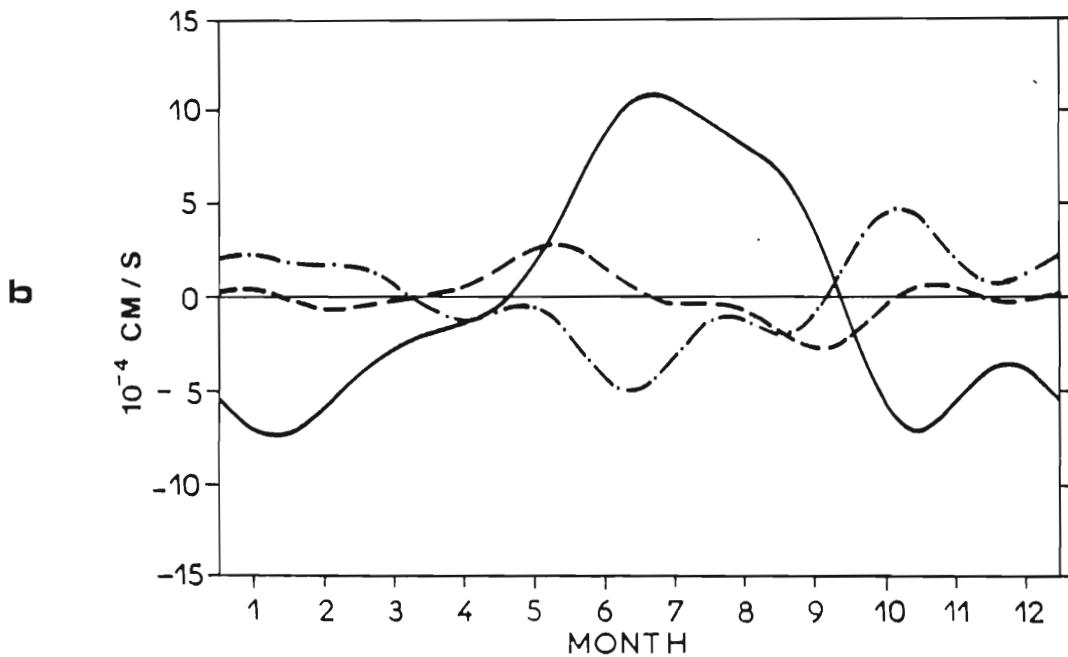
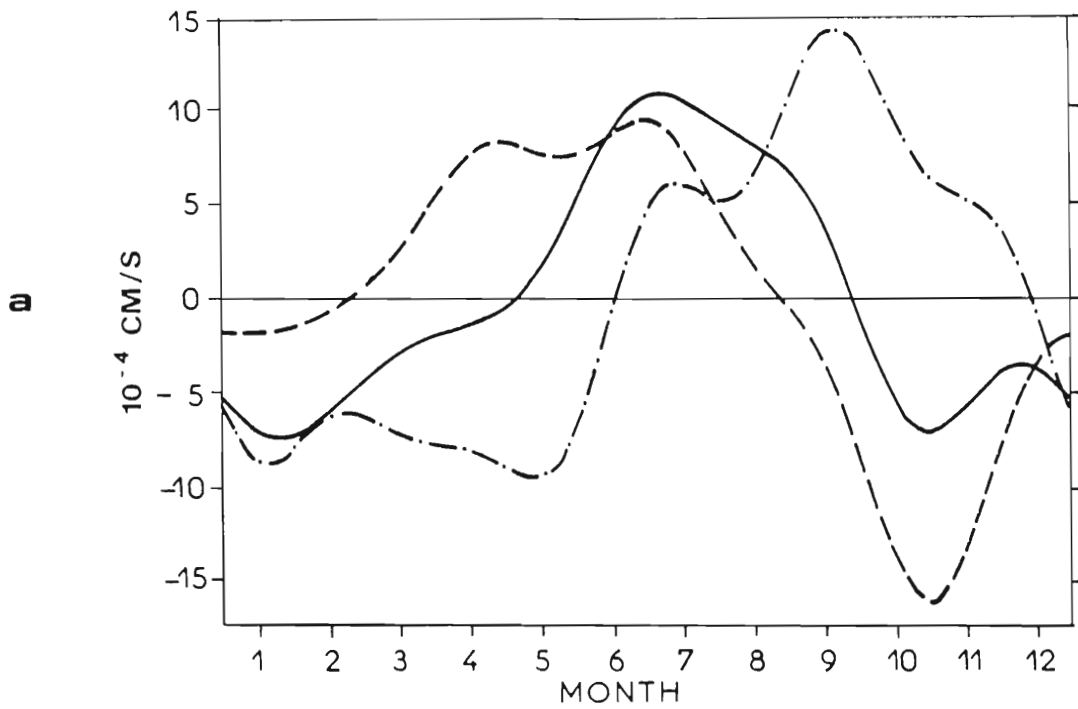


Fig. 33. Comparison at 3°N, 43°W of

a)  $\frac{\partial h}{\partial t}$  (solid), Ekman pumping (dash-dot), and Rossby wave

Fig. 33. Comparison at 3°N, 43°W of

a)  $\frac{\partial h}{\partial t}$  (solid), Ekman pumping (dash-dot), and Rossby wave wave (dashed) contributions

b)  $\frac{\partial h}{\partial t}$  (solid),  $-\frac{1}{\beta y} \frac{\partial^2 U}{\partial y \partial t}$  (dash-dot) and  $\frac{1}{\beta y^2} \frac{\partial U}{\partial t}$  (dashed) (dashed) contributions to Eq. (2).

of the southeast trades results in an anticyclonic perturbation to the wind stress curl. The combination of the two effects causes a seasonal deepening of the pycnocline from May through September. The pycnocline deepens at the equator during the same period in response to strengthening equatorial easterlies.

These large pycnocline displacements are in locations where seasonal variations in the NECC may be produced. The mean position of the NECC in the western model basin is between a pycnocline ridge (sea surface trough) near  $8^{\circ}\text{N}$  and an equatorial pycnocline trough (Fig. 24). The pycnocline displacements at  $10^{\circ}\text{N}$  determine the seasonal depth and location of the pycnocline ridge forming the north flank of the NECC. Similarly, the large annual changes near  $3^{\circ}\text{N}$  influence the location and strength of the low-latitude trough south of the NECC. Since the two regions are out of phase there are large seasonal changes in the meridional pressure gradient. The pycnocline ridge is most shallow and the equatorial trough is deepest from July through December (Fig. 30). Both features are north of their mean position at this time. During the first part of the year the ridge and trough are weak and not well defined.

The simulated NECC undergoes significant spatial and temporal variations in response to the pressure field changes in the model. Early in the year the current is weak and close to the equator. From May to September the NECC progresses northward and becomes well formed between  $5^{\circ}\text{N}$ - $8^{\circ}\text{N}$ . This displacement of the NECC is similar to the observations at  $35^{\circ}\text{W}$ - $50^{\circ}\text{W}$  compiled by Boisvert (1967). As in the observations, the longitudinal extent of the current is not clearly

defined. The zonal current within a rectangle from  $3^{\circ}\text{N}$ - $9^{\circ}\text{N}$  and  $30^{\circ}\text{W}$ - $42^{\circ}\text{W}$  has been averaged to provide an indication of the seasonal variability of the NECC (Fig. 34). Within this region the NECC is strongest in August and is non-existent in April. Dynamic height differences across the NECC at 5/500 db averaged between  $20^{\circ}\text{W}$ - $40^{\circ}\text{W}$  imply that the current is weakest from February to June and strongest from July to November (Merle, 1977).

In the Southern Hemisphere there is no well formed convergence zone in the atmosphere. The western South Atlantic is always under the influence of a single trade wind system. Therefore, there is only one area of large pycnocline displacements south of the equator. Off the coast of Brazil at  $6^{\circ}\text{S}$  the seasonal pycnocline displacements are produced by Ekman pumping and Rossby waves. The Ekman pumping contribution is downwelling favorable from July through January due to a seasonal increase in the southeast trades. The Rossby wave influence has the same phase as north of the equator. The combined effect of the two processes is a downward displacement of the pycnocline from June through November.

### 3) equatorial response

The seasonal changes in the height field along the equator are presented in Fig. 35a. The mean zonal tilt of the pycnocline has been included to aid in discussing the pressure gradient variations. The western side of the model ocean is characterized by a deep pycnocline which has a minimum depth in April-May and maximum depth in September-October. The seasonal variation is dominantly annual. The eastern side which has a minimum depth in April-May and maximum depth in September-October. The seasonal variation is dominantly annual. The eastern side is characterized by a shallow pycnocline which attains a maximum

# NORTH EQUATORIAL COUNTERCURRENT

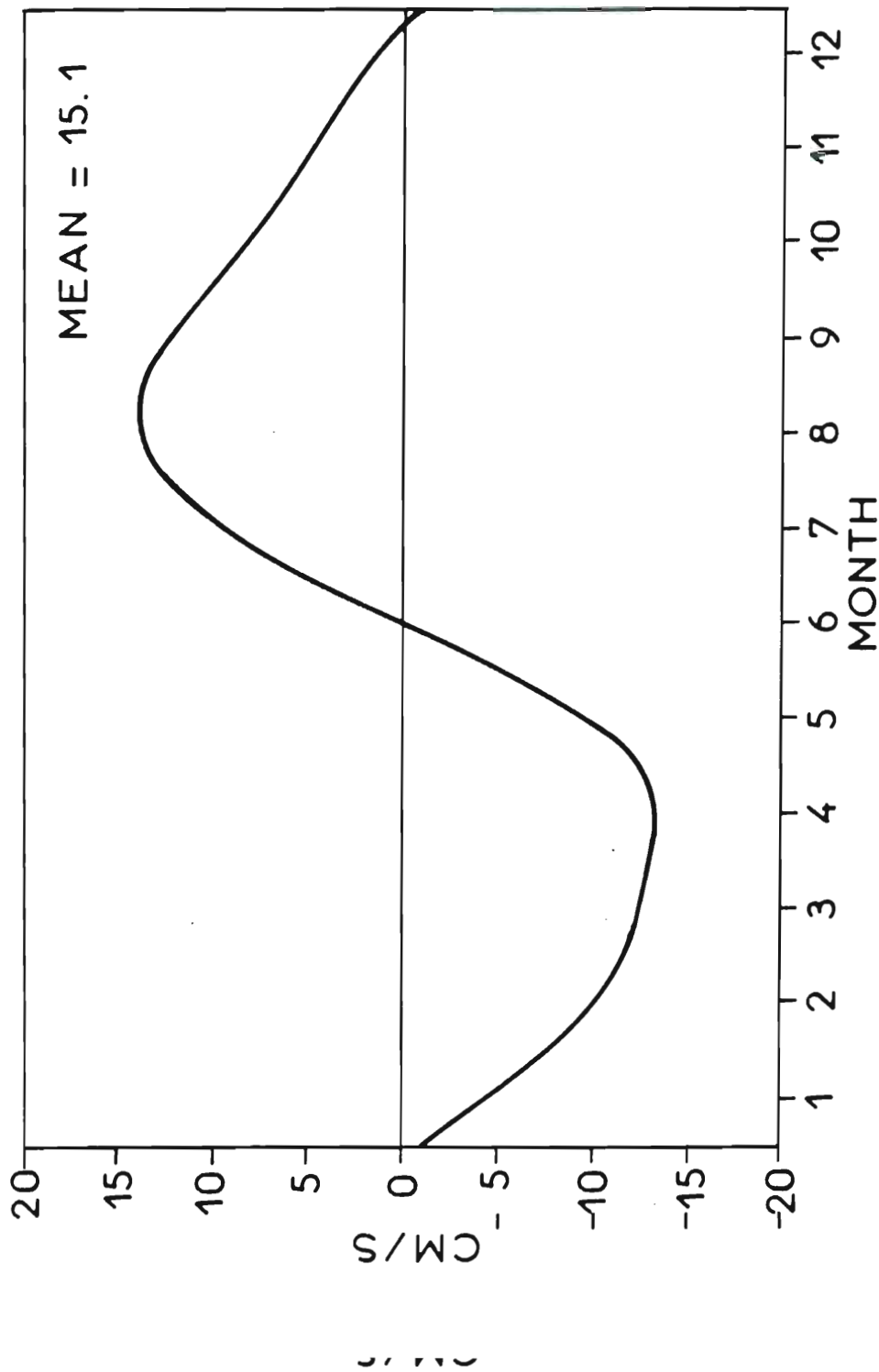
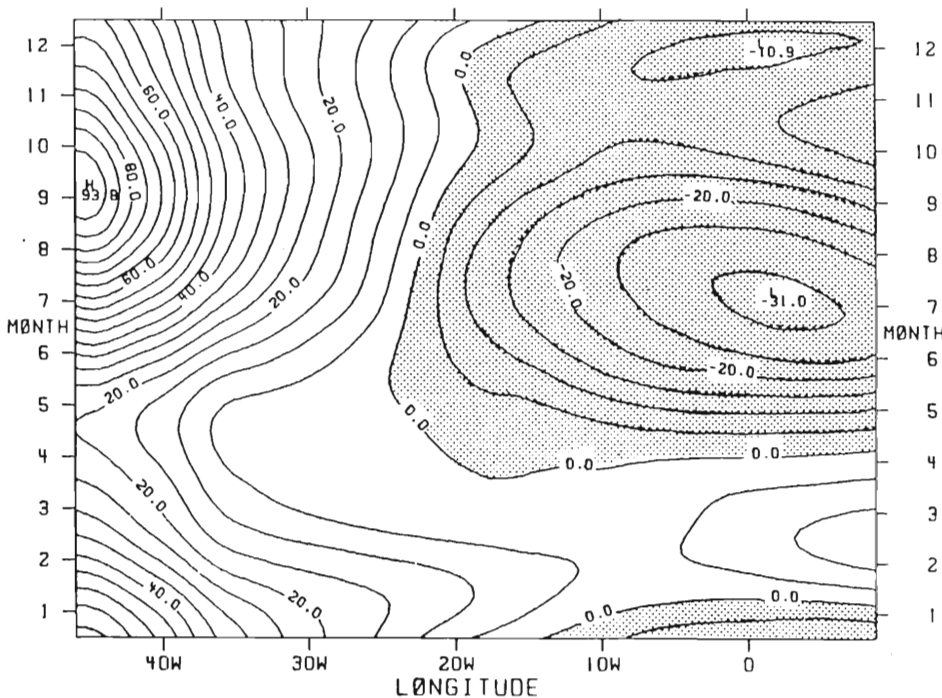


Fig. 34. Zonal velocity corresponding to a simulated North Equatorial Countercurrent averaged between 3°N-9°N and 30°W-42°W.

### H FIELD AT EQUATOR WITH ANNUAL MEAN

a



### H FIELD AT EQUATOR WITHOUT ANNUAL MEAN

b

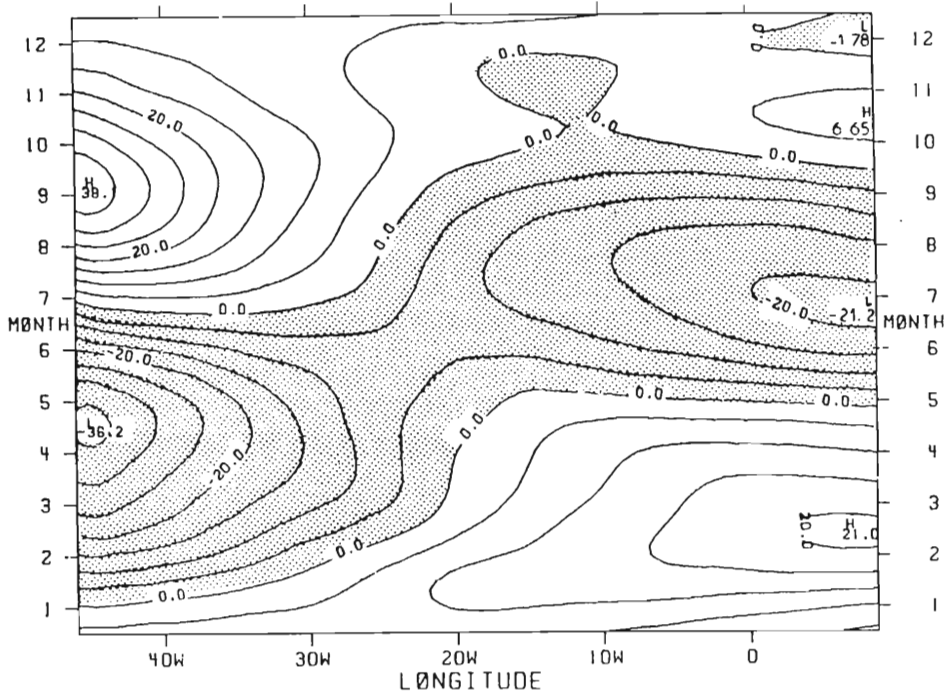


Fig. 35. Temporal variability of the model pycnocline (meters) along the equator. a) Shaded regions indicate the pycnocline is shallower than the initial state of no motion.

Fig. 35. Temporal variability of the model pycnocline (meters) along the equator. a) Shaded regions indicate the pycnocline is shallower than the initial state of no motion. The annual mean east-west pycnocline tilt is included in this plot. b) The annual mean east-west pycnocline tilt has been removed. Shaded regions indicate the pycnocline is shallower than the annual mean.



depth in February-March and minimum depth in July. A secondary maximum is present in October-November followed by a secondary minimum. The timing of the shallow model pycnocline in July is very close to that of the observed minima of thermocline depth and SST in July-August. The small upwelling episode later in the year has also been observed. These seasonal pycnocline displacements on each side of the basin are linked through a pivot point between  $20^{\circ}\text{W}$ - $30^{\circ}\text{W}$ . The oscillation along the equator is not a simple east-west tilting or "seesaw" because of the phase and amplitude differences on opposite ends.

Katz et al. (1977) studied the seasonal change in slope of the dynamic topography along the equator from  $10^{\circ}\text{W}$  to  $40^{\circ}\text{W}$ . It was noted that the zonal pressure gradient was weak in spring and maximum in summer. A reasonable agreement was found between the vertically integrated pressure gradient and the zonal wind stress. Additional calculations by Lass et al. (1982) also indicated the zonal pressure gradient was weak in March-April and maximum in September-October. The east-west slope of the model pycnocline undergoes a similar seasonal cycle. A comparison of the zonal wind stress along the equator (Fig. 36a) and the equatorial height field (Fig. 35a) suggests this simple equilibrium response, with the ocean lagging slightly, holds true in the western half of the basin. In the east, changes in pycnocline depth do not appear to be consistent with local wind stress changes. Thus, the zonal pressure gradient is strongly dependent on the location in time and space. A high degree of temporal and spatial resolution by ocean measurements is needed to fully understand the seasonal pressure in time and space. A high degree of temporal and spatial resolution by ocean measurements is needed to fully understand the seasonal pressure gradient.

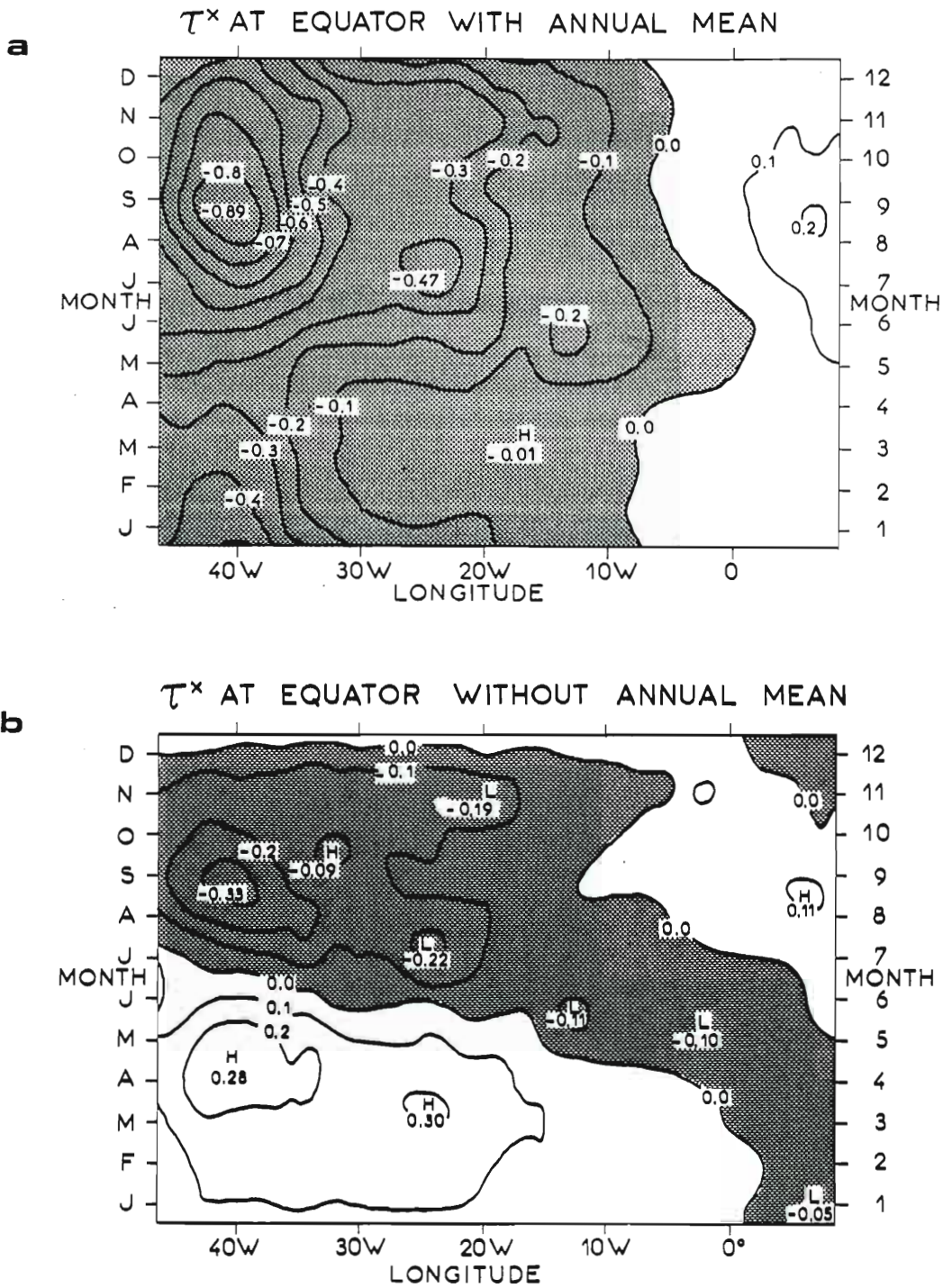


Fig. 36. Temporal variability of the zonal wind stress (dynes  $\text{cm}^{-2}$ ) along the equator. a) The annual mean has been included. Shaded regions indicate easterly wind stress. b) The annual mean has been removed. Shaded regions indicate an easterly wind stress perturbation.

Analysis of the pycnocline and zonal wind stress variability is simplified if the annual mean at each point in space is removed. It is now more evident (Fig. 35b) that the height field change is not a rigid oscillation about a fulcrum in the mid-Atlantic. The amplitude of the variability is largest in the west as are the winds. The annual and semiannual pycnocline displacements in the eastern Atlantic are significant but the overlying wind changes are small. The response at each boundary is in phase for roughly one-third of the basin width. There is also a lag between the minimum pycnocline depth in the east (July) and the maximum depth in the west (September-October). A similar lag appeared in the heat content calculations by Merle (1980a) and has recently been detected in thermocline depth variations (Houghton and Garzoli, personal communication, 1982).

The seasonal cycle of the equatorial model pycnocline indicates the upwelling season at the eastern boundary is not associated with any explicit eastward phase propagation. Based on climatology, the largest intensification of the equatorial easterlies (Fig. 36b) is in the western Atlantic from April to September. In terms of a single train of impulsive Kelvin waves, this would result in remotely forced upwelling at the eastern boundary on into October. Hence, there is no indication that the shallow pycnocline in July is induced by an eastward-propagating Kelvin wave front.

Kindle (1979) and Cane and Sarachik (1981) have studied the linear response of a zonally bounded equatorial ocean to periodic zonal forcing. The resulting periodic solution is a complex superposition of response of a zonally bounded equatorial ocean to periodic zonal forcing. The resulting periodic solution is a complex superposition of a locally forced response, equatorial Kelvin waves, Rossby waves, and

multiple wave reflections. The phase and amplitude of the total response depends on the Kelvin wave speed, the frequency of the forcing, and the width of the basin. These in turn determine the interference pattern set up by the various waves. Zonal phase gradients are therefore not necessarily indicative of any single propagating wave.

The analytical study of  $x$ -independent forcing by Cane and Sarachik (1981) included a case where an equatorial basin having the width of the Atlantic was driven by annual symmetric zonal winds. The equatorial response consisted of an east-west tilting of the pressure field about a point one-third of the basin width away from the western boundary. The maximum amplitude of the response was at the eastern boundary. Upwelling at the eastern boundary led downwelling at the western boundary by one month. The solution from the numerical calculation presented here is similar. Some of the differences are that the response in this study is largest at the western boundary and upwelling at the eastern boundary leads downwelling at the western boundary by two months. The influences of  $x$ -dependent forcing, higher frequency forcing, and non-constant basin width are among the reasons why the solutions will differ.

The importance of the local response and remotely forced equatorial waves will vary across the basin because there is a definite zonal structure to the equatorial wind field. Observations suggest that an equilibrium response exists between the zonal wind stress and the pressure gradient between  $10^{\circ}\text{W}$  and  $40^{\circ}\text{W}$ . In the western part of that an equilibrium response exists between the zonal wind stress and the pressure gradient between  $10^{\circ}\text{W}$  and  $40^{\circ}\text{W}$ . In the western part of the model basin the height field changes appear to be in qualitative

agreement with zonal wind stress fluctuations (Figs. 35, 36). The time history of each term in the x-momentum equation has been analyzed for several intervals along the equator. The seasonal cycles of  $c^2h_x$  and  $\frac{\tau^x}{\rho}$  in the western equatorial Atlantic are large in amplitude and nearly in phase. Most of the annual pycnocline variability in the western equatorial Atlantic is therefore associated with the overlying zonal wind stress changes. The influence of remote effects is small when compared with the magnitude of the locally forced signal. The pressure gradient lags the wind by about 10 days. This slight time delay produces a seasonal acceleration of the equatorial current. Lass et al. (1982) reported that the observed pressure gradient lags the wind stress by approximately one month. The seasonal amplitudes of the pressure gradient and wind stress terms in the eastern Atlantic are smaller than in the western Atlantic. The amplitude of the pressure gradient variation in the Gulf of Guinea is larger than the local wind stress amplitude. The seasonal cycles of the two are not in phase. It appears the response in the western equatorial Atlantic is predominantly local but not in the Gulf of Guinea.

The case studies incorporating partial forcing show that the annual equatorial variability in the western Atlantic is dominated by the local wind (Fig. 31a). Annual fluctuations of the zonal wind stress east of 25°W (Fig. 31b) have a measurable effect on the pycnocline depth in the west but the amplitude is much smaller than the locally forced response. The remote effect from the semiannual wind changes in the east are more important than the local 6 month period locally forced response. The remote effect from the semiannual wind changes in the east are more important than the local 6 month period wind oscillations in the west (Figs. 31c,d). However, the total

amplitude of the semiannual pycnocline displacements is much smaller than the annual cycle.

The annual pycnocline motion in the eastern equatorial Atlantic is comprised of equal contributions from zonal wind stress changes east and west of  $25^{\circ}\text{W}$  (Figs. 31a,b). The amplitude of the semiannual pycnocline displacement is half of the annual signal. This relatively large semiannual variation is responsible for the intriguing secondary upwelling season. The entire semiannual response induced by the zonal wind stress (Fig. 29) is a result of the forcing east of  $25^{\circ}\text{W}$  (Fig. 31d), there is no contribution from the semiannual wind field in the western Atlantic.

#### 4) eastern tropical response

Several mechanisms have been proposed in theoretical and observational studies to explain the coastal and equatorial variability in the eastern tropical Atlantic. A detailed review is provided by Picaut (1982). Philander and Pacanowski (1981a) modelled the relation between southerly winds, Rossby waves, advection, and coastal upwelling south of the equator. Berrit (1976) correlated SST with the local wind field along the southern coast of the Guinea Gulf. South of  $15^{\circ}\text{S}$  there was good agreement between strong southerly winds and low SST, but there was no correlation at all further north. Comparisons of offshore Ekman transports and coastal SST, provided by W. Wooster, yield the same conclusion (Picaut, 1982).

Along the northern coast of the Gulf of Guinea, Houghton (1976) determined there was no significant correlation between the coastal

Along the northern coast of the Gulf of Guinea, Houghton (1976) determined there was no significant correlation between the coastal wind and observed upwelling. Clarke (1978) tried to explain the

seasonal coastal upwelling off Ghana and the Ivory Coast using coastally trapped wave dynamics since the maximum alongshore wind stress (Fig. 23a) occurs to the east. Philander (1979) proposed that the seasonal variations of the cross-equatorial wind contribute to the intensification of the Guinea Current. An associated shoaling of the thermocline, needed to satisfy the geostrophic balance, would result in low SST.

Since there was a lack of evidence throughout the Gulf of Guinea in support of locally forced coastal upwelling, a remote forcing mechanism was offered by Moore et al. (1978). As illustrated by O'Brien et al. (1978) and Adamec and O'Brien (1978), a rapid increase of the zonal wind observed in the western Atlantic would excite an equatorially trapped Kelvin wave. The eastward-propagating wave front would reflect at the eastern boundary and induce a coastally trapped, poleward-propagating upwelling response symmetric about the equator. For nonseasonal events, Servain et al. (1982) found a good correlation between the zonal wind stress in the west and SST in the Gulf of Guinea. The correlation between local wind stress and SST was small. Picaut (1982) noted a southward propagation of the primary low SST episodes along the coast south of  $1^{\circ}\text{S}$ , westward propagation along the coasts of Benin-Togo-Ghana-Ivory Coast ( $3^{\circ}\text{E}$  to  $8^{\circ}\text{W}$ ), and a one month delay between the upwelling events at the equator and the Benin coast ( $5^{\circ}\text{N}$ ). An upward propagation of phase was detected for the summer upwelling event south of Abidjan and has recently been studied using a three-dimensional, remote-forcing model (McCreary et al., 1982). The upwelling event south of Abidjan and has recently been studied using a three-dimensional, remote-forcing model (McCreary et al., 1982). The secondary upwelling event observed later in the year has never been

explained satisfactorily. This event also propagates westward along the northern coast (Roy, 1981).

The seasonal displacement of the model pycnocline along the eastern boundary is presented in Fig. 37. Annual and semiannual coastal upwelling/downwelling events are symmetric about the equator. Poleward propagation of the seasonal signal is evident in both hemispheres. The amplitude of the coastal response decreases offshore while the phase increases. The variability along the northern and southern coasts is a symmetric response to equatorial Kelvin waves impinging on the boundary. Upon reflection, the zonal velocity associated with the incoming Kelvin waves must be eliminated to satisfy the no-flux condition at the coast. Thus, a finite number of Rossby waves and an infinite series of Hermite modes which asymptote to coastal Kelvin waves are generated to satisfy the boundary condition (Moore, 1968).

The most extensive monitoring of the thermal structure in the Gulf of Guinea has been performed by the Oceanographic Research Centers (ORSTOM) off of Abidjan, Ivory Coast and Pointe Noire, Congo. The seasonal movements of the model pycnocline are compared with the mean seasonal cycles of dynamic height (surface/300 db) at Abidjan and Pointe Noire in Fig. 38. Four marine seasons are simulated by the model with similar phase. The seasonal cycle of SST in these areas consists of a secondary cold season in December-January, a primary warm season from February to May, a major cold season from June to mid-October, and a secondary warm season around November (Berrit, 1961, 1962). Annual and semiannual contributions dominate the model



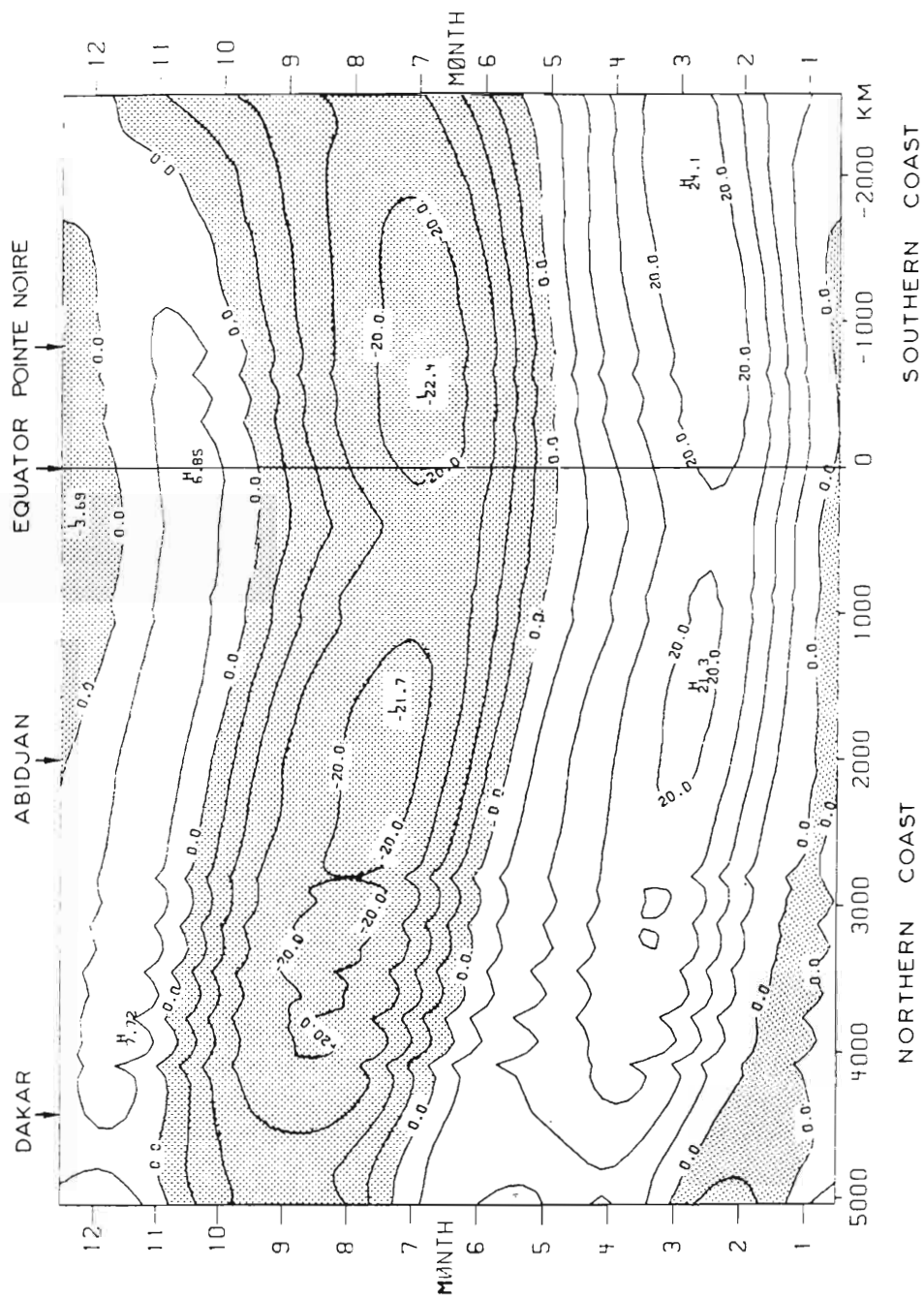


Fig. 37. Seasonal pycnocline displacements (meters) north and south along the eastern boundary. Shaded regions indicate the pycnocline is shallower than the annual mean. The zonal coast in the Guinea Gulf extends from +500 km to +2800 km.

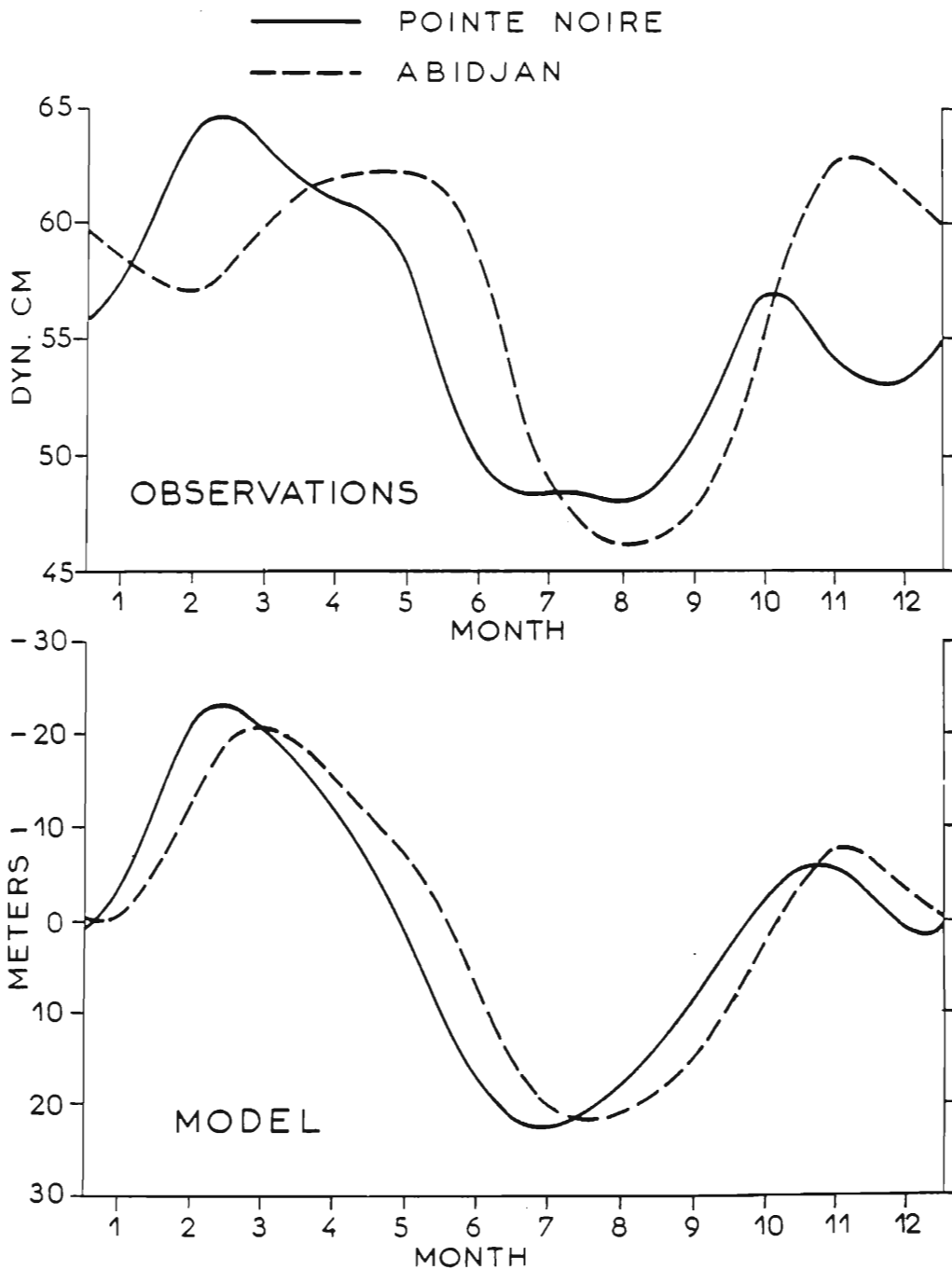


Fig. 38. Comparison of a) dynamic height for 0/300 db and b) model pycnocline depth at Abidjan (dashed) and Pt. Noire (solid). Negative values indicate the pycnocline is deeper than the annual mean.

Noire (solid). Negative values indicate the pycnocline is deeper than the annual mean.

pycnocline, observed thermocline depth, SST, and dynamic height. Temperature measurements at a depth of 15 m indicate the seasonal variability at Pointe Noire leads the comparable signal at Abidjan by one and a half months (Morliere, 1970). A similar lag is evident in the dynamic height signal (Fig. 38). The model pycnocline deviations at Pointe Noire have the same amplitude as at Abidjan but lead by two to three weeks.

The main region of low summer SST ( $22^{\circ}$ - $24^{\circ}$ C) extends along the northern coast of the Guinea Gulf west to  $8^{\circ}$ W,  $\sim$ 2500 km from the equator in Fig. 37 (Morlière and Rébert, 1972). The outbreak of low SST follows a dramatic upwelling of the thermal structure from April to August. In the model there is a notable diminution of this main upwelling signal 1000 km north of the observed limit (Fig. 37). Northward along the coasts of Senegal and Mauritania the surface waters are warm from July to October (Rossignol, 1972; Wooster et al., 1976), at this time atmospheric heating is maximum and the deviation from the mean coastal winds is downwelling favorable. Off Dakar a subsurface upwelling is present in late summer-early fall (Rossignol, 1972; Servain, personal communication, 1982) and may be related to the main upwelling occurrence in the Gulf of Guinea. The subsurface upwelling signal is strong enough to result in a sea level minimum at Dakar in September (Portolano, 1981); one month later than the sea level minimum at Abidjan. This apparent sinking of the upwelling event has been studied with a three-dimensional model by McCreary et al. (1982) via downward propagation of energy. In the present model we sacrifice studied with a three-dimensional model by McCreary et al. (1982) via downward propagation of energy. In the present model we sacrifice vertical resolution in order to treat the wind field and horizontal structure more realistically than in McCreary et al. (1982). Thus, the

main upwelling event along the coast of the Guinea Gulf, though weaker, is still present along the Senegal-Mauritania coasts.

Observations and the model results indicate an upwelling event along the coasts of Senegal and Mauritania early in the year. A large part of this event in the model is locally forced. The largest response to alongshore winds occurs in this region of the model. The local meridional wind stress is predominantly annual. The prevailing northerly wind is maximum in February and March. As suggested by Wooster et al. (1976) and Speth and Detlefsen (1982), the February upwelling along Senegal and Mauritania is mainly driven by the local winds. During the remainder of the year the local winds are not in phase with the pycnocline motion.

Many current measurements in the Gulf of Guinea have been taken on the continental shelf of the Ivory Coast within the Guinea Current. Observations by Lemasson and Rebert (1973) indicate the current is strongest in early summer and weakest in fall and again in late winter. The zonal coastal current from the model has been averaged between  $4^{\circ}\text{E}$  and  $11^{\circ}\text{W}$  (Fig. 39). The seasonal variations compare favorably with the observations: the maximum eastward current is in June-July and is near zero or reverses in February-March and October-November. The majority of the Guinea Current signal is associated with the basin-wide response to the zonal wind field. The meridional wind stress induces seasonal Guinea Current fluctuations one-fourth the size of the total response.

Away from the coastal regions much less is known about the seasonal variability in the eastern Atlantic. The model results

Away from the coastal regions much less is known about the seasonal variability in the eastern Atlantic. The model results indicate that the pycnocline displacements near the Guinea Dome are

# GUINEA CURRENT

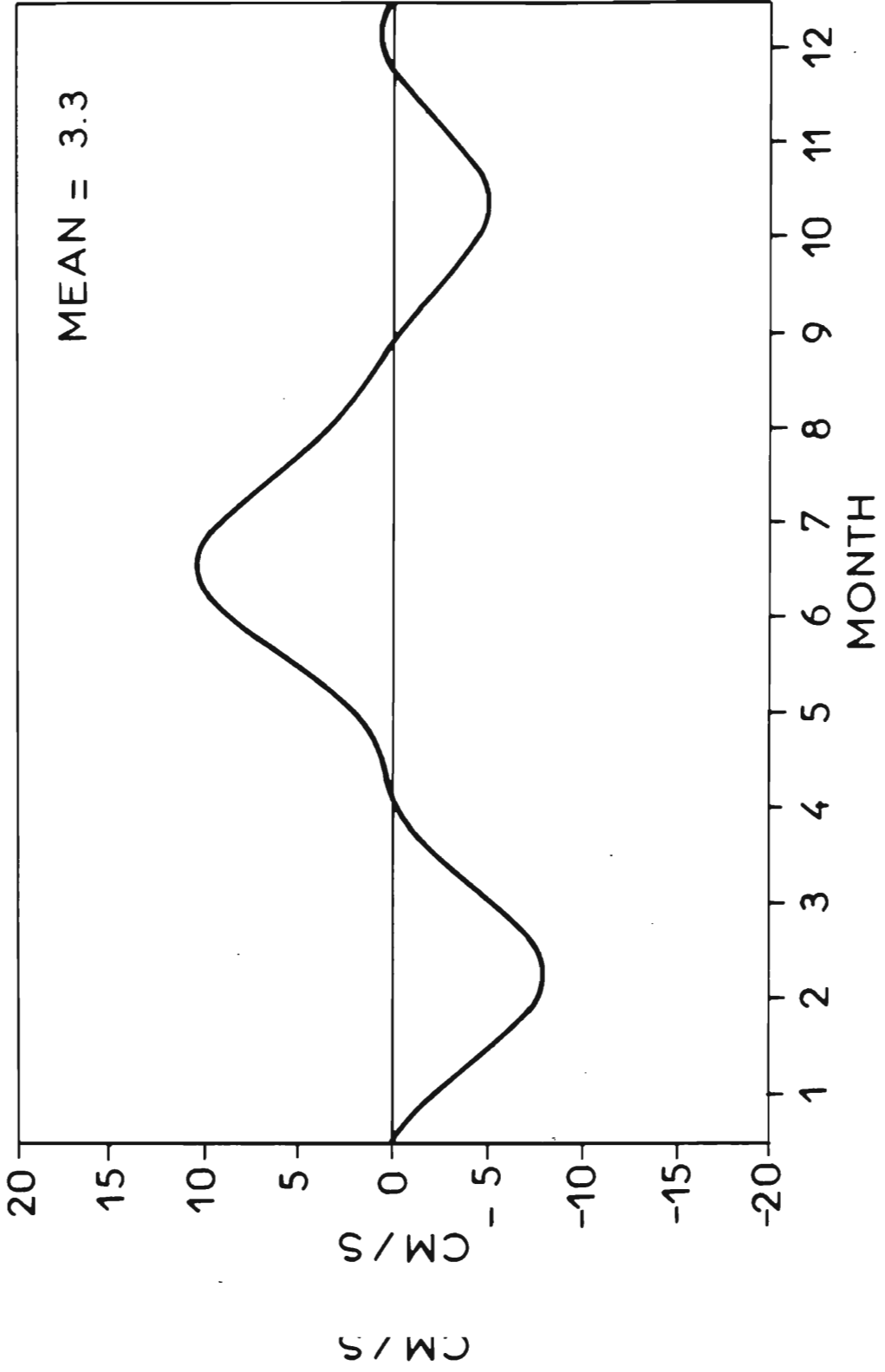


Fig. 39. Zonal velocity corresponding to a simulated Guinea current averaged along the coast between 4°E and 11°W.

small compared with the pycnocline excursions in the western and southeastern parts of the basin (Fig. 26). The pycnocline is deepest from March through May and shallow from August through October. The terms in (2) indicate the pycnocline movement north of the pivot line is governed by Ekman pumping. A cyclonic perturbation to the wind stress curl causes upwelling from May to September. The upwelling favorable wind stress curl is due to an increase in the meridional gradient of the zonal wind stress as the ITCZ migrates northward. Rossby wave effects are not important north of the pivot line. The Guinea Dome in this model is therefore more stationary than the Costa Rica Dome in a numerical simulation of the eastern Pacific discussed by Hofmann et al. (1981).

Near the eastern terminus of the pivot line ( $24^{\circ}\text{W}$ ,  $13^{\circ}\text{N}$ ) the pycnocline deviations are small (Fig. 26). The pycnocline is slightly deeper during the first six months of the year. There is little seasonal change in this area because the Ekman pumping and Rossby wave contributions are out of phase and have similar amplitudes. The pycnocline displacements are much larger to the south in a region of westward increasing phase. At  $20^{\circ}\text{W}$ ,  $7^{\circ}\text{N}$  the pycnocline is deepest in June and shallow in October-November. The seasonal signal is determined by Rossby waves which radiate away from the boundary throughout the year. Ekman pumping is second order. Observations in this area during GATE suggest that the local summer upwelling is not related to Ekman pumping (Perkins, 1981). The Rossby waves are upwelling favorable from June to November. The zonal phase gradient related to Ekman pumping (Perkins, 1981). The Rossby waves are upwelling favorable from June to November. The zonal phase gradient represents the phase speed of the nondispersive, westward-propagating

Rossby waves at this latitude. As evidenced by the phase distribution, the pivot line in the northeastern model basin separates regions influenced by the wind stress curl from regions influenced by Rossby waves.

The pycnocline movement at the center of the Angola Dome is smaller than and out of phase with the pycnocline motion within the Guinea Dome. Small contributions from the wind stress curl and Rossby waves produce the pycnocline deviations. The wind stress curl variability is several times smaller than in the Northern Hemisphere. Northeast of the Guinea Dome the influence of Ekman pumping is still small but the seasonal response is much larger. The phase lines and the vorticity equation imply that Rossby waves determine the seasonal cycle.

In the previous subsection it was demonstrated that the annual equatorial variability within the Gulf of Guinea was formed by equal contributions from the zonal wind stress on either side of 25°W. The entire semiannual pycnocline response was caused by wind forcing east of 25°W. The choice of 25°W as a dividing line had no *a priori* geographical significance because it is difficult to choose a mid-line for such a non-rectangular basin. It did however prove *a posteriori* to be a good choice for isolating the wind stress effects of different regions. Yet, the case studies did little to answer the question of whether the annual and semiannual variability in the Gulf of Guinea are locally or remotely forced.

A convenient definition of the Gulf of Guinea for the model are locally or remotely forced.

A convenient definition of the Gulf of Guinea for the model coastline geometry chosen is the region between the eastern boundary

and approximately  $10^{\circ}\text{W}$ . Additional case studies were performed in which the model ocean was driven by the zonal wind stress west of the Gulf of Guinea and another with the zonal forcing limited within the Guinea Gulf (Fig. 40). Comparison with Figs. 26 and 29 indicates that most of the annual variability in the Gulf of Guinea is remotely forced. This remotely forced periodic response is formed by the superposition of a train of equatorial Kelvin waves and their reflections as Rossby waves. The influences of annual zonal and meridional winds within the interior of the Gulf of Guinea are much smaller than the influence of the zonal wind stress west of  $10^{\circ}\text{W}$ . There is however a notable annual pycnocline response along the zonal coast driven by the zonal component of the southwesterly wind within the gulf (Fig. 40b), but this coastal signal is cancelled in the total forcing solution (Fig. 26a) by the effects of the meridional wind stress fluctuations at the eastern boundary ( $0^{\circ}$ - $4^{\circ}\text{N}$ ).

The response to semiannual forcing is somewhat different (Figs. 28b, 29b, 40c,d). Only half of the semiannual pycnocline signal is remotely forced by the zonal wind stress. The remaining half of the response is formed by equal contributions from zonal and meridional wind stress fluctuations within the Gulf of Guinea.



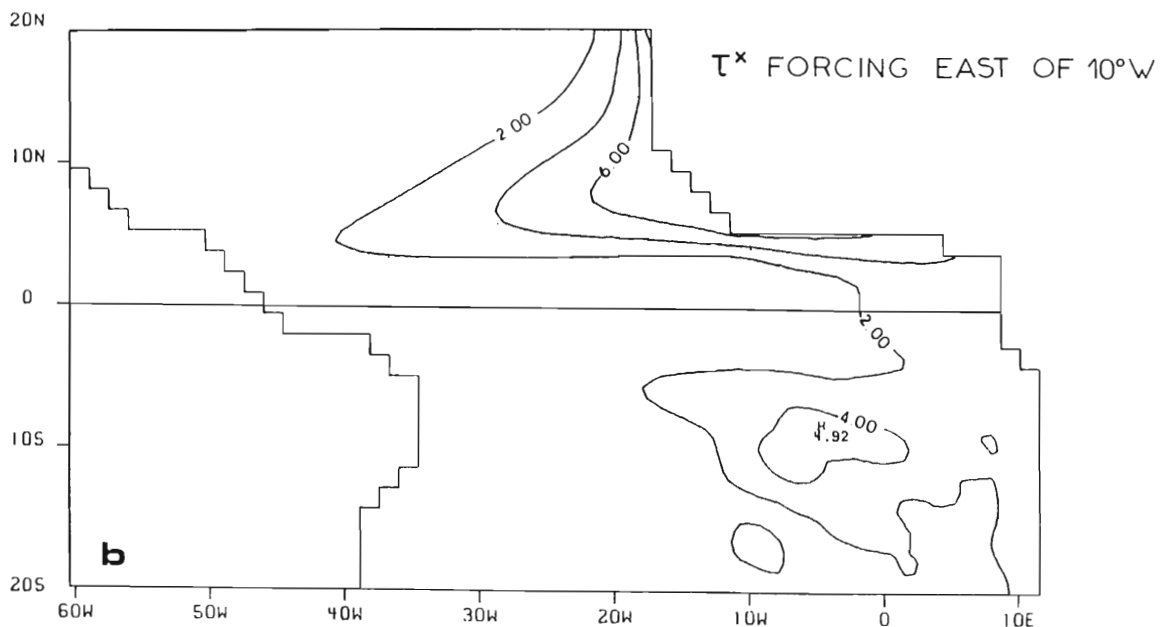
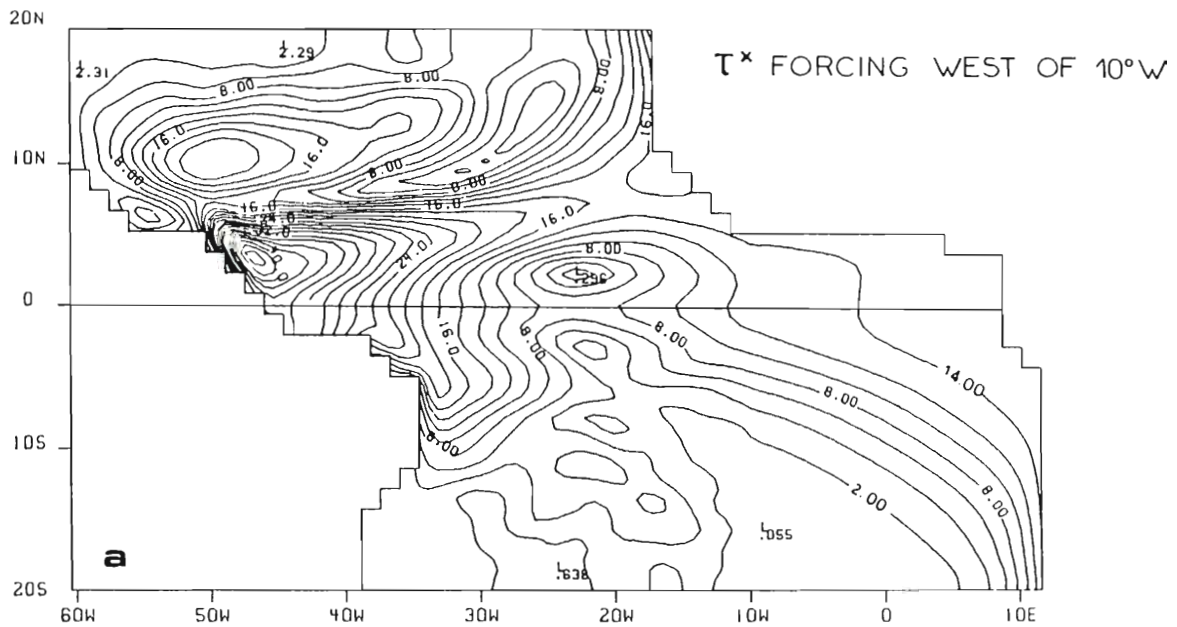


Fig. 40. Amplitude distributions for the pycnocline response to

- a) annual  $\tau^x$  forcing west of  $10^\circ\text{W}$
- b) annual  $\tau^x$  forcing east of  $10^\circ\text{W}$

Fig. 40. Amplitude distributions for the pycnocline response to

- a) annual  $\tau^x$  forcing west of  $10^\circ\text{W}$
- b) annual  $\tau^x$  forcing east of  $10^\circ\text{W}$

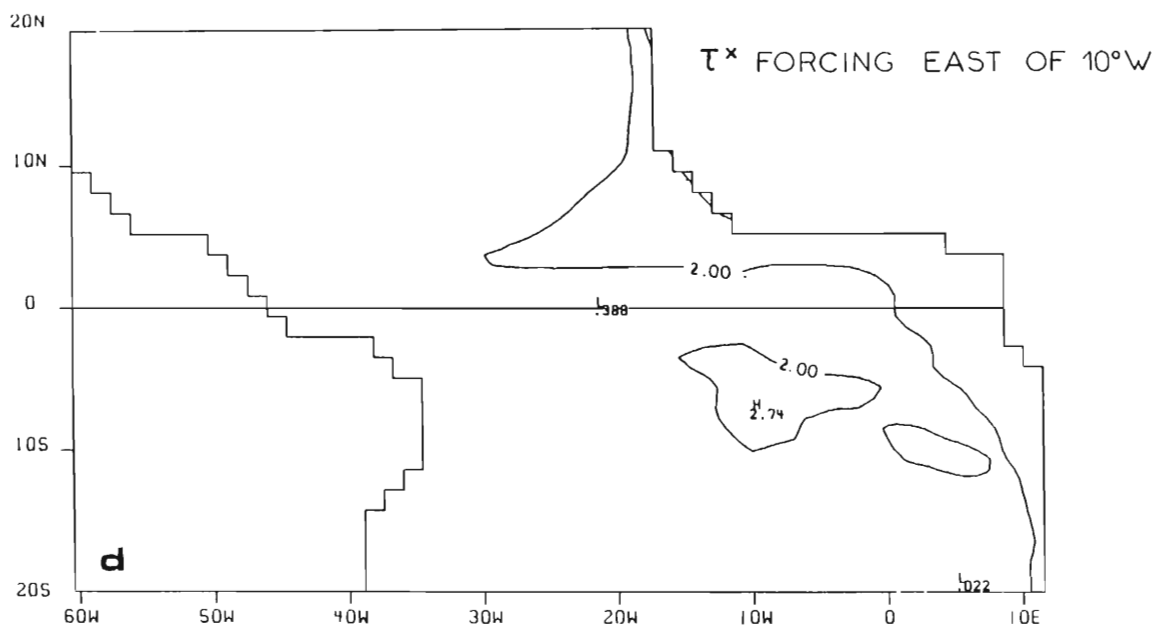
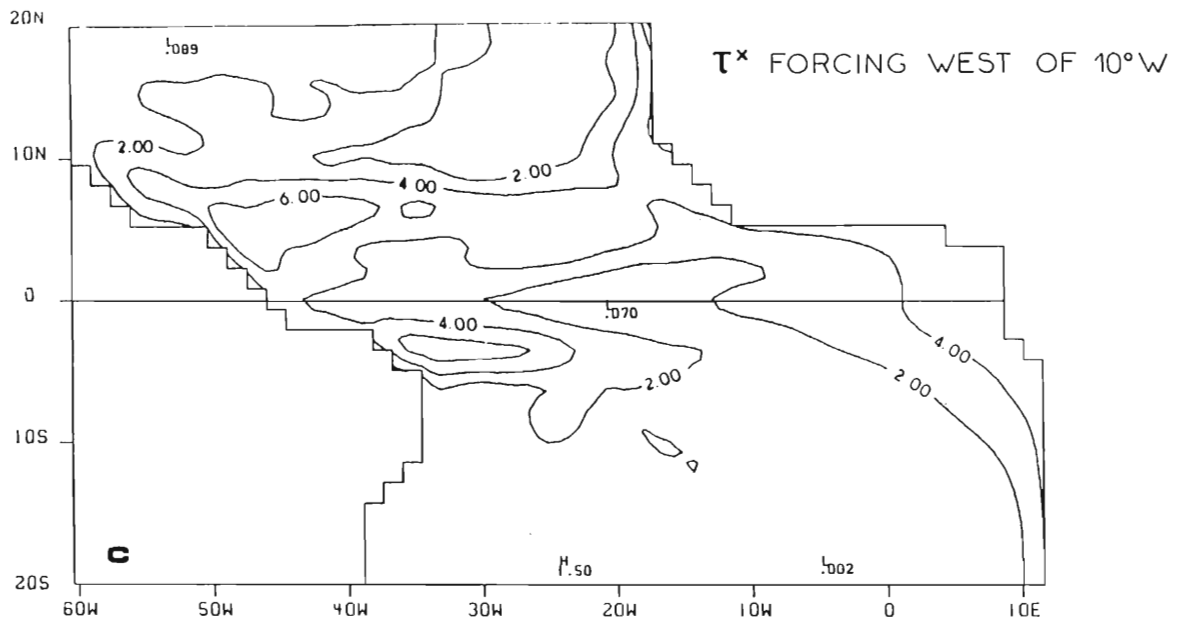


Fig. 40. Amplitude distributions for the pycnocline response to  
 c) semiannual  $\tau^X$  forcing west of  $10^\circ\text{W}$   
 d) semiannual  $\tau^X$  forcing east of  $10^\circ\text{W}$

Fig. 40. Amplitude distributions for the pycnocline response to  
 c) semiannual  $\tau^X$  forcing west of  $10^\circ\text{W}$   
 d) semiannual  $\tau^X$  forcing east of  $10^\circ\text{W}$

#### IV. SUMMARY

Linear numerical models incorporating a single baroclinic mode, realistic coastline geometries, and ship-board estimates of the surface wind fields have been used to interpret the wind-driven responses of two different tropical oceans. The first objective of this work was to analyze the interannual variability of the eastern, central equatorial, and western Pacific for a span of 18 years. The Pacific Ocean model was forced by monthly estimates of the observed surface wind field for 1961-1978. Such a model provides a straightforward way of assessing the basin-wide response to the overlying wind field in a manner that would not be possible by studying the wind field variability. Of interest during the period of study were several Los Niños. The character of these events in the model results and their relation to the forcing were described in detail.

The model pycnocline variability in the eastern Pacific was induced by internal, equatorially trapped Kelvin waves excited by fluctuations in the equatorial zonal wind stress in the western and central Pacific. The model pycnocline variability at the Galapagos Islands was remarkably similar to the observed sea level variability there. Cross correlation between the model pycnocline variability and observed sea level indicated a maximum significant correlation at zero lag. One important discrepancy between the model pycnocline time series and observed sea level was the presence of more high frequency lag. One important discrepancy between the model pycnocline time series and observed sea level was the presence of more high frequency

fluctuations in the pycnocline record.

The five Los Niños years of 1963, 1965, 1969, 1972, and 1976, were depicted as years when the pycnocline was anomalously deep. Los Niños of 1965 and 1969 have been classified as being the strongest for the 1960's. The variability of the southeast trades on both sides of the dateline was the cause of these two events in the model. The onset of the 1965 and 1969 Los Niños was due to the excitation of a large amplitude downwelling Kelvin wave front west of  $180^\circ$ . This Kelvin wave front was excited by a  $0.4 \text{ dynes cm}^{-2}$  relaxation of the easterly wind stress during the latter half of the year preceding El Niño. The relaxation in 1964 and 1968 was so large that the zonal wind stress changed from easterly to westerly. The timing of this Kelvin wave is such that it enhanced the remotely forced seasonal downwelling at the eastern boundary.

Besides the initial downwelling impulse, the 1965 and 1969 Los Niños were characterized by the persistence of a downwelled pycnocline. The pycnocline remained deep because the seasonal intensification of the central Pacific easterlies was not as strong as during non-El Niño years. The upwelling Kelvin waves excited were small in amplitude. Hence, the pycnocline was not significantly upwelled. This lack of a normal seasonal upwelling kept the pycnocline deeper than normal throughout the Los Niños years. Towards the end of 1965 and 1969 the semiannual variability of the interior easterlies was reestablished. The resulting downwelling Kelvin wave front generated towards the end of the year created the second major downwelling pulse of the El Niño. The resulting downwelling Kelvin wave front generated towards the end of the year created the second major downwelling pulse of the El Niño.

year. This completed the double-peak downwelling signature characteristic of the 1965 and 1969 Los Niños events.

In contrast, the minor El Niño of 1963 was only influenced by the wind stress variability east of  $180^\circ$ . During 1962 there was not a large relaxation of the wind field west of the dateline. After the seasonal downwelling at the beginning of 1963 there was a cessation of the semiannual intensification of the southeast trades. The pycnocline remained depressed throughout 1963 and did not recover until 1964.

Anomalous changes in the wind field leading up to the model expression of the 1972 El Niño began with an eastward progression of weakening trade winds west of the dateline in late 1971. A nearly simultaneous intensification of the central equatorial easterlies negated any influence from the west. This resulted in mean annual pycnocline depths at the eastern boundary in early 1972. From January through April a significant decrease of the zonal wind stress between  $120^\circ\text{W}$  and  $180^\circ$  excited a downwelling Kelvin wave front responsible for deep pycnocline depths at the eastern boundary in June. Observations indicated unusually high sea level for the same period. Late in the year, a relaxation of the easterlies at  $100^\circ\text{W}$ - $140^\circ\text{W}$  created a second downwelling episode, smaller relative to that in June. A second peak in sea level was observed at the end of the year. Intensification of the trade winds in January of 1973 led to a recovery from the 1972 El Niño.

Wind changes and their effects associated with the 1976 El Niño were similar to 1972. An eastward progression of weakening trade winds  
Wind changes and their effects associated with the 1976 El Niño  
were similar to 1972. An eastward progression of weakening trade winds

began west of  $160^{\circ}\text{E}$  in late 1975 and generated a downwelling Kelvin wave front. As opposed to late 1971, the winds in the central Pacific did not intensify. Thus, the model pycnocline was deep along the eastern boundary at the beginning of 1976. A decrease in the equatorial easterlies between  $140^{\circ}\text{W}$  and  $180^{\circ}$  during the first several months of 1976 was once again responsible for the deep model pycnocline at the eastern boundary in June of the El Niño year. Additional weakening of the wind stress in the central Pacific produced a final downwelling burst later in the year. The recovery phase began with intensified easterlies in December.

There was one major difference between the simulated Los Niños of the 1970's and those of 1965 and 1969. For the 1960's events, observed sea level was highest and the model pycnocline was deepest towards the beginning and end of the El Niño year in the eastern Pacific. During the 1972 and 1976 El Niño occurrences, elevated sea level and maximum pycnocline depth were in June. Common to all these events was a weakening of the trade winds west of the dateline late in the preceding year. The model pycnocline was deep in June of 1972 and 1976 because the central equatorial easterlies had decreased considerably from January to April. The pycnocline was not deep in mid-1965 or mid-1969 because the trade winds in the central Pacific did not weaken during the first four months of the year. Thus, during the 1970's the easterlies in the central equatorial Pacific had more of an active role in the evolution of El Niño than in the previous decade. This in turn implies there are important differences in the location and timing of in the evolution of El Niño than in the previous decade. This in turn implies there are important differences in the location and timing of the wind changes responsible for each El Niño.

The El Niño sequence of initial wind relaxation west of the dateline followed by weakening or quiescent winds in the central Pacific did not apply to 1975. This event began when winds west of the dateline decreased in late 1974 similar to the type of relaxation prior to an El Niño. A downwelling Kelvin wave was excited and resulted in a deep pycnocline at the eastern boundary in early 1975. The similarity with an El Niño event stopped there. After the initial weakening, the winds intensified and remained anomalously strong for the remainder of the year. At the eastern boundary, there was a rapid upwelling and the model pycnocline remained shallow. Hydrographic observations in the eastern Pacific indicated El Niño type conditions were present at the beginning of 1975 but soon deteriorated (Wyrтки et al., 1976).

The interannual variability in the western tropical Pacific was characterized by a shoaling of the model pycnocline and an observed drop in sea level in all El Niño years. Maximum changes in model pycnocline depth and observed sea level occurred at 5°N-10°N. Truk Island at 7.5°N, 151.9°E is in a strategic position to monitor these fluctuations. The model pycnocline time series at Truk was highly correlated at zero lag with the observed sea level record. A majority of the pycnocline variability at Truk was due to westward-propagating, third latitudinal mode Rossby waves.

The shallow pycnocline and low sea level at the end of the El Niño year was attributed to an upwelling Rossby wave front excited by a decrease in the trade winds to the east. Related wind changes at the equator were responsible for downwelling at the eastern boundary in the decrease in the trade winds to the east. Related wind changes at the equator were responsible for downwelling at the eastern boundary in the

middle and end of the El Niño year. This accounts for the out-of-phase relation between the eastern and western tropical Pacific during the El Niño simulations.

The meridional structure of the zonal wind stress variability between 160E and 140W indicated that the largest perturbation to the wind field during El Niño was not symmetric about the equator and involved the northeast trades. The seasonal weakening of the northeast trades was larger in area and closer to the equator ( $5^{\circ}\text{N}$ - $10^{\circ}\text{N}$ ) during the 1972 and 1976 Los Niños. A simple analytical model forced by an idealization of this weakening yielded an upwelling Rossby wave response in both hemispheres west of the forcing with maximum upwelling at  $7^{\circ}\text{N}$ , 1.5 months after the minimum wind forcing. When the idealized forcing consisted of decreasing southeast trades symmetric about the equator at the beginning of the El Niño year, followed by the El Niño weakening of the northeast trades, and a subsequent recovery of the northeast trades, the response at  $7^{\circ}\text{N}$ - $8^{\circ}\text{N}$  was in qualitative agreement with the model pycnocline variability at Truk during the 1972 and 1976 events. The oceanic response is strongly dependent on the location of the weakened trade winds. This may account for differences between the seasonal and nonseasonal response in the western tropical Pacific. When the center of the northeast trade wind forcing was shifted to  $10^{\circ}\text{N}$ , similar to the normal location of the maximum seasonal weakening, the low-latitude response was considerably smaller and the maximum response was displaced northward more than the shift of the forcing.

response was displaced northward more than the shift of the forcing.



In the central equatorial Pacific, limited sea level records were available for Canton Island and Christmas Island. This is an area for which there are important wind changes to the east and west during El Niño. These islands are therefore subject to the influence of equatorially trapped Kelvin waves excited to the west and long Rossby waves generated to the east. Since these islands are located  $2^{\circ}$ - $3^{\circ}$  from the equator, the Kelvin wave amplitude is reduced and the Rossby wave amplitude is increased relative to that at the equator.

Decomposition of the model pycnocline variability at these islands indicated that almost all of the signal was due to Kelvin waves and first latitudinal mode Rossby waves. The superposition of Kelvin and Rossby waves during El Niño, changes from one event to another depending on the location and timing of the forcings. Analysis of sea level variability in the central equatorial Pacific is therefore difficult because Kelvin wave signals generated in the west and ultimately causing pycnocline displacements in the east may be masked temporarily by a superposition with Rossby waves of opposite sign.

The second objective of this work was to study the linear, dynamic oceanic response to the seasonally varying wind field of the tropical Atlantic. A linear, single baroclinic mode model driven by the climatological seasonal wind stress was used. Based on previous studies implying the dominance of the second baroclinic mode in the tropical Atlantic, an equivalent depth of 19 cm ( $c = 137 \text{ m s}^{-1}$ ) was chosen for the gravest mode of this calculation. The coastline geometry of the model was an idealization of the tropical Atlantic chosen for the gravest mode of this calculation. The coastline geometry of the model was an idealization of the tropical Atlantic

basin from 20°N to 20°S. Monthly estimates of the Atlantic surface wind field on a 1° x 1° mesh averaged over 60 years (Hastenrath and Lamb, 1977) provided the basis for the seasonal periodic forcing function. Important regions of variability were identified for the atmosphere and ocean. Of interest were the physical mechanisms responsible for the seasonal signal of key features such as the meridional topography in the western Atlantic, the equatorial pressure gradient, and the response within the Gulf of Guinea. Observations of the seasonal cycle throughout the tropical Atlantic were compared with the results of the simple model to ascertain whether the simulated response had any relevance.

The mean topography of the model pycnocline consisted of a series of troughs and ridges bounding the various equatorial currents. The combined effects of wind stress curl and cross-equatorial winds determined the meridional structure. The distribution of the pycnocline features compared favorably with observed dynamic topography except at 8°S off the Brazilian coast. At this location sparse data indicate a ridge is present in the dynamic topography but there is no corresponding permanent formation in the model.

The modelled seasonal response to the Atlantic wind field, depending on the location, consists of a combination of a locally forced response, Kelvin waves, Rossby waves, and multiple wave reflections. Throughout the tropical Atlantic basin the seasonal cycles of the atmospheric forcing, the observed dynamic height, and the model pycnocline depth are largely annual and semiannual. In general, there atmospheric forcing, the observed dynamic height, and the model pycnocline depth are largely annual and semiannual. In general, there

is a reasonable comparison between the phase and amplitude distributions of the observed dynamic height and the model pycnocline depth.

The largest amplitudes of the dynamic height and pycnocline fields are in the western Atlantic. Observations and the model results indicate the northwest part of the basin is characterized by a north-south tilting about a pivot line which roughly parallels the mean position of the ITCZ. The pivot line separates two regions of large amplitude pycnocline displacements which are out of phase. North of the pivot line ( $\sim 10^\circ\text{N}$ ) wind stress curl and divergence of the Ekman transport govern the annual response. An increase of the zonal wind stress and an anticyclonic perturbation to the wind stress curl during the first half of the year cause the pycnocline to deepen. The ITCZ is displaced southward at this time. The pycnocline response south of the pivot line is a combination of local and remote effects. An influx of the southeast trades from June to November when the ITCZ is shifted northward produces an anticyclonic perturbation to the wind stress curl. From March to August westward-propagating Rossby waves are downwelling favorable. The two processes combine to produce a seasonal deepening of the pycnocline from May through September. Close to the equator the pycnocline deepens during the same period as the easterlies intensify. These two regions of significant pycnocline fluctuations determine the seasonal strength and location of the trough and ridge which bound the NECC in the western Atlantic. The meridional pressure gradient between these features has a large annual signal. The resulting NECC is strongest in August and is non-descript in April. The meridional pressure gradient between these features has a large annual signal. The resulting NECC is strongest in August and is non-descript in April.

There is only one area of large pycnocline variations south of the equator because only one trade wind system is present, i.e., there is no analog to the ITCZ. Notable pycnocline displacements at  $6^{\circ}\text{S}$  are induced by Ekman pumping and Rossby waves. An increase in the southeast trades from July through January causes a locally forced downwelling contribution. Remotely forced Rossby waves have the same phase as north of the equator. The total response results in downwelling from June through November.

Observations and model results along the equator indicate an east-west tilting of the pycnocline. Large model pycnocline displacements in the west are a locally forced near-equilibrium response between the annual zonal wind stress and the zonal pressure gradient. Effects from the annual zonal wind stress in the east and the basin-wide semiannual zonal wind field are present but smaller in comparison to the locally forced annual response. The equatorial zonal pressure gradient in the eastern Atlantic is not balanced by the local wind stress. Annual equatorial pycnocline movements in the east are the response to equal contributions of the zonal wind stress on each side of  $25^{\circ}\text{W}$ . All the semiannual pycnocline motion in the eastern equatorial Atlantic is associated with wind changes east of  $25^{\circ}\text{W}$ . In agreement with observations, the minimum pycnocline depth in the east (July) leads the maximum depth in the west (September-October).

The pivot line in the northeastern part of the basin separates regions influenced by the wind stress curl from areas influenced by Rossby waves. The curl of the wind stress north of the pivot line regions influenced by the wind stress curl from areas influenced by Rossby waves. The curl of the wind stress north of the pivot line determines the vertical displacement of the model pycnocline. The

pycnocline is shallow from August through October in this area which includes the Guinea Dome. Large pycnocline movements south of the pivot line are produced by Rossby waves radiating away from the eastern boundary. The influence of Ekman pumping is small there. The pycnocline displacements between these two regions are negligible because Rossby waves and Ekman pumping have similar amplitudes and are out of phase along the pivot line.

The seasonal variations of the wind stress curl in the southeastern part of the basin are much smaller than north of the pivot line. Most of the pycnocline motion is driven by Rossby waves. Pycnocline fluctuations within the Angola Dome are smaller than within the Guinea Dome and have opposite phase.

The simulated seasonal signal at the eastern boundary is symmetric about the equator. Pycnocline displacements along the northern and southern coasts are related to the reflection of annual and semiannual frequency equatorial Kelvin waves which are part of the forced periodic response of the basin. The phase of the eastern boundary response is similar to that observed at various coastal stations. Of particular importance are the simulations of the major (mid-year) and secondary (year-end) upwellings and the isolation of the forcing responsible. The only significant contribution from meridional winds is along the coasts of Mauritania and Senegal. Large fluctuations in the alongshore wind stress produce an upwelling season in February.

Case studies in which the model was forced by various partitions of the wind field indicate the annual wind-driven variability in the

Case studies in which the model was forced by various partitions of the wind field indicate the annual wind-driven variability in the Gulf of Guinea is remotely forced. Fluctuations of the zonal wind

stress west of  $10^{\circ}\text{W}$  are responsible for a majority of the simulated annual pycnocline displacements in the Gulf of Guinea. The annual zonal wind east of  $10^{\circ}\text{W}$  has only a secondary influence along the zonally oriented coast which is cancelled by meridional wind stress variations at the eastern boundary. The dominant response in the Guinea Gulf is a superposition of annual Kelvin waves excited by zonal equatorial wind changes to the west and Rossby waves generated by the reflection of the Kelvin waves at the boundary. Thus, the major summer upwelling is primarily a response to changes in the equatorial easterlies remote from the Gulf of Guinea. Half of the semiannual pycnocline signal in the Gulf of Guinea is forced by 6 month period zonal wind stress oscillations west of  $10^{\circ}\text{W}$ . The remaining portion of the signal comes from zonal and meridional winds within the gulf. This suggests the secondary winter upwelling season is an expression of wind variability remote from and within the Gulf of Guinea.

## V. DISCUSSION AND CONCLUSIONS

The results of the Pacific Ocean model demonstrate that interannual changes of the zonal wind stress in the central and western Pacific are very important in determining the sea level/pycnocline responses of El Niño. For most Los Niños during the period of study the onset phase was linked to perturbations to the zonal wind field in the western Pacific. How the El Niño event progressed and matured was subsequently determined by the nature of the wind field in the central Pacific. Recently, it was noted (Keen, 1982) that there is often a greater incidence of tropical cyclone pairs in the western Pacific prior to El Niño. A succession of these disturbances, at times penetrating east of 180°, results in strong eastward perturbations to the wind field several times per month. In the future it will be necessary to determine how these high frequency disturbances affect the wind field monthly means. It would be of interest to know how the model results would change if there was a greater temporal resolution of the wind field.

The season in which an anomalously deep pycnocline occurs might have important ramifications for determining the size of anomalous SST. For the El Niño events of the 1960's the model pycnocline was anomalously deep during the periods of seasonal warming in the Southern Hemisphere. For the El Niño events of the 1970's the pycnocline was deepest during the low SST season and SST anomalies were larger than Hemisphere. For the El Niño events of the 1970's the pycnocline was deepest during the low SST season and SST anomalies were larger than

in the previous decade. Does a depression of the thermocline during the auroral fall and winter result in a larger positive SST anomaly than a thermocline depression in summer? Modelling efforts including thermodynamics will provide the information needed to understand relations between thermocline depth, vertical velocity, and SST.

The results of this numerical simulation have also provided some information regarding monitoring the tropical Pacific wind field. In view of the correlations between the model results and observations at several locations, important fluctuations in the low latitude surface wind field must have been large enough in space and time to have been resolved by ship-board estimates. Admittedly, there are several problems with this method of observing the wind field, but it is the only data set available suitable for interannual modelling studies. Nonetheless, this study has demonstrated a definite need for continuous monitoring of the detailed structure of the entire tropical Pacific wind field.

With respect to real-time wind monitoring, the simulations of the El Niño events for 1961-1978 indicate that a predictive capability for El Niño will not be straightforward. At the present time, persistence of anomalous conditions in the tropical atmosphere cannot be predicted. An example of why this is important is the aborted event of 1975 when the winds in the western Pacific initially weakened in a manner similar to the onset of previous El Niño events. Shortly thereafter the winds abruptly intensified and remained strong. Monitoring a significant abruptly intensified and remained strong. Monitoring a significant



wind relaxation without knowledge of a subsequent intensification may lead to an erroneous El Niño prediction. Furthermore, equal weight must be given to all regions when monitoring the tropical Pacific wind field. As illustrated by the conditions during the first several months of 1972, an anomalous decrease in the trade winds in the western Pacific may be followed by an intensification of the winds in the central Pacific. The net result of such circumstances being no change in the eastern Pacific.

The wind-driven modelling results presented here have shown that a significant amount of the observed interannual sea level variability in the eastern, central equatorial, and western Pacific can be accounted for by linear theory when reasonable estimates of the wind field are provided. Internal Kelvin and Rossby waves play important roles in determining the variability throughout the tropical Pacific. Drastic shoaling of the pycnocline in the western Pacific during El Niño may be induced by Rossby waves excited by changes in strength and position of the northeast trades. In the eastern tropical Pacific, remotely forced Kelvin waves generated in the central and western equatorial Pacific are responsible for the El Niño pycnocline displacements. By definition El Niño is associated with elevated SST but at present the cause and effect relation of a Kelvin wave induced deep thermocline and SST is not understood.

Even though there was some agreement between observations and the results of the Atlantic Ocean model there were several limitations to results of the Atlantic Ocean model there were several limitations to

this work. The model was constrained to be linear and consisted of a single baroclinic mode. The vertical resolution was therefore poor and wind induced changes to features such as the undercurrent could not be studied. In addition, the effects of downward energy propagation could not be determined. It is not known whether nonlinearities or the vertical propagation of Kelvin waves and Rossby waves will significantly alter the superposition constituting the forced periodic response. The lack of any thermodynamics precluded any firm understanding of the SST variability in regions where pycnocline depth and SST are uncorrelated. A prime example is the Senegal and Mauritania coasts where there are important differences between the surface and subsurface thermal structure.

Another limitation of this study was the use of climatological wind data to represent the seasonal cycle. Averaging the wind field over many decades results in smaller temporal variations than may occur in a particular year. This approach was chosen rather than having to make a subjective judgement of which year had "typical" seasonal variations. This was not a severe limitation for the present study since most descriptions of the seasonal cycle in the tropical Atlantic Ocean are based on time averaged observations. The results from the numerical calculation were dependent on this wind field having the same periodicity from one year to the next. A periodic solution was thereby allowed to develop. This was achieved at the equator in less than one year.

Since annual local forcing was not important in the Gulf of Guinea, the phase of the annual response was dependent on the interfer-

Since annual local forcing was not important in the Gulf of Guinea, the phase of the annual response was dependent on the interference pattern of a continuous series of annual frequency Kelvin waves

excited by the equatorial wind field in the west and the Rossby waves reflected at the boundary. In contrast, the response of an equatorial ocean to impulsive forcing is a single eastward-traveling Kelvin wave front which reflects at an eastern boundary as a train of westward-propagating Rossby waves. This was the premise used by Moore et al. (1978), O'Brien et al. (1978), and Adamec and O'Brien (1978) as a possible explanation of the seasonal upwelling in the Gulf of Guinea. A rapid seasonal increase of the easterlies in the western equatorial Atlantic would excite an upwelling Kelvin wave front.

The impulsive remote forcing hypothesis assumes that the upwelling at the eastern boundary lags the wind change in the west by the time required for a Kelvin wave to travel from the forcing region to the eastern boundary. Climatology indicates the initial strengthening of the easterlies takes place in the mid-Atlantic and then progresses westward (Fig. 27). The most dramatic wind changes are in the western Atlantic where the easterlies continue to increase after the peak upwelling in the Gulf of Guinea. This suggests the timing may not be correct for the impulsively excited Kelvin wave concept. However, a rapid increase of the easterly wind in spring 1979 at St. Paul Rocks,  $0^{\circ}55'N$ ,  $29^{\circ}21'W$  (Katz et al., 1981), which is not unusual (Servain et al., 1982), indicates that the impulsive forcing idea might still be relevant for specific years. Servain et al. (1982) also found a good correlation between nonseasonal perturbations of the zonal wind stress in the western Atlantic and nonseasonal SST in the Gulf of Guinea. The SST lagged the remote winds by one month; the time it would take a in the western Atlantic and nonseasonal SST in the Gulf of Guinea. The SST lagged the remote winds by one month; the time it would take a

$1 \text{ m s}^{-1}$  phase speed Kelvin wave to travel from the forcing area to the Gulf of Guinea. Interannual short time scale events observed in the Gulf of Guinea thermal structure have also been compared with the El Niño phenomena of the eastern Pacific (Hisard, 1980; Merle, 1980b). It has been suggested that these episodes may have important implications for fisheries, coastal rainfall, and cyclogenesis.

An interannual calculation similar to the Pacific Ocean study is needed to address these differences between the climatological seasonal cycle and the seasonal signal of an individual year. The difference between the forced periodic response and the seasonal cycle from one year to the next could then be determined. It would also be of interest to know how the seasonal response would change if the temporal resolution of the wind field was increased. At present no such data set exists.

The Atlantic study has demonstrated that a significant part of the seasonal dynamic height signal can be accounted for via linear, periodic, wind-driven processes. As previous modelling studies of the seasonal and interannual variability of the tropical Pacific have shown, the oceanic response can be studied with some degree of skill if a realistic estimate of the wind field variability is provided. The degree of comparability is affected by the limitations of the observations and the model. Since the observed variability is imprecise a simple linear model is adequate for simulating the oceanic response. The wind driven response in this simulation was a combination of local and remote forcing effects which were strongly response. The wind driven response in this simulation was a combination of local and remote forcing effects which were strongly

dependent on location. Only the northernmost and western equatorial parts of the basin were totally dominated by local forcing. Therefore, continuous monitoring of the entire tropical Atlantic surface wind field at small time and space scales is vital to our understanding of the seasonal oceanic response.

## REFERENCES

- Adamec, D., and J. J. O'Brien, 1978: The seasonal upwelling in the Gulf of Guinea due to remote forcing. J. Phys. Oceanogr., 8, 1050-1060.
- Anderson, D., 1979: Low latitude seasonal adjustment in the Atlantic (unpublished manuscript).
- Bakun, A., 1978: Guinea current upwelling. Nature, 271, 147-150.
- Barnett, T. P., 1977: An attempt to verify some theories of El Niño. J. Phys. Oceanogr., 7, 633-647.
- Berrit, G. R., 1961: Contribution à la connaissance des variations saisonnières dans le Golfe de Guinée. Observations le long des lignes de navigation. Cah. ORSTOM, sér. Océanogr., 13, 715-727.
- \_\_\_\_\_, 1962: Contribution à la connaissance des variations saisonnières dans le Golfe de Guinée. Observations le long des lignes de navigation. Cah. ORSTOM, sér. Océanogr., 14, 663-673.
- \_\_\_\_\_, 1976: Les eaux froides côtières du Gabon à l'Angola sont-elles dues à un upwelling d'Ekman? Cah. ORSTOM, sér. Oceanogr., 14, 273-278.
- Bogorov, V. G., and Collaborators, 1973: Tropical cyclonic macrocirculation systems and their role in the formation of the ocean structure. in Formation of biological productivity and bottom sediments as related to ocean circulation in the south-eastern Atlantic, Transactions of the P.P. Shirsov Institute of Oceanology, 95, 1-13.
- Boisvert, W. E., 1967: Major currents in the North and South Atlantic Oceans between 64°N and 60°S. Naval Oceanographic Office. Technical Report 193, pp. 92.
- Bunker, A. F., 1976: Computations of surface energy flux and annual air-sea interaction cycles of the North Atlantic Ocean. Mon. Wea. Rev., 104, 1122-1140.
- Busalacchi, A. J., and J. J. O'Brien, 1980: The seasonal variability in a model of the tropical Pacific. J. Phys. Oceanogr., 10, 1929-1951.
- Camerlengo, A. L., and J. J. O'Brien, 1980: Open boundary conditions in rotating fluids. J. Comp. Phys., 35, 12-35.
- Cane, M. A., and E. S. Sarachik, 1977: Forced baroclinic ocean motions: I. The linear equatorial bounded case. J. Mar. Res., 35, 395-432.
- Camerlengo, A. L., and J. J. O'Brien, 1980: Open boundary conditions in rotating fluids. J. Comp. Phys., 35, 12-35.
- Cane, M. A., and E. S. Sarachik, 1977: Forced baroclinic ocean motions: II. The linear equatorial bounded case. J. Mar. Res., 35, 395-432.

- \_\_\_\_\_, and E. S. Sarachik, 1981: The response of a linear equatorial ocean to periodic forcing. J. Mar. Res., 39, 651-693.
- Clarke, A. J., 1978: On the generation of the seasonal coastal upwelling in the Gulf of Guinea. J. Geophys. Res., 84, 3743-3751.
- Davis, R. E., 1976. Predictability of sea surface temperature and sea level pressure anomalies over the North Pacific Ocean, J. Phys. Oceanogr., 6, 249-266.
- Emery, W. J., 1975: Dynamic height from temperature profiles. J. Phys. Oceanogr., 5, 369-375.
- Enfield, D. B., and J. S. Allen, 1980: On the structure and dynamics of monthly mean sea level anomalies along the Pacific coast of North and South America. J. Phys. Oceanogr., 10, 557-578.
- Goldenberg, S. B., and J. J. O'Brien, 1981: Time and space variability of tropical Pacific wind stress. Mon. Wea. Rev., 109, 1190-1207.
- Hastenrath, S., 1976: Variations in low-latitude circulation and extreme climatic events in the tropical Americas. J. Atm. Sci., 33, 202-215.
- \_\_\_\_\_, and P. J. Lamb, 1977: Climatic atlas of the tropical Atlantic and Eastern Pacific Oceans. University of Wisconsin Press, Madison, 97 charts.
- Hellerman, S., 1980: Charts of the variability of the wind stress over the tropical Atlantic. GATE Sup. II Deep Sea Res., 26, 63-75.
- Hickey, B., 1975: The relationship between fluctuations in sea level, wind stress and sea surface temperature in the equatorial Pacific. J. Phys. Oceanogr., 5, 460-475.
- Hickie, B. J., 1977: The effects of coastal geometry on equatorial waves (Free modes of the Gulf of Guinea). (unpublished manuscript)
- Hisard, P., 1980: Observation de réponses de type <<El Niño>> dans l'Atlantique tropical oriental Golfe de Guinée. Océan. Acta, 3, 69-78.
- \_\_\_\_\_, and B. Piton, 1981: Interannual variability in the eastern tropical Atlantic during the last decades. in Recent 69-78.
- \_\_\_\_\_, and B. Piton, 1981: Interannual variability in the eastern tropical Atlantic during the last decades. in Recent Progress in Equatorial Oceanography. Nova University Press, 297-306.

- Hofmann, E. E., A. J. Busalacchi and J. J. O'Brien, 1981: Wind generation of the Costa Rica Dome, Science, 214, 552-554.
- Houghton, R. W., 1976: Circulation and hydrographic structure over the Ghana continental shelf during the 1976 upwelling. J. Phys. Oceanogr., 6, 909-924.
- Hurlburt, H. E., 1974: The influence of coastline geometry and bottom topography on the eastern ocean circulation. Ph.D. dissertation, Florida State University, 104 pp.
- \_\_\_\_\_, J. C. Kindle and J. J. O'Brien, 1976: A numerical simulation of the onset of El Niño. J. Phys. Oceanogr., 6, 621-631.
- Katz, J., 1981: Dynamic topography of the sea surface in the equatorial Atlantic. J. Mar. Res., 39, 53-63.
- \_\_\_\_\_, R. Belevitsch, J. Bruce, V. Bubnov, J. Cochrane, W. Duing, P. Hisard, H. U. Lass, J. Miencke, A. deMesquita, L. Miller, and A. Rybnikov, 1977: Zonal pressure gradient along the equatorial Atlantic. J. Mar. Res., 35, 293-307.
- Keen, R. A., 1982: The role of cross-equatorial tropical cyclone pairs in the Southern Oscillation, Mon. Wea. Rev., in press.
- Kidson, J. W., Tropical eigenvector analysis and the southern oscillation, Mon. Wea. Rev., 103, 187-196, 1975.
- Kindle, J. C., 1979: Equatorial Pacific Ocean variability - seasonal and El Niño time scales. Ph.D. dissertation, Florida State University, 134 pp.
- Knox, R. A., and D. Halpern, 1982: Long range Kelvin wave propagation of transport variations in Pacific Ocean equatorial currents, J. Mar. Res., 40, 329-339.
- Lamb, P. J., 1978: Case studies of tropical Atlantic surface circulation pattern during recent sub-Saharan weather anomalies, 1967-1968. Mon. Wea. Rev., 106, 282-291.
- Lass, H. U., V. Bubnov, J. M. Huthance, E. J. Katz, J. Meincke, A. deMesquita, F. Ostapoff, and B. Voituriez, 1982: Seasonal changes of the zonal pressure gradient in the equatorial Atlantic west of 10°W during the FGGE year. Submitted to Océan. Acta.
- Lemasson, L., and J.-P. Rébert, 1973: Les courants marins dans le Golfe Ivoirien. Cah. ORSTOM, sér. Oceanogr., 11, 67-95.
- \_\_\_\_\_, J. C. Kindle and J. J. O'Brien, 1977: Sea surface temperature  
Lemasson, L., and J.-P. Rébert, 1973: Les courants marins dans le Golfe Ivoirien. Cah. ORSTOM, sér. Oceanogr., 11, 67-95.
- Markham, C. G., and D. R. McLain, 1977: Sea surface temperature related to rain in Ceara, northeastern Brazil. Nature, 265, 320-323.



- Mazeika, P. A., 1967: Thermal domes in the eastern tropical Atlantic Ocean. Limnol. Oceanogr., 12, 537-539.
- McCreary, J., 1976: Eastern tropical response to changing wind systems: with application to El Niño. J. Phys. Oceanogr., 6, 632-645.
- \_\_\_\_\_, 1977: Eastern ocean response to changing wind systems, Ph.D. dissertation, University of California, San Diego.
- \_\_\_\_\_, J. Picaut and D. W. Moore, 1982: Effect of annual remote forcing in the eastern tropical Atlantic. (manuscript in preparation)
- Merle, J., 1977: Seasonal variations of temperature and circulation in the upper layers of the equatorial Atlantic Ocean. Paper presented at the GATE workshop -Miami, Feb. 28 -March 10, 1977 (unpublished manuscript)
- \_\_\_\_\_, 1978: Atlas hydrologique saisonnier de l'océan Atlantique intertropical. Travaux et documents de l'O.R.S.T.O.M. No. 82.
- \_\_\_\_\_, 1980a: Seasonal heat budget in the equatorial Atlantic Ocean. J. Phys. Oceanogr., 10, 464-469.
- \_\_\_\_\_, 1980b: Variabilité thermique annuelle et interannuelle de l'océan Atlantique équatorial Est. L'hypothèse d'un <<El Niño>> Atlantique. Ocean Acta., 3, 209-220.
- \_\_\_\_\_, 1982: Seasonal variability of subsurface thermal structure in the tropical Atlantic (to appear in the proceedings of the 14<sup>th</sup> international Liège Colloquium on ocean hydrodynamics)
- \_\_\_\_\_, and J. F. Le Floch, 1978: Cycle annuel moyen de la température dans les couches supérieures de l'océan Atlantique intertropical. Ocean. Acta., 1, 271-276.
- \_\_\_\_\_, M. Fieux and P. Hisard, 1980: Annual signal and interannual anomalies of sea surface temperature in the eastern equatorial Atlantic. Deep Sea Res., GATE sup. II 26, 77-101.
- \_\_\_\_\_, and S. Arnault, 1982: Seasonal variability of dynamic topography in the tropical Atlantic Ocean. (manuscript in preparation).
- Meyers, G., 1979: Annual variation in the slope of the 14°C isotherm along the equator in the Pacific Ocean. J. Phys. Oceanogr., 9, 885-891.
- \_\_\_\_\_, 1982: Annual variation in the depth of the 14°C isotherm along the equator in the Pacific Ocean. J. Phys. Oceanogr., 9, 885-891.
- \_\_\_\_\_, 1982: Annual and interannual variation in sea level near Truk Island, J. Phys. Oceanogr., in press.

- Moore, D. W., 1968: Planetary-gravity waves in an equatorial ocean. Ph.D. thesis, Harvard University, 201 pp.
- \_\_\_\_\_, and S. G. H. Philander, 1977: Modeling of the tropical oceanic circulation. The Sea, Vol. 6, E. Goldberg, et al., Eds., Wiley-Interscience, 319-361.
- \_\_\_\_\_, P. Hisard, J. P. McCreary, J. Merle, J. J. O'Brien, J. Picaut, J. M. Verstraete and C. Wunsch, 1978: Equatorial adjustment in the eastern Atlantic. Geophys. Res. Letters, 5, 637-640.
- Morlière, A., 1970: Les saisons marines devant Abidjan. Doc. Sc. Centre Rech. Océanogr. Abidjan, 1, 1-15.
- \_\_\_\_\_, and J. P. Rébert, 1972: Etude hydrologique du plateau continental ivoirien. Doc. Sci. Centre Rech. Oceanogr. Abidjan, 3, 1-30.
- Namias, J., 1969: On the causes of the small number of Atlantic hurricanes in 1968. Mon. Wea. Rev., 97, 346-348.
- O'Brien, J. J., D. Adamec and D. W. Moore, 1978: A simple model of equatorial upwelling in the Gulf of Guinea. Geophys. Res. Letters, 5, 641-644.
- \_\_\_\_\_, A. Busalacchi and J. Kindle, 1981: Ocean models of El Niño. Resource Management and Environmental Uncertainty: Lessons from Coastal Upwelling Fisheries. M. H. Glantz and J. D. Thompson, Eds., Wiley-Interscience, 159-212.
- Orlanski, I., 1976: A simple boundary condition for unbounded hyperbolic flows. J. Comp. Phys., 21, 251-269.
- Patton, R. J., 1981: A numerical model of equatorial waves with application to the seasonal upwelling in the Gulf of Guinea. M.S. thesis, Massachusetts Institute of Technology.
- Perkins, H., 1981: Low-frequency forcing of the tropical Atlantic Ocean under the ITCZ during GATE, Deep Sea Res., GATE sup. I 26, 225-236.
- Philander, S. G. H., 1977: The effect of coastal geometry on equatorial waves (forced waves on the Gulf of Guinea). J. Mar. Res., 35, 509-523.
- \_\_\_\_\_, 1979: Variability of the tropical oceans. Dyn. Atm. Ocean., 3, 191-208.
- \_\_\_\_\_, 1979: Variability of the tropical oceans. Dyn. Atm. Ocean., 3, 191-208.
- \_\_\_\_\_, 1979: Upwelling in the Gulf of Guinea. J. Mar. Res., 37, 23-33.

- Philander, S. G. H., and R. C. Pacanowski, 1980: The generation and decay of equatorial currents. J. Geophys. Res., 85, 1123-1136.
- \_\_\_\_\_, and \_\_\_\_\_, 1981a: The oceanic response to cross-equatorial winds (with application to coastal upwelling in low latitudes). Tellus, 33, 204-210.
- \_\_\_\_\_, and \_\_\_\_\_, 1981b: Response of equatorial oceans to periodic forcing. J. Geophys. Res., 86, 1903-1916.
- Picaut, J., 1982: Propagation of the seasonal upwelling in the eastern equatorial Atlantic. To appear in J. Phys. Oceanogr.
- \_\_\_\_\_, J. M. Verstraete and A. Morlière, 1978: Ondes forcées par la marée et l'atmosphère le long des cotes du Golfe de Guinée. CNEXO report. Université de Bretagne Occidentale, 78 pp.
- Portolano, P., 1981: Contribution à l'étude de l'hydroclimat des cotes Sénégalaises. ORSTOM, Centre Océanogr. Dakar-Thiaroye, 69 pp.
- Quinn, W. H., 1974: Monitoring and predicting El Niño invasions, J. Appl. Meteor., 13, 825-830.
- \_\_\_\_\_, D. O. Zopf, K. S. Short, and R. T. W. Kuu Yang, 1978: Historical trends and statistics of the Southern Oscillation, El Niño and Indonesian droughts. Fish. Bull., 76, 663-678.
- Romea, R. D., and R. L. Smith, 1982. Further evidence for coastal trapped waves along the Peru coast. Submitted to J. Phys. Oceanogr.
- Rosignol, M., 1972: Contribution à l'étude du "complexe guinéen". Doc. Sci. ORSTOM, Rép. du Sénégal Serv. Océanogr. et Pêches. 143 pp.
- \_\_\_\_\_, and M. Meyrueis, 1964: Campagne océanographique de Gerard-Treca. ORSTOM, Centre Oceanogr. Dakar-Thiaroye. 53 pp.
- Roy, C., 1981: Sur le phénomène de la petite saison froide dans le Golfe de Guinée. D.E.A. Report, Université de Bretagne Occidentale, France, 38 pp.
- Schopf, P. S., and D. E. Harrison, 1982: On equatorial Kelvin waves and El Niño: I. Model SST changes with different mean conditions. Submitted to J. Phys. Oceanogr.
- Servain, J., J. Picaut and J. Merle, 1982: Evidence of remote forcing in the equatorial Atlantic Ocean. J. Phys. Oceanogr., 12, submitted to J. Phys. Oceanogr.
- Servain, J., J. Picaut and J. Merle, 1982: Evidence of remote forcing in the equatorial Atlantic Ocean. J. Phys. Oceanogr., 12, 457-463.
- Smith, R. L., 1978: Poleward propagating perturbations in currents and sea levels along the Peru coast. J. Geophys. Res., 83, 6083-6092.

- Speth, P., and H. Detlefsen, 1982: The relationship between sea surface temperatures and winds off Northwest Africa and Portugal (submitted to Océanogr. Tropicale)
- Stommel, H. S., 1947: Note on the use of the T-S correlation for dynamic height anomaly computations. J. Mar. Res., 5, 85-92.
- Verstraete, J. M., J. Picaut and A. Morlière, 1980: Atmospheric and tidal observations along the shelf of the Guinea Gulf. Deep Sea Res., GATE Sup. II, 26, 343-356.
- Voituriez, B., 1981a: The equatorial upwelling in the eastern Atlantic: Problem and paradoxes, in Coastal Upwelling, F. A. Richard, Editor, A.G.U., Washington, D.C.
- \_\_\_\_\_, B., 1981b: The equatorial upwelling in the eastern Atlantic Ocean in Recent Progress in Equatorial Oceanography. Nova University Press, 229-247.
- \_\_\_\_\_, B., 1981c: Les sous-courants équatoriaux nord et sud et la formation des dômes thermiques tropicaux. Oceanologica Acta, 4, 497-506.
- Wooster, W. S., A. Bakun and D. R. McClain, 1976: The seasonal upwelling cycle along the eastern boundary of the North Atlantic. J. Mar. Res., 34, 131-141.
- Wyrtki, K., 1964: Upwelling in the Costa Rica Dome. Fish. Bull., 63, 355-372.
- \_\_\_\_\_, 1974a: Sea level and the seasonal fluctuations in the western Pacific Ocean. J. Phys. Oceanogr., 4, 91-103.
- \_\_\_\_\_, 1974b: Equatorial currents in the Pacific 1950 to 1970 and their relations to the trade winds. J. Phys. Oceanogr., 4, 372-380.
- \_\_\_\_\_, 1975: El Niño -The dynamic response of the equatorial Pacific Ocean to atmospheric forcing. J. Phys. Oceanogr., 5, 572-584.
- \_\_\_\_\_, 1977: Sea level during the 1972 El Niño, J. Phys. Oceanogr., 6, 779-787.
- \_\_\_\_\_, 1979: The response of sea surface topography to the 1976 El Niño. J. Phys. Oceanogr., 9, 1223-1231.
- \_\_\_\_\_, Stroup, E., Patzert, W., Williams, R., and Quinn, W., 1976: Predicting and observing El Niño, Science, 191, 343-346.
- \_\_\_\_\_, Stroup, E., Patzert, W., Williams, R., and Quinn, W., 1976: Predicting and observing El Niño, Science, 191, 343-346.
- Yoshida, K., 1955: Coastal upwelling off the California Coast. Records of Oceanogr. Works in Japan, 2, 8-20.